PB2003-100457

Creep Characterization of Residual Tropical Soils for Engineering Design and Analysis

Horst G. Brandes

Kerwin Chang

Devin D. Nakayama

Research Report UHM/CE/02-01

March 2002

UNIVERSITY OF HAWAII
COLLEGE OF ENGINEERING

DEPARTMENT OF CIVIL ENGINEERING

Technical Report Documentation Page

1. Report No.	2. Government Accession No.	3. Recipient's Catalog No.
HWY-L-UH-97-01		

4. Title and Subtitle	5. Report Date
CREEP CHARACTERIZATION OF RESIDUAL TROPICAL SOILS FOR ENGINEERING DESIGN AND ANALYSIS	MARCH 2002
	6. Performing Organization Code
7. Author(s) H. G. Brandes, Ph.D., P.E., K. Chang and D. D. Nakayama	8. Performing Organization Report No.
9. Performing Organization Name and Address University of Hawaii - College of Engineering Department of Civil Engineering 2540 Dole Street, Holmes Hall 383 Honolulu, HI 96822	10. Work Unit No. (TRAIS)
	11. Contract or Grant No. Contract No. 43012
12. Sponsoring Agency Name and Address HAWAII DEPARTMENT OF TRANSPORTATION, HIGHWAYS DIV. 869 Punchbowl Street Honolulu, HI 96813	13. Type of Report and Period Covered Final Report
	14. Sponsoring Agency Code

15. Supplementary Notes

Prepared in cooperation with the U.S. Department of Transportation, Federal Highway Administration

16. Abstract

The objective of this study was to investigate the time-dependent behavior of tropical soils from Hawaii by conducting carefully controlled long-term creep tests under drained conditions. Time dependency issues investigated include creep behavior under sustained anisotropic stresses, rate effects during deviatoric loading, as well as strength changes associated with secondary consolidation and aging. Correlations were sought between creep deformation and Atterberg limits to provide empirical correlations that can be referred to when time consuming and expensive tests of the type conducted herein are not feasible. In addition, the testing program was aimed at determining specific material constants for constitutive model development and verification.

In terms of friction angles, two of the soils yielded values significantly different from what would be expected based on their Atterberg linits. Strain rate effects during drained and undrained loading varied depending on the type of soil, hence proposed guidelines for either type of loading may not be appropriate for all the soils investigated. A general relationship is proposed between the Singh-Mitchell creep parameter m and plasticity. Post-creep strength tests revealed an increase in deviatoric stress needed to reach failure, compared to similar tests conducted on non-aged specimens.

17. Key Words	18. Distribution Statement
Creep, strain rate effects, strength, tropical soils, aging	Document is available to the U.S. public through the National Technical Information Service, Springfield, Virginia 22161

19. Security Classif. (of this report)	20. Security Classif. (of this page)	21. No. of Pages	22. Price
Unclassified	Unclassified	133	

Final Research Report

Creep Characterization of Residual Tropical Soils for Engineering Design and Analysis

By:

Horst G. Brandes
Kerwin Chang
Devin D. Nakayama

Department of Civil Engineering
University of Hawaii

Prepared in cooperation with:

State of Hawaii Department of Transportation
Highways Division
&
U. S. Department of Transportation
Federal Highway Administration

March 2002

Table of Contents

1. Summary and Recommendations 1
2. Project Contributions: Students, Theses, Publications 5
3. Journal Manuscript: *Creep and Time-Dependent Strength Effects in Volcanic Soils* 7
4. Appendix A – Background 69
5. Appendix B – Index Properties and Strength Tests 84
6. Appendix C – Creep Tests 106
7. Appendix D – Post-Creep Strength Tests 117
8. Appendix E1 – Publication 1 122
9. Appendix E2 – Publication 2 128

1. Summary and Recommendations

The objective of this study was to investigate the time-dependent behavior of residual tropical soils from Hawaii by conducting carefully controlled long-term creep tests under drained conditions, in an effort to provide the necessary experimental data to characterize the soil response beyond primary consolidation. Time dependency issues investigated include creep behavior under sustained anisotropic stresses, rate effects during deviatoric loading, as well as strength changes associated with secondary consolidation and aging. Correlations were sought between creep deformation and Attergerg limits to provide empirical correlations that can be referred to when time consuming and expensive tests of the type conducted herein are not feasible. In addition, the testing program was aimed at determining specific material constants for constitutive model development and verification.

This section summarizes the work conducted, presents the principal findings, and makes recommendations for future studies. The scientific aspects of the research program are described in further detail in Section 3 of this report, which constitutes a manuscript that is being submitted for publication in a peer reviewed journal for dissemination of the research findings. Miscellaneous results from the testsing program are included in the appendices.

Four soils with distinctive sets of geotechnical properties were selected for this study (Table 1). They included a high plasticity clay from the Alani-Paty landslide area in Manoa, a residual silt and a residual clay from the Kapolei area, and an ash soil from the South Hilo District with extremely high plasticity properties (Figure 1). All the soils were mixed with water to their respective liquid limits. They were reconstituted with a high-speed mixer to brake up all vestiges of in situ structure and reconsolidated uniformly in submerged cylinders to yield normally consolidated specimens. Sufficient identical samples were prepared for both the strength and creep testing programs.

Triaxial tests were conducted to characterize the strength properties of the four soils. They included isotropicaly consolidated undrained and drained tests. Some specimens were loaded under strain-controlled conditions, whereas others were loaded under stress-controlled conditions, the latter to simulate the loading conditions in the creep tests. This testing program was aimed at determining maximum deviatoric stresses from which appropriate drained strengths and stress levels could be determined for the creep tests (Figures 4, 8, 11, 14). In addition, as expanded on in Section 3, a number of rate dependency issues important to the way the creep tests were conducted were investigate as well.

The creep testing program began with the Manoa clay samples. Five drained triaxial creep tests were conducted at stress levels ranging between 0% and 90% (Figure 15). The longest of these, the 90% test, lasted for 482 days (1.32 years) and is among the longest creep tests ever conducted. As expected, accumulated creep strains increased with increasing stress levels. This does not imply that field conditions in which stresses are close to failure will lead to the largest amount of creep prior to rupture. Most of the deformations observed in Figure 15 are associated with the loading phases of the tests. In contrast, true creep conditions require uniform stress conditions. In order to isolate the creep deformations in the tests, it is necessary to focus on the behavior beyond the end of loading. This is best accomplished by calculating the rate of axial

strain and ignoring the loading phase. The results are shown as a function of time in a log-log plot in Figure 16. Aside from the anomalous results of the 30% test, all other tests are characterize by linear fits that are more or less parallel to each other but are shifted upward with stress level. This means that the higher the stress level, the higher the rate of strain. The slope of these lines is the Singh-Mitchell parameter m. The results indicate that this parameter is independent of stress level and appears to be a soil constant. In general, the higher the parameter m, the higher the rate of creep attenuation, and hence the faster that creep deformations can be expected to cease in the field. Of course, the total amount of creep that will occur still depends on the initial rate of deformation once constant stress conditions are reached. Thus the parameter m should not be used by itself to compare creep susceptibility. An intercept is needed as well. Such an intercept depends on the stress intensity at which creep is occurring.

Four creep tests were conducted or the Kapolei Red silt (Figure 17). Stress levels ranged between 0% and 50%. Higher intensities were not possible since the material appeared to fail under drained conditions at deviatoric stresses well below what was predicted from the undrained strength tests. Again, m-parameters were more or less constant for all the tests, with the exception of the 30% one. It is not clear why the 30% tests for the Manoa clay and the Kapolei Red silt did not agree with the rest of the data.

In the case of the Hilo Ash soil, creep tests were conducted at 70% and 90% stress levels (Figure 19). Interestingly, the accumulated creep strains were the largest for any of the soils, even at comparable stress levels. As noted earlier, however, the vast majority of the creep strains occurred during the loading phases with only scant deformations following during the constant stress phases. This is reflected in strain rates that are comparable to those of the other soils (Figure 21). The 70% creep test is the only one that failed during the creep stage, in this case well beyond the end of deviatoric loading (331 days after the start of the test).

One creep tests was conducted for the Kapolei Brown Clay at 70% (Figure 22). It lasted for 278 days and yielded an m-parameter of 1.37. Additional creep tests were not carried out due to time constraints but should be conducted in the future.

A comparison among the different soil types in terms of the m-parameter is presented in Figure 27, where the results are correlated with plasticity index. Included also are the results from a series of deep sea illite creep tests conducted under similar test conditions by the first author in an earlier study. It appears that, with the exception of the Hilo Ash soil, the parameter m increases linearly with plasticity index. At present, this is deemed a preliminary correlation due to the limited number of soil types. The results are surprising since they indicate that in high plasticity soils such as the Manoa clay creep deformations will attenuate much faster than in lower plasticity soils such as the Kapolei Red silt, for which creep deformations can continue to be significant over longer periods of time. Of course, as already discussed, the amount of deformation that will occur, due strictly to creep phenomena, are highly dependent on in situ stresses, which may be quite different from those used in this study. Furthermore, field drainage conditions, changes in moisture content and saturation, as well as ionic fluctuations due to leaching processes and changes in pore water chemistry, all are bound to have an important effect on long term displacements in the field.

The average *m*-parameter for the Hilo ash soil does not agree with the correlation indicated in Figure 27. Despite the high plasticity indices for this soil, the *m*-parameter is not very high. In general, it appears that high Atterberg limits for the Hilo Ash soil do not translate into unusually low friction angles, high compressibility, or unexpected creep behavior. In fact, other than for identification purposes, Atterberg limits for this type of soil should not be used for correlation with engineering behavior using conventional empirical relationships without further study. Also, given the dramatic changes in Atterberg limit values and gradation upon drying and wetting, classification of these soils using the Unified Soil Classification System is questionable. In general, it is advisable that these soils not be allowed to dry unduly in the laboratory and that fluctuation in field moisture be considered prominently when evaluating their long-term performance.

The Manoa clay and the Kapolei Brown clay creep specimens were subjected to undrained deviatoric loading upon completion of the creep tests to investigate how strength changes with time. The results are summarized in terms of stress paths and strength parameters in Figures 33 and 34. In each case the stiffness of the soil increases upon reloading with failure reached at quite low axial strains. Maximum deviatoric stresses were significantly higher than those predicted from non-aged strength tests. The increase is attributed largely to the formation of additional bonds during long-term creep. The effect is such that the Mohr-Coulomb failure envelope is shifted upward but with no change in friction angle. When aging is allowed to continue for longer periods of time, as in the 90% Manoa clay creep test, the maximum deviatoric stress is seen to increase proportionally. Additional creep tests conducted under anisotopic stress conditions are necessary to clarify the role that such anisotropy has on strength changes.

This study has resulted in significant findings that compliment prior investigations on the creep aspects of Hawaiian soils. Nonetheless, time-dependency is a complex phenomenon that is not yet fully understood. Much remains to be done. Given that creep has been identified as a major problem in Hawaii, leading to slope displacements, secondary settlement of foundations, continued deformation of fills, and even to unexpected failures that develop over time, it is necessary that additional studies be conducted to better understand how particular soil masses may behave in the long term. The following recommendations follow from this study:

- A comprehensive testing program needs to be conducted on the strength properties of common Hawaiian soils that focuses on rate dependency, stress versus strain modes of loading, differences between drained and undrained strengths, as well as isotropic and anisotropic methods of consolidation. Although some strength values are reported in the literature for selected soils, there does not exist a comprehensive database of strength properties for the vast number of soils that are encountered in Hawaii. In many cases these soils are significantly different from those found elsewhere. Of particular interest are extreme soils such as the class of Ash deposits found on the Big Island and elsewhere. Strength properties are essential for most aspects of geotechnical engineering practice associated with roads and highways.

- The creep testing program needs to be continued to include additional tests on the Kapolei Brown clay, the Hilo Ash soil, and a number of other soil types that were not

included in this investigation. Given that the time dependency of low plasticity soils may also be significant in some instances, soil types such as low plasticity calcareous sediments and estuarine materials should be included as well. This would allow for more reliable empirical correlations with plasticity indices or other soil characteristics. Additional test conditions should include anisotropic consolidation prior to creep, a range of different types of stress paths before and after creep testing, and an expanded set of post-creep strength tests.

- Finally, laboratory tests need to be supplemented with field measurements. These may include the installation of long-term inclinometers on slopes, settlement plates, extensometers, and pore pressure piezometers. In situ tests should include borehole shear tests, cone penetrometer tests, and permeability tests. The results from a comprehensive investigation of this type should be used to conduct a numerical prediction of time-dependent deformations for a selected case study. A preliminary analysis of this type was conducted as part of an investigation related to this study, the results of which are outlined in the manuscripts that are included in Appendices E1 and E2. A much more thorough study of this type should provide the required link between laboratory results and field measurements.

2. Project Contributions: Students, Theses, Publications

2.1 Students

A number of students contributed to the project at various times and were supported partially with funds from the research grant. Their work included laboratory testing, analysis, and preparation of the findings. The following students made significant contributions:

Devin D. Nakayama: He carried out the bulk of the strength, creep, post-creep, and classification tests conducted for this study. In addition, he prepared all the soils for testing. The work conducted under this study comprised the bulk of his M.S. thesis research project. He received a Research Assistantship through this grant for his efforts. His thesis is listed below.

Candy S. L. Tsui: She assisted with the testing during one semester and received partial funding for it. Her M.S. thesis, also related to this project, was closely related to this study and lead to two publications in 2001 (Appendices E1 and E2).

Kerwin Chang: An undergraduate student at present, he assisted with completing the remaining creep tests, updating the data files, and preparing this report

2.2 Thesis

Two Department of Civil Engineering M.S. theses were completed during the project. They were also published as Department technical reports:

Drained creep characteristics in normally consolidated tropical Hawaiian soils, M.S. Thesis, Devin D. Nakayama, 2000 (Department of Civil Engineering Technical Report UHM/CE/00-03, D. Nakayama and H. Brandes).

Modeling the slope stability and creep behavior of the Alani-Paty landslide area, Manoa valley, Honolulu, Hawaii, M.S. Thesis, Candy Sau Lan Tsui, 1999 (Department of Civil Engineering Technical Report UHM/CE/99-07, Candy Sau Lan Tsui and H. G. Brandes).

2.3 Publications

In addition to this report, quarterly reports were submitted to the Research Committee throughout the duration of the project. The following publications have resulted to date:

Brandes, H. G. and Nakayama, D. D. (2002). Creep and time-dependent strength effects in volcanic soils. *Geotechnique* (Journal manuscript in Section 3 to be submitted January 2002, possibly to be split into two articles due to its length and breath).

Brandes, H. G. and Tsui, C. S. L. (2001). Modeling the effectiveness of groundwater-lowering remediation techniques in the Alani-Paty landslide area, Oahu, Hawaii. *Computer Methods and Advances in Geomechanics, Proceedings of the 10th International Conference on Computer Methods and Advances in Geomechanics,* **2**:1543-1547.

Tsui, C. S. L., Brandes, H. G. and Nakayama, D. D. (2001). Creep behavior of the slow-moving Alani-Paty landslide, Oahu, Hawaii. *Computer Methods and Advances in Geomechanics, Proceedings of the 10th International Conference on Computer Methods and Advances in Geomechanics,* **2**:1629-1633.

3. Journal Manuscript

Creep and Time-Dependent Strength Effects in Volcanic Soils

H. G. Brandes and D.D. Nakayama
Department of Civil Engineering
University of Hawaii

Abstract

Time-dependent characteristics of four contrasting volcanic soils from Hawaii were investigated under triaxial conditions. Short-term strength, creep, and post-creep strength tests revealed that these types of soils are sensitive to loading rates and aging, often along the lines of what previous studies have found for other types of fine-grained soils. In terms of creep deformations, there appear to be differences among the four soil types in terms of creep strain attenuation over time. Significant strength and stiffness gains are observed after long periods of deformation under constant anisotropic stresses. These are attributed largely to aging phenomena associated with the development of interparticle bonds. The effect of aging is reflected in an upward shift of the Mohr Coulomb failure envelope, but not in a change in friction angle. The amount of the shift depends on the length of the aging period.

Introduction

The time-dependent behavior of fine-grained soils has been the focus of numerous investigations over the past 40 years that have included laboratory tests conducted under various configurations, as well as a number of constitutive studies (Murayama and Shibata, 1961; Singh and Mitchell, 1968; Bishop and Lovenbury, 1969; Vaid and Campanella, 1977; Tavenas et al., 1978; Adachi and Oka, 1982; Borja and Kavazanjian, 1984; Tavenas and Leroueil, 1987; Imai, 1995; Leroueil and Marques, 1996; Adachi et al., 1996; Silva and Brandes, 1996). Of particular note is the development of material models that treat rate effects, and in some cases temperature, within the context of soil elasto-plasticity (Sekiguchi, 1984; Borja and Kavazanjian, 1984; Oka et al., 1988; Kaliakin and Dafalias, 1990; Adachi et al., 1996). This allows their consistent implementation within the general framework of critical state soil behavior. However, much remains to be done. Only a handful of creep models have found widespread use in finite element codes such as PLAXIS, AFINA, and other widely used programs. Virtually none of the constitutive models in these codes take into account rate-dependent effects during loading. Another shortcoming is that most models have been developed based on a limited number of soil types and a restricted set of laboratory test conditions. This places limits on their usefulness for general geotechnical applications. The purpose herein is to report on a set of triaxial creep and strength tests conducted on tropical volcanic soils of varying plasticity and mineralogy in order to contribute to the data set on creep characteristics of fine-grained soils. Rate effects during triaxial loading and changes in strength following creep deformation under sustained stresses are investigated as well.

Soils Tested

The four soils obtained for this study were collected from the islands of Oahu and Hawaii (Figure 1). They represent common tropical Hawaiian soils with distinctive sets of geotechnical properties, particularly in terms of mineralogy and plasticity. Volcanic soils across the islands are highly variable. They reflect the igneous processes that gave birth to the parent basaltic rocks and assorted pyroclastic ejecta, the chemical composition of the source magma, and the climatic conditions under which weathering has occurred. Hawaii's location in the path of North Pacific trade winds, along with its rugged geography, has resulted in a series of microclimates that range from very dry conditions along much of the leeward sides of the islands to extremely wet conditions along the volcanic ridges. Annual rainfall at many locations exceeds 2500 mm per year. It is thought that today's weather patterns have remained relatively unchanged since the major islands were formed, starting some five million years ago (Stearns, 1966). Due to generally warm temperatures year round, chemical weathering has proceeded at a high rate in areas with abundant precipitation. As a result, many types of soils have been identified, each reflecting unique complex processes of clay mineral formation. A major criterion in selecting soils for this study was to choose materials with widely ranging plasticity characteristics, which presumably would lead to contrasting types of stress-strain-time-strength behavior. All the soils were tested for basic index properties in general accordance with ASTM procedures. The results are summarized in Table 1 and Figure 2.

The Manoa clay (MC) is a dark brown clayey soil found on alluvial fans and talus slopes bordering steep and moderately steep ridges on the islands of Oahu and Kauai. The representative soil sample used in this study was taken from the Hulu-Woolsey landslide area in Manoa Valley, Honolulu. It consists of material that has descended from Waahila Ridge and has weathered on the debris apron to form vertisols. Vertisols are pedologic soils that are typically dark brown to gray, clay-rich, and are of high plasticity. The Manoa clay is highly expansive and is locally known as adobe soil. It is found at numerous locations and has continually presented slope stability problems in urban areas (Peck, 1958; Peck and Wilson, 1968; De Silva, 1974; Baum and Reid, 1992; Ellen et al., 1995; Brandes and Tsui, 2001; Tsui et al., 2001). Although most of the damage to residential structures, roads and utilities is strongly related to cumulative failures following intense rainfall events, some of the observed deformations have been attributed to creep (Baum et al., 1991).

Lateritic soils are among the most widespread classes of soils in Hawaii. They are found in basins and on alluvial fans, particularly on the older islands of Oahu and Kauai. Although common throughout the world, tropical conditions in Hawaii result in intense leaching processes, with all but the youngest soils substantially depleted of silica-rich minerals. Left behind in the weathered residuum are high concentrations of oxides, aluminum, titanium, and manganese (Mitchell and Sitar, 1982). High iron oxide fractions give these soils their red color. Locally, the term for highly and moderately lateritic soils is red soils. The Kapolei Red (KR) silt belongs to this class of soils, although in this case the precise extent of laterization is not clear. The red soil tested in this study has

plasticity, specific gravity and gradation characteristics similar to tropical acrisols from South America and Africa (Morin, 1982). ML soils such as this one, and even those lateritic soils that are nominally classified as MH, are considered reasonably good for construction purposes and are used extensively in road embankments, earthfill dams, and as subgrade for lightweight structures (Lum, 1982). The KR silt was chosen for this study because of its abundance and common use as a construction material, but principally because its Atterberg limits are significantly lower than those of the other three soils tested (Figure 2).

Hilo Ash (HA) soil is found on the windward side of the Mauna Kea volcano on the Island of Hawaii. The representative sample used for this investigation was collected in the South Hilo district area at a depth between 0.5 m and 2.0 m. Ash soils occur in Japan, many Pacific and Caribbean Islands, and the Rift Zone of Africa (Uehara, 1982). They typically consist of weathered and often weakly cemented fine particles of volcanic glass. The plasticity and gradation characteristics are highly variable and depend on many factors, particularly past fluctuations in moisture content. Ash soils that have remained steadily moist can at times be characterized by extremely high water contents and Atterberg limits, as well as moderate to high sensitivities and low specific gravities. That is the case for the HA soil selected for testing (Table 1, Figure 2). Oven drying the HA soil resulted in irreversible microstructural changes that were reflected in large changes in Atterberg limits and gradation (Table 1). The exact nature of these fabric changes is poorly understood, although they may be due in some cases to the collapse of halloysite and allophane structures upon drying (Mitchell and Sitar, 1982). A complicating factor is that some of these soils also have a significant organic content (Wieczorek et al., 1982), the drying of which is also irreversible. In any case, all the soils in this study were kept moist at all times. Ash soils in Hawaii are generally rated as poor materials due to their high compressibility, high swelling, low density upon compaction and poor workability. Nonetheless, they typically have high friction values and steep cuts remain stable over prolonged periods of time under static conditions. Because of their medium to high sensitivity, ash soils can be susceptible to slope instability from earthquake shaking (Nielson et al., 1977). Due to high water contents, they likely would amplify seismic shaking propagating from beneath. There is anecdotal information that this is indeed the case for some deposits in the general vicinity of Hilo.

The Kapolei Brown (KB) clay was collected from the broad coastal Ewa plain on the island of Oahu. It was taken from a site not too distant from where the KR silt was obtained. The KB clay is dark reddish to brown and pedologically probably a distant cousin of the KR silt. However, it has significantly higher plasticity indices and shrink-swell potential. In this regard it is probably closer to the Manoa clay and classifies as a CH soil. The use of KB clay is normally avoided in road subgrades, foundations, and engineered fills. Its high plasticity and swell potential causes frequent headaches to homeowners who complain of cracked slabs, walls, and other forms of structural distress. Because it is often found close to lateritic soils that are similar in color, texture and moisture content, it is sometimes misidentified and erroneously used in construction.

Preparation of Samples

All the strength and creep tests were conducted in triaxial cells. The inherent variability in most natural soil deposits makes obtaining multiple undisturbed specimens that are reasonably similar in all respects almost impossible. Instead, the soils in this study were reconstituted and reconsolidated using a consistent set of procedures so that a sufficient number of comparable specimens would be available for testing. Each soil was sieved in a moist condition through a No. 4 sieve to remove any particles larger than one-fourth the sample diameter to be used in the triaxial tests (49.1 mm). All the soils were then brought to moisture contents close to their respective liquid limits and blended thoroughly with a handheld electric drywall mixer. After mixing, the soils were carefully placed in smooth cylindrical containers, taking care that no air was being entrapped. Filter paper was placed at the ends and along the sides of the cylinders. Porous stones were added to the top and bottom to provide for double drainage conditions.

The cylinders were immersed in water and the soils consolidated in stages to a vertical stress of 25 kPa. The vertical displacement of the upper stones was monitored using dial gages. Loads were left on until the deformations ceased. Standard one-dimensional consolidation tests were conducted to confirm that adequate time was allotted for the soil in each cylinder to reach at least 90% consolidation. At the end of consolidation, the soils were subsampled by inserting thin stainless steel tubes to obtain the triaxial specimens. These tubes were inserted with the aid of a piston that was outfitted with a set of O-rings to minimize drag-down effects, in much the same way that piston assemblies are used for field coring of soft clays. Final moisture contents indicated that the specimens obtained using these procedures were relatively uniform (Table 2)

Strength Tests

The strength test program consisted of isotropically consolidated undrained (CIU) and drained (CID) triaxial strength tests. Specimens were back-pressured to at least 150 kPa, with measured B-values well in excess of 0.95. Final consolidation pressures were all above the 25 kPa used during the prior reconsolidation process in order for normally consolidated conditions to prevail during deviatoric loading.

The stress-strain behavior and strength of normally consolidated fine-grained soils is rate-dependent. Vaid and Campanella (1977) found that increases in strain rate, longer periods of aging, and thixotropic hardening all result in stiffer undrained stress-strain response and higher undrained shear strength in clays. Mitchell (1976) has noted that a ten-fold increase in loading rates could lead to a five to ten percent increase in shear strength in undrained tests, with the magnitude of the effect increasing with plasticity. Therefore, care was taken in selecting appropriate rates. Loading rates were calculated using the ASTM D4767-95 standard for undrained tests (Appendix A) and Bishop and Henkel's (1962) procedure for drained tests (Appendix B). Both strain-controlled and stress-controlled tests were conducted. In most cases strain-controlled tests were chosen since they better define peak deviatoric stress and post-peak behavior. One advantage of the stress-controlled type is that appropriate stress rates can be selected without having to

assume an axial strain at failure (Appendix A). Perhaps more important herein is that strength tests conducted in this manner are a better simulation of the stress-controlled loading conditions during the creep tests. Calculated rates are listed for each soil type in Table 3 for undrained tests and in Table 4 for drained tests, respectively.

Results of the Manoa clay strength tests are presented in Figures 3 and 4 and are summarized in Table 5. One stress-controlled CIU (100 kPa) and four strain-controlled CIU tests (30 kPa, 50 kPa, and two at 100 kPa) were conducted. No drained tests were attempted due to time constraints. A loading period on the order of 40 days would have been necessary to reach 15% axial strain. Volume changes during the isotropic consolidation phases were consistent among all the CIU tests and produced an average t_{50} value of 540 minutes. According to the ASTM procedure, a loading rate of 0.00074%/min was determined for undrained loading. In order to reach 15% axial strain, as recommended, would have taken approximately two weeks. Again, due to time constraints and inherent difficulties in conducting undrained tests over such long periods of time, it was decided to conduct the tests at a higher rate of 0.05%/minute instead. According to Mitchell (1976), it is possible that strengths determined in this study are as much as 10 to 20% above those that could be expected if the ASTM recommended strain rate had been used. The stress-controlled test was conducted at a loading rate within the range of loading rates used in the creep tests. As is evident from Figure 3, the stress-strain behavior up to failure is similar to that of the two strain-controlled tests, although the pore pressure response, and hence the stress path, are somewhat different. In each test there is a clearly defined peak deviator stress. Failure occurred with the development of well-defined failure planes. Slight adjustments to the equipment following the early Manoa clay strength tests allowed the reliable use of very slow strain and stress rates, as necessary, in the remaining testing program.

The 14^0 friction angle for the Manoa clay is quite low, despite the fact that the strain rates used were substantially higher than recommended by ASTM. This friction value plots well below the classic Kenney relationship (Kenney, 1959) for normally consolidated soils. Back-analysis of slope stability in the area suggests that undisturbed friction values are not much higher than about 14^0 (Brandes and Tsui, 2001). It would therefore appear that this type of material must be significantly different from other normally consolidated soils in terms of mineralogy and/or fabric. X-ray diffraction tests conducted by Wan et al. (1999) on similar soils in East Honolulu revealed a low percentage of well-defined clay minerals, at times as low as 25% on a weight basis. The large amorphous fraction, which is an indication of the relative youth of the soil, is of unknown composition and poor crystalline structure and may very well be the reason for such low shear strengths.

Strength tests conducted on the Kapolei Red silt included 3 strain-controlled CIU tests, three stress-controlled CID tests, and one strain-controlled CID test. The results are shown in Figures 6 through 8 and in Table 6. The three CIU tests resulted in a friction angle of 36^0, which attests to the inherent strength of these lateritic soils alluded to earlier. This strength is in line with previous reports by Lum (1982) and others for similar Hawaiian soils. All the tests showed continuous deviatoric stress increase with strain and no softening. Failure in each case resulted in a barrel-shaped specimen.

Based on the results in Figure 8, a drained strength of 285 kPa would be predicted for an effective confining pressure of 100 kPa. All drained creep tests in this study were carried out at such a consolidation stress and stress levels for the Kapolei Red silt referred to when discussing the creep tests are defined with reference to this value. The CID strength tests were conducted to verify that 285 kPa is indeed the correct drained strength to be used for this soil. Three of the CID tests were loaded under stress-controlled conditions at rates of 12.5 kPa/hr, 4 kPa/hr, and 2 kPa/hr (Figure 7). An average value of 3 hours for t_{100} yielded a recommended loading rate of 4 kPa/hr according to the procedure in Appendix B. The 12 kPa/hr test was actually a creep test that failed prematurely. The sample failed at a deviatoric stress of 138 kPa, or about 48% of the maximum deviatoric strength predicted from the undrained tests (Figure 8). When the stress rate was reduced to the recommended 4 kPa/hr, the maximum deviatoric stress increased to 186 kPa, or about 65% of what had been expected based on the undrained tests. At 2 kPa/hr a maximum deviatoric value of 156 kPa was measured. In all three tests the stiffness prior to failure is similar. Since the rate of loading did not appear to have a clear influence on the maximum deviatoric stress reached in the drained tests, it was hypothesized that perhaps the reason that the drained strengths were incompatible with the undrained ones was the difference in the loading modes. To test this idea, a fourth CID test was conducted under strain-controlled conditions at a rate of 0.003 %/min, or about three times as fast as recommended by the procedure in Appendix B (Figure 7). In this case the maximum deviatoric stress reached 241 kPa, or 85% of the expected value.

It is possible that the selected rates of loading in the drained tests, whether strain or stress-controlled, were too high and resulted in the generation of significant excess pore pressures. The stress-controlled CID test in particular suggests that substantially lower rates than those recommended by Bishop and Henkel (1962) may be necessary in order to achieve truly drained conditions, at least for the Kapolei Red silt. The 2 kPa/hr and 4 kPa/hr tests show sharp increases in the rate of volume change shortly before failure, which indicates that the rate of loading may have been too high at the end of the tests. Volume changes in the 12 kPa/hr test are the smallest, probably because failure was reached much faster and thus not sufficient time was allowed for volume compression to take place.

Four strength tests were conducted on Hilo Ash soil, one strain-controlled CID and three strain-controlled CIU tests (Figures 9 through 10, Table 7). All specimens revealed a ductile deviatoric stress response with no clear peak stages and barrel-shaped configurations throughout loading. Given the high plasticity of this soil, it was anticipated that a low friction angle would follow. Nonetheless, a substantial value of 39^0 was obtained from the CIU tests, which agrees well with values reported by others for Hawaiian ash soils (for example, see Wieczorek et al. 1982). The extremely high plasticity of the Hilo ash soil places it well above the Kenney (1959) relationship (Figure 5). As was the case with the Manoa clay, such an unusual behavior in a normally consolidated soil is probably due to a unique fabric and mineralogy. The drained strength test was sheared under stress-controlled conditions at a rate of 3.5 kPa/hr, as suggested by

Bishop and Henkel (1962). In this case the maximum deviatoric stress was within 2% of what was predicted from the CIU tests.

Strength tests for the Kapolei Brown clay included 3 CIU tests and one strain-controlled CID test (Figures 12 through 14, Table 8), the latter conducted at the very slow rate of 0.0025%/min that follows from the procedure in Appendix B. In this case, the soil plots near the Kenney (1959) relationship (Figure 5). On the other hand, the maximum drained deviatoric stress reached only 77% of the estimated value based on the undrained tests (Figure 14). Clearly, rate effects are dependent on soil type. Procedures that have been suggested to determine appropriate loading rates for triaxial tests, such as the ones in Appendices A and B, may in fact be inappropriate for certain types of materials, such as the Kapolei Red silt and the Kapolei Brown clay.

Creep Tests

Long-term triaxial creep tests were conducted on all four soil types. Procedures for set-up, back-pressuring and consolidation were similar to those used for the strength tests. In each case specimens were back-pressured to 300 kPa and consolidated isotropically to 100 kPa. Once consolidation was completed, individual samples were subjected to a constant deviatoric stress under drained conditions by means of a loading frame, lead shot and dumbbell weights. Both axial and volumetric deformations were measured with electronic transducers at regular intervals. Drained conditions were chosen since they are thought to be representative of most field applications where the very long-term response is of interest. In order to maintain drained conditions throughout the deviatoric phase, axial loads were applied in a slow and systematic fashion to avoid generating significant excess pore pressures during loading. In general, small weights on the order of 100 grams were added every hour until the desired deviatoric stress was reached. Loading was applied around the clock with the help of three automatic fish feeders that released lead shot unto the loading frame at regular intervals. As indicated, volume changes were measured electronically with an automatic volume change device. Nevertheless, axial deformations are deemed more accurate. It is inherently more difficult to measure volume flow precisely over long periods of time due to the possibility of small leaks, osmotic flow across the membrane, small fluctuations in back pressure and cell pressure, and even fouling of the stagnant fluid in the drainage lines, the cell, and the specimen itself. In some cases, small corrections were applied to the volume change measurements by considering the moisture content of the sample at the end of the test.

A series of creep tests were conducted on each soil type. Specimens were loaded to various deviatoric stresses. The stress level for each test is defined as the percentage of the applied deviatoric stress relative to the maximum drained deviatoric stress that would be based on the short-term CIU strength envelope. Applied loads were adjusted periodically to account for changes in sample area as determined from accumulated axial and volumetric deformations.

Manoa Clay

Four Manoa clay specimens were tested at single stress levels of 30%, 50%, 70%, and 90% (Figure 15, Table 9). As expected, the higher the deviatoric stress, the higher the axial strain. The procedure in Appendix B yields a recommended drained loading rate of 0.085 kPa/hr for the Manoa clay. Significantly higher rates were used for the first three tests since the fish feeder technique had not yet been implemented successfully in these early tests. The 30% and 70% specimens were loaded at a rate of 0.575 kPa/hr, whereas the 50% test was loaded at a rate of 1.13 kPa/hour. On the other hand, the 90% test was indeed loaded at the recommended rate of 0.085 kPa/hr. It took 32.3 days to reach a stress level of 90%. It is apparent from Figure 15 that the much lower rate of loading in the 90% test does affect the initial axial strain behavior when compared to the other three tests, although at times well beyond the end of loading the accumulated axial strain in the 90% test is still the highest. The effect of loading rate is much more apparent in the volume change behavior. Volumetric strain in the 70% test is much higher than in the 90% test, which is attributed to the substantially higher loading rate in the 70% test. It is possible that in the 70% test significant pore pressures may have accumulated during loading, yielding primary consolidation in addition to creep. On the other hand, the comparatively lower difference in loading rates between the 30% and 50% tests does not appear to have as pronounced an effect on the accumulated volume changes at long times.

In all the creep tests conducted in this study axial strain rates are observed to decrease exponentially with time and therefore we consider power laws of the Singh-Mitchell (1968) type:

$$\dot{\varepsilon}_d = Ae^{\alpha D}\left(\frac{t_o}{t}\right)^m \tag{1}$$

where $\dot{\varepsilon}_d$ is the deviatoric strain rate, A, α, and m are material creep parameters, D is the stress level, and t_o is a convenient reference time. Since the interest herein is on creep deformations over long periods of time, it is useful to consider the parameter m, which is a measure of how fast creep rates decrease with time. This equation was originally developed from relatively short-term (1000 minutes) undrained creep tests. Singh and Mitchell (1968) note that this general relationship was also expected to apply for drained conditions and we can write a similar expression for the axial strain rate, $\dot{\varepsilon}_a$, during drained creep:

$$\dot{\varepsilon}_a = G\left(\frac{t_o}{t}\right)^m \tag{2}$$

where G is a stress-dependent parameter, and m is now the absolute value of the slope of the log of axial strain rate versus log of time:

$$\log\left(\frac{\dot{\varepsilon}}{\dot{\varepsilon}_o}\right) = -m\log\left(\frac{t}{t_o}\right) \tag{3}$$

in which $\dot{\varepsilon}_o$ is the axial strain rate at the reference time t_o. A similar expression to (2) can also be written for the volumetric strain. For triaxial conditions, where the specimen is assumed to remain approximately cylindrical, the axial, deviatoric, and volumetric strains are related by:

$$\varepsilon_d = \varepsilon_a - \frac{1}{3}\varepsilon_v \tag{4}$$

Singh and Mitchell (1968) propose that the parameter m is dependent only on the material type, although they do not explain how. This constant was determined for all tests in order to investigate how it may depend on soil type and stress level.

Calculated creep strain rates for the 50% and 70% Manoa clay tests are shown in Figure 16, along with the best fit lines for all four tests. The linear fits stretch from the end of deviatoric loading through the end of each test (see Table 9 for these times). In all the tests the log of axial strain rate decreases linearly with the log of time through the duration of the creep phase. With the exception of the 30% test, the computed linear best fits are approximately parallel to each other and clearly indicate that at any given time the axial strain rate increases with stress level, as expected from equation (1). It is not clear why the 30% test resulted in a comparatively lower m parameter.

Kapolei Red Silt

For the Kapolei Red silt a recommended loading rate of 3 kPa/hr is estimated using the procedure in Appendix B. Four tests were loaded at this rate and were held at deviatoric stresses corresponding to stress levels of 0%, 30%, 40% and 50%. As discussed in the previous section, an earlier creep test that was loaded at a rate of 12 kPa/hr failed prematurely at a stress level of 48%. For the remaining tests it was decided to lower the loading rate to the recommended 3 kPa/hr and to keep stress levels at 50% or less. The results in Figure 17 (Table 9) indicate an axial strain response qualitatively different from what was observed in the Manoa clay tests. There is a much sharper transition from the loading stage to the constant deviatoric stress stage. Comparison between the 0% test and the other three tests indicates that the majority of the axial strain in each test is due to axial deformation during loading. It should be noted that the deviatoric stress versus axial strain behavior during the loading phase of all three creep tests is similar to the one observed in the CID strength test (Figure 7). Once a constant stress was achieved, strains continued at much lower rates. Volume changes in the creep tests developed primarily during deviatoric loading as well. Use of the same rate of axial loading for the 30%, 40% and 50% tests resulted in volumetric strains that increase with stress level. The large volume change fluctuations in the 30% test are attributed to malfunction of the volume change device.

As was the case with the Manoa clay, the axial strain rate linear fits are relatively parallel to each other, also with the exception of the 30% test (Figure 18). Once again, it is not immediately apparent why this test shows such a different behavior. Perhaps because the

strain rate at the end of deviatoric loading was about an order of magnitude larger than for any other test, the material compensated henceforth with a much faster rate of strain rate decrease.

Hilo Ash Soil

The loading rate for the Hilo Ash soil was estimated to be 3.5 kPa/hr. One creep specimen was loaded to 70% stress level and another one to 90% using this rate, except for occasional six hour breaks followed by accelerated catch-up loading periods (Figure 19, Table 9). If the axial strain was observed to accelerate substantially, the rate of loading was decreased temporarily in order to avoid premature failure. Nonetheless, axial strains were higher than for any other soil types at equivalent stress levels. When comparing the loading phase of the creep tests to that of the CID strength test, it is apparent that the selected loading scheme for the creep tests resulted in a somewhat lower stiffness, hence presumably with drainage conditions at least as efficient as in the CID test (Figure 20).

Both tests lasted close to one year. Most of the axial strain again developed during the deviatoric loading phase, with a relatively sharp transition to much lower strain rates during the constant stress stage. The 70% stress level test failed unexpectedly after 331 days. This is the only test that underwent failure well into the creep phase. However, the reason for the failure is unknown. There is no tertiary creep phase prior to rupture. The only aspect about this test that is noteworthy is the acceleration in volumetric strain during the period preceding failure.

There is not a large difference in terms of axial strain rates at equivalent times between the two tests (Figure 20). The calculated values near the end of the 70% test do not show any indication that the specimen was about to fail. There is no transition to larger strain rates, i.e. tertiary creep, prior to failure.

Kapolei Brown Clay

One creep test was completed for the Kapolei Brown clay (Figure 22, Table 9). Loading was applied at a rate of 0.30 kPa/hr, as estimated with the procedure in Appendix B, to a stress level of 70%. This took 13 days. The transition in axial strain rate from the loading phase to the constant stress phase is relatively gradual, more like what is observed for the Manoa clay tests. Axial strain stiffness during the loading phase is comparable to that of the CID strength test, even though loading had to be slowed down at times when substantial jumps in axial strain were observed. This test was terminated after 278 days. It is interesting to note that volumetric strain accelerates after about 150 days, similar to what occurred in the 70% Hilo Ash soil test that failed during creep. It is possible that the Kapolei Brown clay test was headed toward failure in a similar fashion. However, there is no sign of axial strain rates entering a tertiary creep phase toward the end of the test that might point to an impending failure (Figure 23).

Comparisons Among All Soil Types

As pointed out earlier, the 30% Manoa clay and the 30% Kapolei Red silt creep tests yielded *m*-parameter linear fits at odds with the rest of the data set for each respective soil type (Figures 16 and 18). Hence, we focus our cross-soil comparisons of axial strains and axial strain rates on the tests conducted at 50%, 70% and 90% stress level. As pointed out earlier, the Kapolei Red silt creep tests show a much sharper transition in axial strain rate from the loading phase to the constant stress phase than the Manoa clay tests, regardless of the creep stress intensity. This point is illustrated in Figure 24a for the two 50% stress level tests. Part of the reason may be that the coefficient of consolidation of the Kapolei Red silt is about an order of magnitude larger than the one for Manoa clay (Table 1), although the rate of loading used in the Kapolei Red silt test was about three times as large as in the Manoa clay test. In order to focus on constant-stress creep behavior over the long term, independent of the loading phase, it is more useful to look at strain rates as a function of the logarithm of time (Figure 24b). The Manoa clay test shows comparatively higher strain rates early on in the test, but values decrease at a higher rate than for the Kapolei Red silt. Both tests approach similar strain rates at about 200,000 minutes. It is surprising that strain rates in the low plasticity Kapolei Red silt do not decrease as fast as in the higher plasticity Manoa clay. This is manifested by significantly lower *m* parameters for the Kapolei Red silt. When the anomalous 30% tests are excluded, the average *m* parameter for the three remaining Manoa clay tests is 1.46, whereas for the three remaining Kapolei Red silt tests it is 0.98 (Table 10).

The three 70% stress level tests allow for a comparison among the Manoa clay, the Hilo Ash soil and the Kapolei Brown clay (Figures 25a and 25b). The Manoa clay and Kapolei Brown clay tests show similar amounts of axial strain, whereas in the Hilo Ash soil test strains are approximately twice as high. In terms of axial strain rates, all three tests show similar values at equivalent times. The *m* parameters are also within reasonable agreement, although the value calculated for the Kapolei Brown clay test is somewhat lower than for the other two tests. At 90% stress level the Hilo Ash soil test reveals a rather large axial strain in excess of 20%, much higher than the 90% Manoa clay test (Figures 26a and 26b). Most of this developed during deviatoric loading and may indicate that the specimen came perilously close to failure during this stage. Nonetheless, strain rates beyond the end of loading are lower than for the Manoa clay. The m parameter for both tests is similar and probably within the margin of experimental error.

The average *m* parameters for the Manoa clay, the Kapolei Red silt, the Hilo Ash soil and the Kapolei Brown clay tests are 1.46, 0.98, 1.04, and 1.14, respectively (Table 10). The significantly larger value for the Manoa clay indicates that creep deformations attenuate much faster than in the other three soils, despite the rather high Atterberg limits for the Manoa clay. The Hilo Ash soil, which has by far the highest Atterberg limits and moisture content, is similar in terms of *m* parameter to the Kapolei red silt and the Kapolei Brown clay. It appears that extreme plasticity characteristics in this case do not translate into unusual creep behavior, much the same way that they do not translate into unusual friction angles or compressibility. One would tend to conclude that the Atterberg

limits for this particular soil type constitute a poor index set for correlation with engineering behavior in the usual sense. It is difficult to see any clear correlation between plasticity properties and creep deformations. One cannot simply state that the higher the plasticity, the higher the amount of creep that will accumulate. On the other hand, higher Atterberg limits appear to result in somewhat larger rates of creep strain rate decrease, i.e. higher m parameters, with the exception of the extreme Hilo Ash soil (Figure 27). The results in Figure 27 appear to agree with a set of eighteen drained creep tests conducted on undisturbed and reconstituted deep sea illites (Silva and Brandes, 1996). A linear trend line is suggested, although the true nature of the relationship between plasticity index and m parameter is not yet clear. Additional tests on soils with different Atterberg limits are necessary.

Post-Creep Strength Tests

Following a period of deformation under constant stress conditions, soils can gain or loose stiffness and strength upon reloading. In some cases soils may even fail during the creep phase at deviatoric loads below what would be expected from short-term strength tests. This was the case for the 70% Hilo Ash soil, which failed after 331 days of creep. In most instances though, studies have indicated that a gain in stiffness and strength can be expected and is attributed to consolidation, aging, fatigue and stress state history (Bjerum and Lo, 1963; Mitchell, 1976; Esu and Grisola, 1977). All the Manoa clay creep tests, as well as the 70% Kapolei Brown soil creep test, were subjected to undrained, stress-controlled deviatoric loading to failure at the end of their respective creep phases. These tests were conducted by closing the drainage valve and adding weights to the axial loading frame at regular intervals. Excess pore pressures and axial strains were recorded during each test.

Additional deviatoric stresses, beyond those applied during the creep phase, are shown for the Manoa clay post-creep strength tests in Figure 28 and for the Kapolei Brown clay in Figure 29. Using the procedure in Appendix A, a loading rate of 0.48 kPa/hr was selected for the Manoa clay and Kapolei Brown clay tests. A single rate was selected for all the tests to focus on strength and stress-strain changes due to long-term creep and not due to loading rate effects. The results of the post-strength creep tests are summarized in Table 11.

Figure 28 reveals that higher creep stress levels resulted in lower added deviatoric stresses necessary to reach failure. This is simply because the higher stress level creep tests were already closer to failure prior to the strength tests. In the case of the 90% test, the maximum deviatoric stress is somewhat higher than for the 70% test, presumably due to the much higher duration of the creep phase, which yielded additional strength gain from the aging process. When the results from the creep and post-creep phases are combined, it becomes clear that the higher the creep stress level, the higher the cumulative deviatoric stress at failure (Figures 30 and 31). Two additional effects that are observed are higher stiffnesses upon reloading and lower axial strains at failure (Table 11). This is readily apparent when comparing the post-creep strength tests with the short-term stress-controlled CIU test conducted at similar initial stresses (Figure 28).

In general, axial strain at failure decreases with increasing creep duration (Table 11). An increase in stiffness and a reduction in axial strain at failure agree with what Bjerrum and Lo (1963) report for undisturbed Skabo clay from the Oslo vicinity. However, they note only modest gains in maximum deviatoric stress, on the order of 6%, for specimens consolidated isotropically for lengths of up to four months. Strength gains herein were larger, amounting to an average deviatoric stress increase on the order of 18 kPa, as discussed below. The reason for this is probably a combination of the use of longer aging periods, more effective methods for removal of geologic in situ aging effects through thorough reconstitution and reconsolidation, and the fact that the soils were quite different and were subjected to different sets of stresses prior to shearing to failure.

The effect of aging is made clear in Figure 32 for the Manoa clay specimens that were consolidated isotropically for different periods of time. Two short term strength tests, one strain-controlled and one stress-controlled, are combined with the 0% post-creep strength test. All specimens had essentially identical initial water contents and yielded similar axial and volumetric strains upon 3.5 days of consolidation at 100 kPa. Shearing was conducted under undrained conditions. In the 0% creep test the consolidation stress was maintained for a total period of 33 days prior to shearing. During the final 29.5 days of consolidation, this specimen underwent an additional volumetric strain of only 0.9%, hardly enough to affect strength due to primary volume compression. The short-term tests reveal a similar maximum deviatoric stress, although the stress-controlled one shows a somewhat higher initial stiffness. On the other hand, the 0% creep test reaches a much higher maximum deviatoric stress, along with a correspondingly higher stiffness (Figure 32). Given the small amount of additional volume compression that occurred in this test past the initial 3.5 days of consolidation, the higher deviatoric stress and stiffness in the 0% test are clearly attributed to aging effects. It is likely that ageing is also responsible for strength and stiffness gain in the other post-creep tests, although it is not clear how the anisotropic aging conditions affect this.

Whereas Bjerrum and Lo (1963) report excess pore pressure versus axial strain behavior that is more or less independent of the age of the specimens, in this study excess pore pressures were not uniform. In general, they decrease with increasing stress level, with the exception of the 90% test. But pore pressure curves only tell part of the story. More useful in many respects is to consider the resulting stress paths (Figures 33 and 34). A short-term CIU strength test with a consolidation stress of 100 kPa under stress-controlled loading is included in Figure 33 for comparison. Also shown is the failure envelope calculated from the set of short-term strain-controlled CIU tests discussed earlier (Figure 4). The 30% and 50% tests reveal almost vertical stress paths, which one associates with elastic, overconsolidated behavior. Stress paths in the 50%, 70% and 90% tests, as well as in the 70% Brown Kapolei clay test, bend slightly to the right, which suggests that at higher creep stress level intensities the volume change tendency upon reloading shifts from none to slightly expansive. The end conditions of all the tests, except for the 90% stress level one, fall close to a failure envelope that is nearly parallel to the short-term one, but that is shifted upward by about 8.9 kPa (Figure 33). Thus with increasing creep time the undrained strength appears to increase due to the development of cohesive bonds rather than due to an increase in friction. As Bjerrum and Lo (1963)

point out, the mobilization of additional frictional resistance would require strain, which has already been noted to decrease substantially with aging time.

Small or no volume change tendency during the post-creep strength tests is also an indication that the strength gain observed is due to time-dependent hardening of the material as a result of aging during the creep phase. Hardening of this type is often described in terms of a quasi-preconsolidation pressure that develops during sustained loading (Leonards and Remiah, 1959; Bjerrum, 1972). The 90% test resulted in a failure point above the two envelopes in Figure 33, which is attributed to the substantially longer creep duration for this test, nearly 500 days, as opposed to durations on the order of 100 days or less for the other Manoa clay tests (Table 11). Thus additional strength would have been gained due to the formation of additional interparticle bonds.

Conclusions

Four tropical volcanic soils with contrasting index properties from the islands of Oahu and Hawaii were reconstituted, reconsolidated and tested for strength and creep properties under triaxial conditions. The objective was to investigate long-term deformations, loading rate effects and aging phenomena. The results can be summarized as follows:

- In terms of friction angles, two of the soils yielded values significantly different from what would be expected based on their Atterberg limits. The Manoa clay soil plots well below Kenney's (1959) classic relationship for normally consolidated soils, the Hilo Ash soil plots well above, and the two lateritic soils fall near the trend line. The unusual values for the first two soils are probably due to complex clay soil formation processes that may still be incomplete, but that are poorly understood.

- The loading rate techniques recommended by ASTM D4767-95 for undrained tests and Bishop and Henkel (1962) for drained tests do not lead to strength values that are always consistent with reference to a single Mohr Coulomb failure envelope. Drained tests in two of the three soils, the Kapolei Red silt and the Kapolei Brown clay, resulted in drained strengths that ranged between 48% and 85% of the value predicted from the undrained tests. Consideration of the loading rates and loading modes (stress and strain-controlled) used in this study, suggests that perhaps the rates recommended by Bishop and Henkel (1962) are too high and result in excess pore pressures, and hence partially drained conditions. On the other hand, for the Hilo Ash soil drained and undrained strengths did match very well.

- Stress-controlled loading rates of 2 kPa/hr, 4 kPa/hr, and 12.5 kPa/hr for the Kapolei Red silt produced similar initial stiffnesses in terms of deviatoric stress versus axial strain, but maximum stress values that varied by as much as 35%. No clear trend was observed from this limited set of tests that would suggest an

appropriate loading rate necessary to maintain truly drained conditions for this type of soil.

- As expected, in the creep tests axial strains and volumetric strains increase with increasing sustained deviatoric stress levels. Axial strain rates decrease exponentially with time and can reasonably be described by a linear relationship of the Singh-Mitchell (1968) type between the logarithm of axial strain rate and the logarithm of time. The slope of such a fit, the m-parameter, in general appears to be a constant that is independent of stress level. However, the intercept does vary with stress level, such that higher strain rates are predicted for higher stress levels at given times.

- With the exception of the Hilo Ash soil, the m-parameter appears to vary linearly with soil plasticity. An increase in plasticity index leads to an increase in m parameter, i.e. in a higher attenuation in axial strain rate with time.

- The high Atterberg limits for the Hilo Ash soil do not translate into unusually low friction angles, high compressibility (Nakayama, 2000), or unexpected creep behavior. In fact, other than for identification purposes, Atterberg limits for this type of soil should not be used for correlation with engineering behavior using conventional empirical relationships without further study. Also, given the dramatic changes in Atterberg limit values and gradation upon drying and wetting, classification of these soils using the Unified Soil Classification System is questionable. In general, it is advisable that these soils not be allowed to dry unduly in the laboratory and that fluctuation in field moisture be considered prominently when evaluating their long-term performance.

- Post-creep, stress-controlled tests conducted under undrained conditions showed that the stiffness of soil increases upon reloading with failure reached at low axial strains. Maximum deviatoric stresses were significantly higher than those predicted from non-aged strength tests. The increase is attributed largely to the formation of additional bonds during long-term creep, at least when creep occurs under isotropic confining stresses. The effect is such that the Mohr-Coulomb failure envelope is shifted upward but with no change in friction angle. When aging is allowed to continue for longer periods of time, as in the 90% Manoa clay creep test, the maximum deviatoric stress is seen to increase proportionally. Additional creep tests conducted under anisotopic stress conditions are necessary to clarify the role that such anisotropy has on strength changes.

Acknowledgements

This study was conducted in part by a grant from the Hawaii Department of Transportation and the Federal Highway Administration. Their support is gratefully acknowledged. In particular, the advice from Clarence Miyashiro, Richard K.So, and U Kuong Ung is appreciated. Kerwin Chang contributed to the preparation of this manuscript.

References

Adachi, T., Oka, F. and Mimura, M., 1996. Modeling aspects associated with time dependent behavior of soils. In: Measuring and Modeling Time Dependent Soil Behavior, T. C. Sheahan and V. N. Kaliakin (Eds.), *ASCE Geotechnical Special Publication No. 61*, 61-95.

Adachi, T. and Ocha, F., 1982. Constitutive equations for normally consolidated clay based on elasto-viscoplasticity. *Soils and Foundations*, **22**(4):57-70.

Baum, R. L. and Reid, M. E., 1992. Geology, hydrology and mechanics of the Alani-Paty landslides, Manoa Valley, Oahu, Hawaii. *U. S. Geological Survey Open-File* Report 92-501.

Baum, R. L., Reid, M. E., Wilburn, C. A. and Torikai, J. D., 1991. Summary of geotechnical and hydrologic data collected from May 1, 1990 through April 30, 1991, for the Alani-Paty landslide, Manoa Valley, Honolulu, Hawaii. *U. S. Geological Survey Open-File Report* 91-598.

Bishop, A. W. and Lovenbury, H. T., 1969. Creep characteristics of two undisturbed clays. *Proceedings of the 7th International Conference on Soil Mechanics and Foundation Engineering*, Mexico, **1**:29-37.

Bishop, A. W. and Henkel, D. J., 1962. The measurement of soil properties in the triaxial test. London: Edward Arnold Ltd.

Bjerrum, L. and Lo, K. Y., 1963. Effect of aging on the shear-strength properties of a normally consolidated clay. *Geotechnique*, 2:147-157.

Bjerrum, 1972. Embankments on soft ground. *Proceedings of the ASCE Specialty Conference on Performance of Earth and Earth-Supported Structures*, **II**:1-54.

Borja, R. I. And Kavazanjian, E., 1984. Finite element analysis of time-dependent behavior of soft clays. *Geotechnical Engineering Research Report* No. GT1, Department of Civil Engineering, Stanford University.

Brandes, H. G. and Tsui, C. S. L., 2001. Modeling the effectiveness of groundwater-lowering remediation measures in the Alani-Paty landslide area, Oahu, Hawaii. *Proceedings of the 10th International Conference on Computer Methods and Advances in Geomechanics*, **2**:1543-1547.

De Silva, G. L. R., 1974. Slope stability problems induced by human modification of soil covered hill slopes of Oahu, Hawaii. *Ph.D. Dissertation*, Department of Geography, University of Hawaii.

Ellen, S. D., Liu, L. A. S. M., Fleming, R. W., Reid, M. E., and Johnson, M. J., 1995. Relation of slow-moving landslides to earth materials and other factors in valleys of the Honolulu District of Oahu, Hawaii. *U. S. Geological Survey Open-File Report* 95-218.

Esu, F. and Grisolia, M., 1977. Creep characteristics of an overconsolidated jointed clay. *Proceedings of the 9th International Conference on Soil Mechanics and Foundation Engineering*, Tokyo, **1**:93-100.

Gibson, R. E. and Henkel, D. J., 1954. Influence of duration of test at constant rate of strain on measured 'drained strength.' *Geotechnique*, **IV**:6-15.

Imai, G., 1995. Analytical examinations of the foundations to formulate consolidation phenomena with inherent time-dependency. *International Symposium on Compression and Consolidation of Clayey Soils – IS-Hiroshima's 95*, 2:891-935.

Kaliakin, V. N. and Dafalias, Y. F., 1990. Theoretical aspects of the elastoplastic-viscoplastic bounding surface model for cohesive soils. *Soils and Foundations*, 30(3):11-24.

Kenney, T. C., 1959. Discussion. *Journal of the Soil Mechanics and Foundations Division, ASCE*, **85**(SM3):67-79.

Leonards and Remiah, 1959. Time effects in the consolidation of clay. *Papers on soils – 1959 Meeting, American Society for Testing and Materials*, Special Technical Publication No. 254, 116-130.

Leroueil, S. and Marques, M. E. S., 1996. Importance of strain rate and temperature effects in geotechnical engineering. In: Measuring and Modeling Time Dependent Soil Behavior, T. C. Sheahan and V. N. Kaliakin (Eds.), *ASCE Geotechnical Special Publication No. 61*, 1-60.

Lum, W. B., 1982. Engineering problems in tropical and residual soils in Hawaii. *Proceedings, Engineering and Construction in Tropical and Residual Soils*, 1-12.

Mitchell, J. K., 1976. Fundamentals of soil behavior. New York: John Wiley & Sons, Inc.

Mitchell, J. K. and Sitar, N., 1982. Enineering properties of tropical residual soils. *Proceedings, Engineering and Construction in Tropical and Residual Soils*, 30-57.

Morin, W. J., 1982. Characteristics of tropical red residual soils. *Proceedings, Engineering and Construction in Tropical and Residual Soils*, 147-171.

Murayama, S. and Shibata, T., 1961. Rheological properties of clays. *Proceedings of the 5th International Conference on Soil Mechanics and Foundation Engineering*, Paris, 269-272.

Nielson, N. N., Furumoto, A. S., Lum, W. and Morrill, B. J., 1977. The Honomu, Hawaii earthquake; report of inspection. *Report to National Academy of Science.*

Oka, F., Adachi, T. and Mimura, M., 1988. Elasto-viscoplastic constitutive models for clays. *Proceedings of the International Conference on Rheology and Soil Mechanics*, 12-28.

Peck, R. B., 1958. Report on causes and remedial measures, Waiomao Slides, Honolulu. *Report prepared for the City and County of Honolulu.*

Peck, R. B. and Wilson, S. D., 1968. Report on the Hind Iuka landslide and similar movements, Honolulu, Hawaii. *Report prepared for the City and County of Honolulu.*

Sekiguchi, H., 1984. Theory of undrained creep rupture of normally consolidated clay based on elasto-viscoplasticity. *Soils and Foundations*, 24(1):129-147.

Silva, A. J. and Brandes, H. G., 1996. Drained creep behavior of marine clays. In: Measuring and Modeling Time Dependent Soil Behavior, T. C. Sheahan and V. N. Kaliakin (Eds.), *ASCE Geotechnical Special Publication No. 61*, 228-242.

Singh, A. W. and Mitchell, J. K., 1968. General stress-strain-time function for soils. *Journal of the Soil Mechanics and Foundations Division, ASCE*, **94**(1):21-46.

Stearns, H. T., 1966. Geology of the State of Hawaii. Palo Alto: Pacific Books Publisher.

Tavenas, F. and Leroueil, S., 1987. State-of-the-art on 'laboratory and in situ stress-strain-time behavior of soft clays. *International Symposium on Geotechnical Engineering of Soft Soils*, **2**:1-46.

Tavenas, F., Leroueil, S., La Rochelle, P. and Roy, M., 1978. Creep behavior of an undisturbed lightly overconsolidated clay. *Canadian Geotechnical Journal*, **15**(3):402-423.

Tsui, C. S. L., Brandes, H. G. and Nakayama, D. D., 2001. Creep behavior and modeling of the slow-moving Alani-Paty landslide, Oahu, Hawaii. *Proceedings of the 10th International Conference on Computer Methods and Advances in Geomechanics*, **2**:1629-1633.

Uehara, G., 1982. Soil science for the tropics. *Proceedings, Engineering and Construction in Tropical and Residual Soils*, 13-26.

Vaid, Y. P. and Campanella, R. G., 1977. Time-dependent behavior of undisturbed clay. *Journal of the Geotechnical Engineering Division, ASCE*, **103**(7):693-709.

Wan, Y., Brandes, H., Kwong, J. and Nicholson, P., 1999. Amorphous clay and its influence on plastic and shear behavior of a colluvial soil in Hawaii. *Research Report* UHM/CE/99-06, Department of Civil Engineering, University of Hawaii.

Wieczorek, G. F., Jibson, R. W., Wilson, R. C. and Buchanan-Banks, J. M., 1982. Geotechnical properties of ash deposits near Hilo, Hawaii. *U. S. Geological Survey Open-File Report* 82-279.

Appendix A – Loading Rates for Undrained Conditions

According toASTM D4767-95, the recommended axial loading rate for undrained testing should be based on t_{50}, i.e. the time required for 50% primary consolidation. The value of t_{50} is determined in accordance with the procedures outlined in test method ASTM D2435, in this case by using the Casagrande technique on the deformation data from the consolidation phases of the triaxial tests. Using an average t_{50} for each soil type, and assuming an axial strain at failure of 4%, the strain-controlled loading rate can be calculated as:

$$\text{loading rate [strain/time]} = \frac{4\%}{10\ t_{50}} \tag{A1}$$

For stress-controlled tests, the loading rate can similarly be determined as:

$$\text{loading rate [stress/time]} = \frac{\sigma_{d-\max}}{10\ t_{50}} \tag{A2}$$

where $\sigma_{d-\max}$ is the estimated maximum deviatoric stress, determined from the strain-controlled tests.

Average values of t_{50}, along with the estimated undrained rates for the four soil types, are presented in Table 3.

Appendix B – Loading Rates for Drained Conditions

An appropriate rate of deformation in drained tests is one that minimizes excess pore pressures throughout the shearing phase. Gibson and Henkel (1954) have estimated, based on the theory of consolidation, that the average degree of pore pressure dissipation at failure, U_f, can be expressed as:

$$U_f = 1 - \frac{h^2}{\eta c_v t_f} \tag{B1}$$

where h is half the sample height, c_v the coefficient of consolidation, t_f the time to failure, and η a factor that accounts for the type of drainage conditions. For radial and end drainage, η is equal to 40.4. A 95% degree of pore pressure dissipation is acceptable according to Bishop and Henkel (1962). In this case the time to failure becomes:

$$t_f = \frac{h^2}{0.05\eta c_v} \tag{B2}$$

The coefficient of consolidation, , is calculated using the following expression for the case of radial and end drainage (Bishop and Henkel, 1962):

$$c_v = \frac{\pi h^2}{4t_{100}}\left(\frac{1}{(1+2h/R)^2}\right) \tag{B3}$$

where R is the radius of the specimen and t_{100} is the time required for 100% primary consolidation according to Casagrande technique. Average values for t_{100} for each soil type were determined from the consolidation phases of the triaxial tests.

Assuming an axial strain at failure of 4%, strain-controlled loading rates can be calculated as:

$$\text{loading rate [strain/time]} = \frac{4\%}{t_f} \tag{B4}$$

Similarly, stress-controlled loading rates are given by:

$$\text{loading rate [stress/time]} = \frac{\sigma_{d-\max}}{t_f} \tag{B5}$$

where $\sigma_{d-\max}$ is determined from the strain-controlled undrained strength tests.

Average values of t_{100}, along with the estimated drained rates for the four soil types are presented in Table 4.

Table 1. Summary of soil properties.

	G_s	Fines (%)	LL (%)	PI (%)	USCS	C_c ($x10^{-3}$ mm^2/s)	C_v ($x10^{-3}mm^2/s$)
Manoa clay	2.88	95	87	54	CH	0.72	1.1
Kapolei Red silt	2.79	98	41	16	ML	0.22	16.9
Hilo Ash soil							
not-dried	2.51	81	210	94	MH	0.75	99.1
oven-dried	2.51	18	non-plastic		SM	-	-
Kapolei Brown clay	2.94	96	62	37	CH	0.49	2.6

Table 2. Consolidation durations and moisture contents.

	Initial moisture content (%)	Final moisture content (%)	Consolidation duration (days)
Manoa clay	87	79	28
Kapolei red silt	41	37	14
Hilo ash soil	210	169	28
Kapolei brown clay	69	55	41

Table 3. Axial strain-controlled loading rates under undrained conditions.

	Average t_{50} (min)	Calculated loading rate (%/min)
Manoa clay	540	0.00074
Kapolei Red silt	36	0.011
Hilo Ash soil	40	0.01
Kapolei Brown clay	150	0.00267

Table 4. Deviatoric stress-controlled loading rates under drained conditions.

	Average t_{100} (hours)	Time to failure (hours)	Maximum deviatoric stress (kPa)	Calculated loading rate (kPa/hour)
Manoa clay	36	841	71.35	0.085
Kapolei Red silt	3	70	284.62	4.07
Hilo Ash soil	4	93	350.49	3.77
Kapolei Brown clay	18	421	136.90	0.325

Table 5. Manoa Clay, strength test results.

Sample	w_o (%)	w_f (%)	σ'_3 (kPa)	$\varepsilon_{a\text{-failure}}$ (%)	σ_d (kPa)	q_f (kPa)	p'_f (kPa)	u_f (kPa)	A_f (kPa)	strain rate / stress rate
MC 30	75	61	30	4.5	19	10	26	14	0.73	0.05%/min
MC 50	75	63	50	2.7	29	15	49	15	0.52	0.05%/min
MC 100a	74	53	100	6.5	50	25	94	32	0.63	0.05%/min
MC 100b	80	58	100	4.5	51	25	90	35	0.70	0.05%/min
MC 100c	70	56	100	5.0	52	26	85	41	0.79	0.48 kPa/min

Table 6. Kapolei Red silt, strength test results.

Sample	w_o (%)	w_f (%)	σ'_3 (kPa)	$\varepsilon_{a\text{-failure}}$ (%)	σ_d (kPa)	q_f (kPa)	p'_f (kPa)	u_f (kPa)	A_f (kPa)	strain rate / stress rate
KR 50	36	32	50	14.8	47	23	41	32	0.69	0.01 %/min
KR 100	36	30	100	14.7	78	39	66	73	0.93	0.01 %/min
KR 200	36	28	200	14.9	144	72	122	150	1.04	0.01 %/min
KR 50	36	29	100	4.3	138	69	169	N/A	N/A	12.5 kPa/hr
KR 100a	36	28	100	7.0	186	93	193	N/A	N/A	4.0 kPa/hr
KR 100b	36	28	100	4.7	156	78	178	N/A	N/A	2.0 kPa/hr
KR 100c	36	28	100	14.9	241	120	220	N/A	N/A	0.003 %/min

Table 7. Hilo Ash soil, strength test results.

Sample	w_o (%)	w_f (%)	σ'_3 (kPa)	$\varepsilon_{a\text{-failure}}$ (%)	σ_d (kPa)	q_f (kPa)	p'_f (kPa)	u_f (kPa)	A_f (kPa)	strain rate / stress rate
HA 50	180	163	50	14.87	73	37	55	31	0.43	0.01 %/min
HA 100	179	158	100	14.9	117	59	97	62	0.53	0.01 %/min
HA 200	176	143	200	12.3	221	111	174	137	0.62	0.01 %/min
HA 100	175	137	100	14.7	357	179	279	N/A	N/A	3.50 kPa/hr

Table 8. Kapolei Brown clay, strength test results.

Sample	w_o (%)	w_f (%)	σ'_3 (kPa)	$\varepsilon_{a\text{-failure}}$ (%)	σ_d (kPa)	q_f (kPa)	p'_f (kPa)	u_f (kPa)	A_f (kPa)	strain rate / stress rate
KB 50	55	46	50	3.9	30	15	33	32	0.95	0.0025 %/min
KB 100	52	39	100	3.1	58	29	71	58	1.00	0.0025 %/min
KB 200	54	37	200	4.3	108	54	132	123	0.88	0.0025 %/min
KB 100	55		100	7.9	105	68	168	-	-	0.25 kPa/hour

Table 9. Creep test results.

		$\sigma_{d\text{-}max}$ (kPa)	$\sigma_{d\text{-}applied}$ (kPa)	Stress level (%)	w_o (%)	w_f (%)	Load rate (kPa/hr)	Loading Phase (days)	End of loading ε_a (%)	End of loading ε_v (%)	End of creep test ε_a (%)	End of creep test ε_v (%)	Test duration (days)
Manoa clay	MC 0%	71	0	0	81	59	0	0	-	-	0.65	1.09	29
	MC 30%	71	21	30	83	58	0.58	1.54	0.68	0.43	2.17	3.45	79
	MC 50%	71	36	50	75	53	1.13	1.33	1.63	1.38	3.90	6.55	128
	MC 70%	71	50	70	84	57	0.57	5.29	4.30	2.07	6.10	10.90	102
	MC 90%	71	64	90	75	39	0.09	31.50	5.17	5.80	8.93	9.51	482
Kapolei Red silt	KR 0%	285	0	0	36	31	-	-	-	-	0.10	0.65	36
	KR 30%	285	85	30	39	31	3.00	1.17	2.61	1.76	4.81	4.43	105
	KR 40%	285	114	40	39	30	3.00	1.58	3.79	2.63	5.71	4.51	105
	KR 50%	285	142	50	39	28	3.00	1.96	4.63	3.26	5.86	4.91	152
Hilo Ash soil	HA 70%	350	315	70	169	147	3.50	3.00	10.16	6.27	13.35	35.48	331
	HA 90%	350	245	90	169	N/A	3.50	4.71	18.47	8.87	23.01	19.79	365
Kapolei Brown clay	KB 70%	137	96	70	55	55	0.30	13.29	5.11	2.76	6.97	7.48	278

Table 10. Summary of *m*-parameters.

Material Type	LL	PL	*m*	*m*-average
Manoa clay	87	33		1.46
0			1.6	
30			1.14	
50			1.55	
70			1.46	
90			1.54	
Kapolei Red silt	41	25		0.98
0			0.88	
30			1.76*	
40			1.10	
50			0.95	
Hilo Ash soil	210	116		1.04
70			1.08	
90			1.00	
Kapolei Brown clay	62	25		1.14
70			1.14	

* excluded from average

Table 11. Post-creep test results.

	$\varepsilon_{v\text{-}consol}$ (%)	$\varepsilon_{v\text{-}creep}$ (%)	$\varepsilon_{a\text{-}creep}$ (%)	Creep Duration (days)	Loading Rate (kPa/hr)	$\sigma_{d\text{-}fail}$ (kPa)	$\Delta\sigma_{d\text{-}fail}$ (kPa)	$\Delta\varepsilon_{a\text{-}f}$ (%)	Δu_f (kPa)	A_f
MC 0%	15.3	1.1	0.7	29	0.48	73	73	5.5	38	0.52
MC 30%	15.6	3.5	2.2	79	0.48	76	53	1.7	29	0.55
MC 50%	14.2	6.6	3.9	128	0.48	86	49	0.6	15	0.31
MC 70%	15.6	10.9	6.1	102	0.48	91	40	0.7	11	0.28
MC 90%	13.7	9.5	8.9	482	0.48	107	43	0.5	16	0.37
KB 70%	14.4	7.5	7.0	278	0.48	168	72	0.4	19	0.26

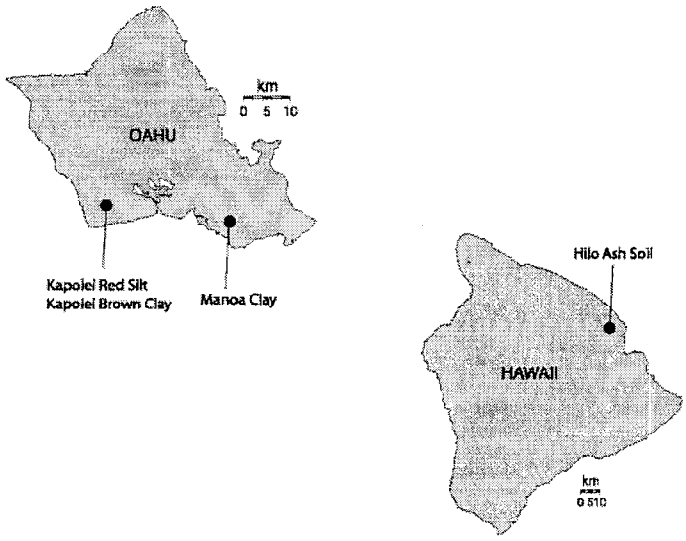

Figure 1. Soil sampling locations (Kapolei: Farrington Highway in Kapolei area; Manoa: Hulu-Woolsey landslide area; Hilo: South Hilo District).

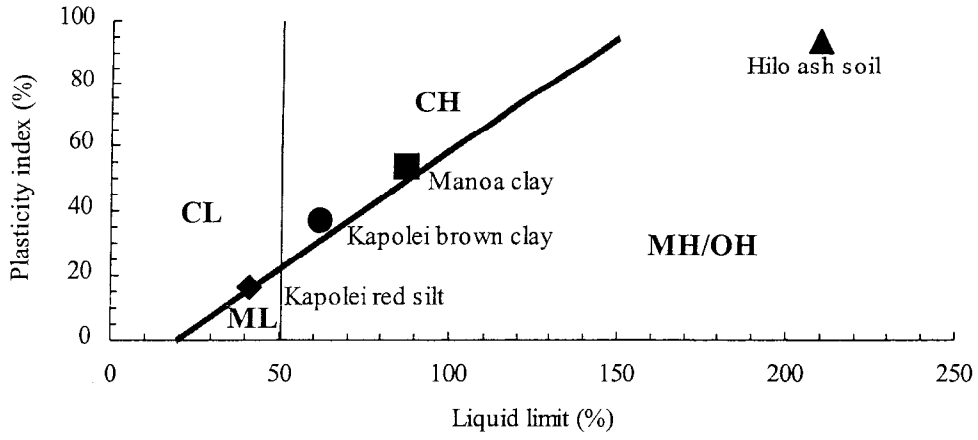

Figure 2. Plasticity characteristics of soils.

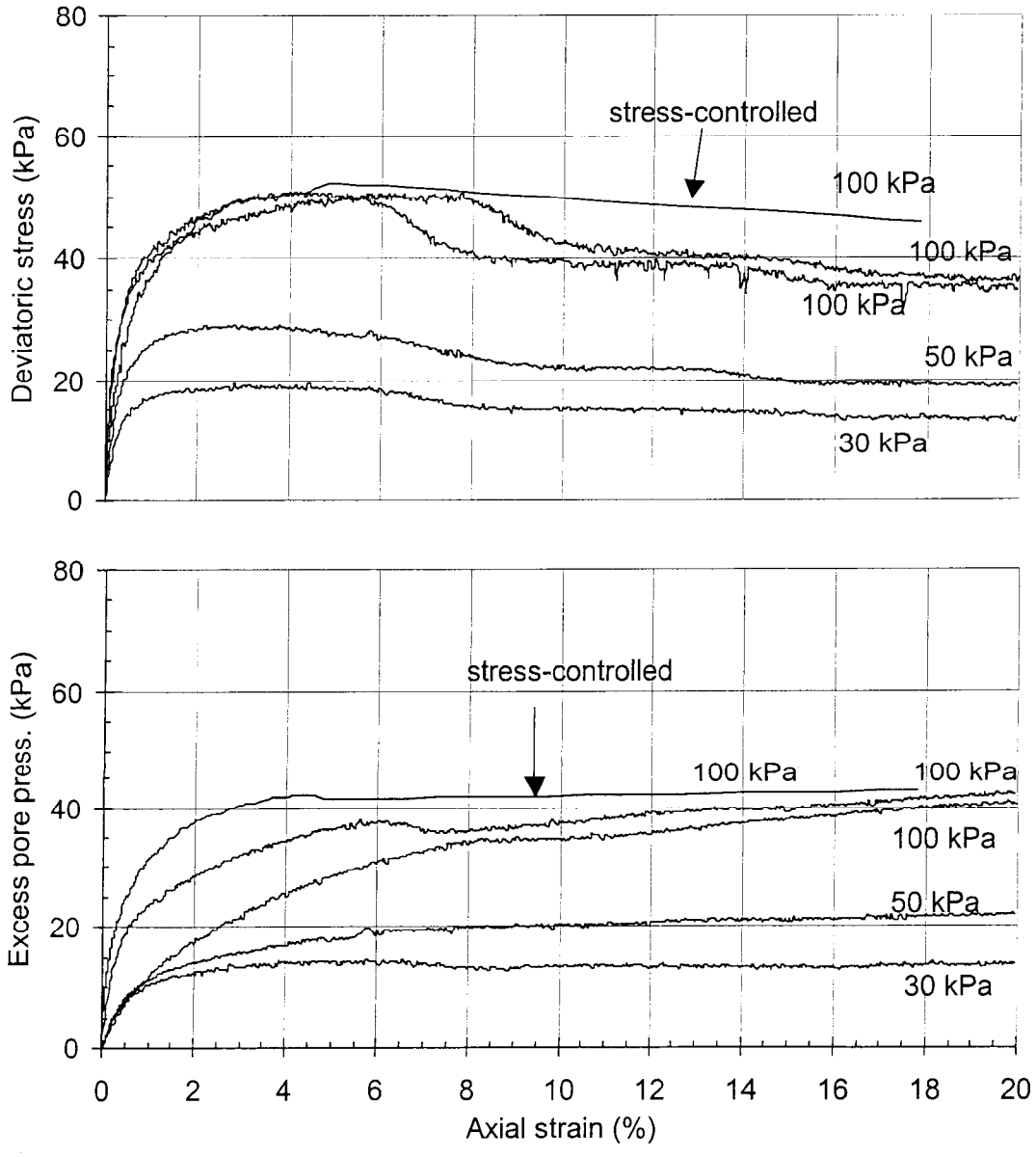

Figure 3. Manoa clay, CIU strength tests: stress-strain behavior. All tests are strain-controlled, expect as noted. Isotropic consolidation stresses are indicated.

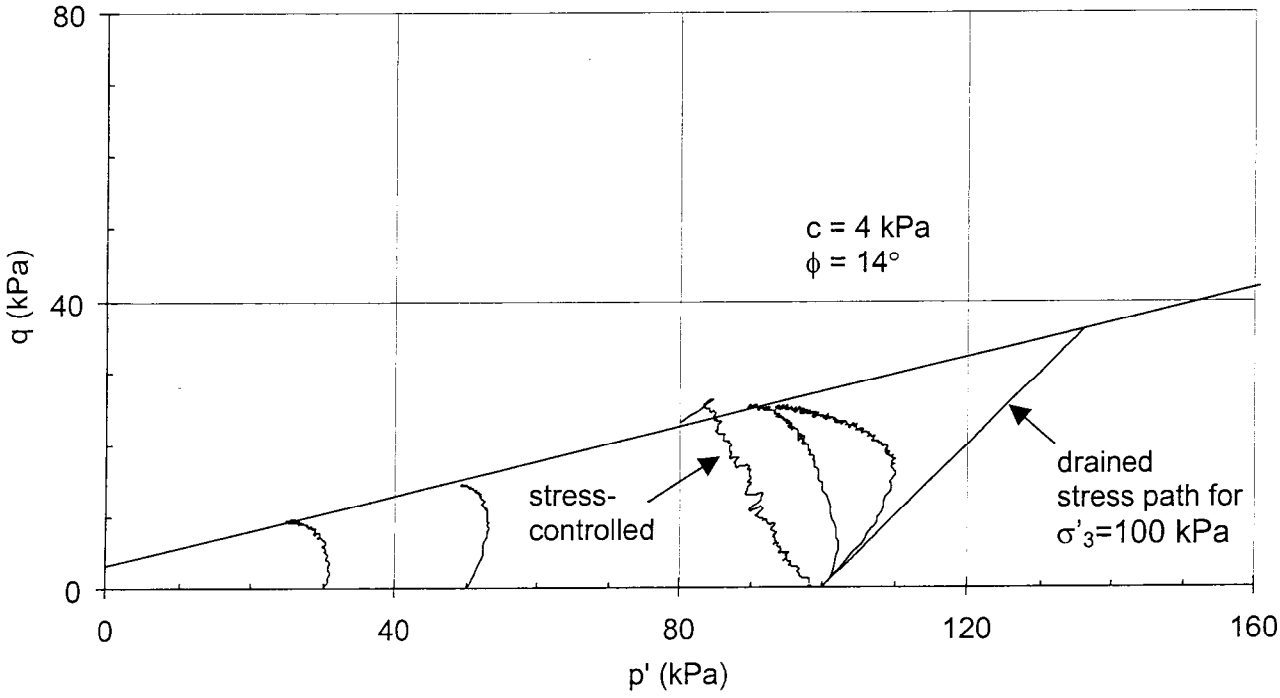

Figure 4. Manoa clay, CIU strength tests: stress paths. All tests are strain-controlled, except as stated.

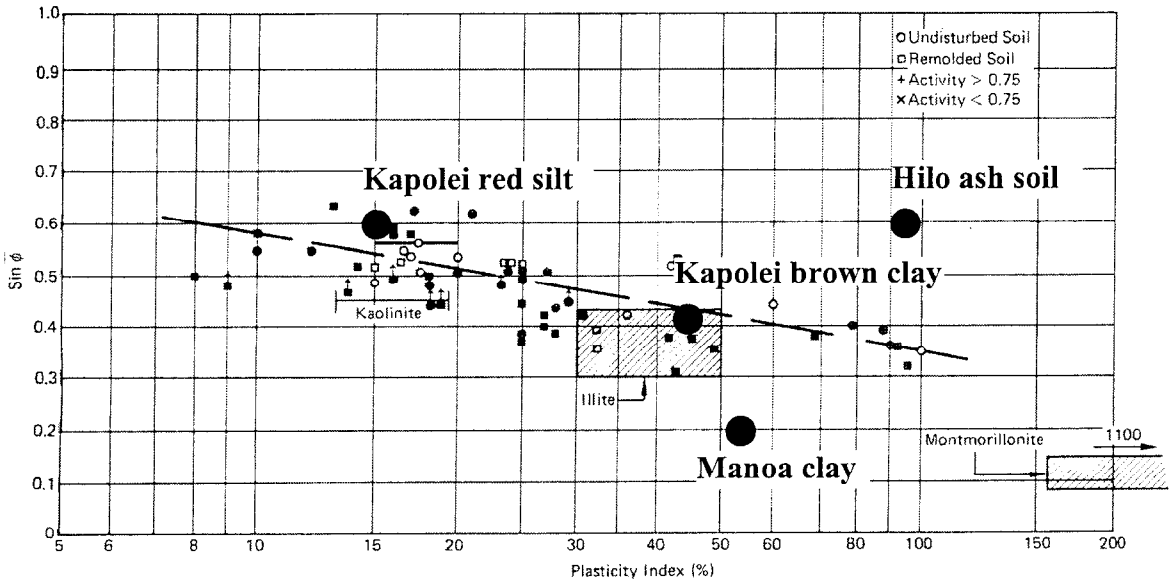

Figure 5. Relationship between sin ϕ and plasticity index for normally consolidated soils (Kenney, 1959, reprinted from Mitchell, 1976).

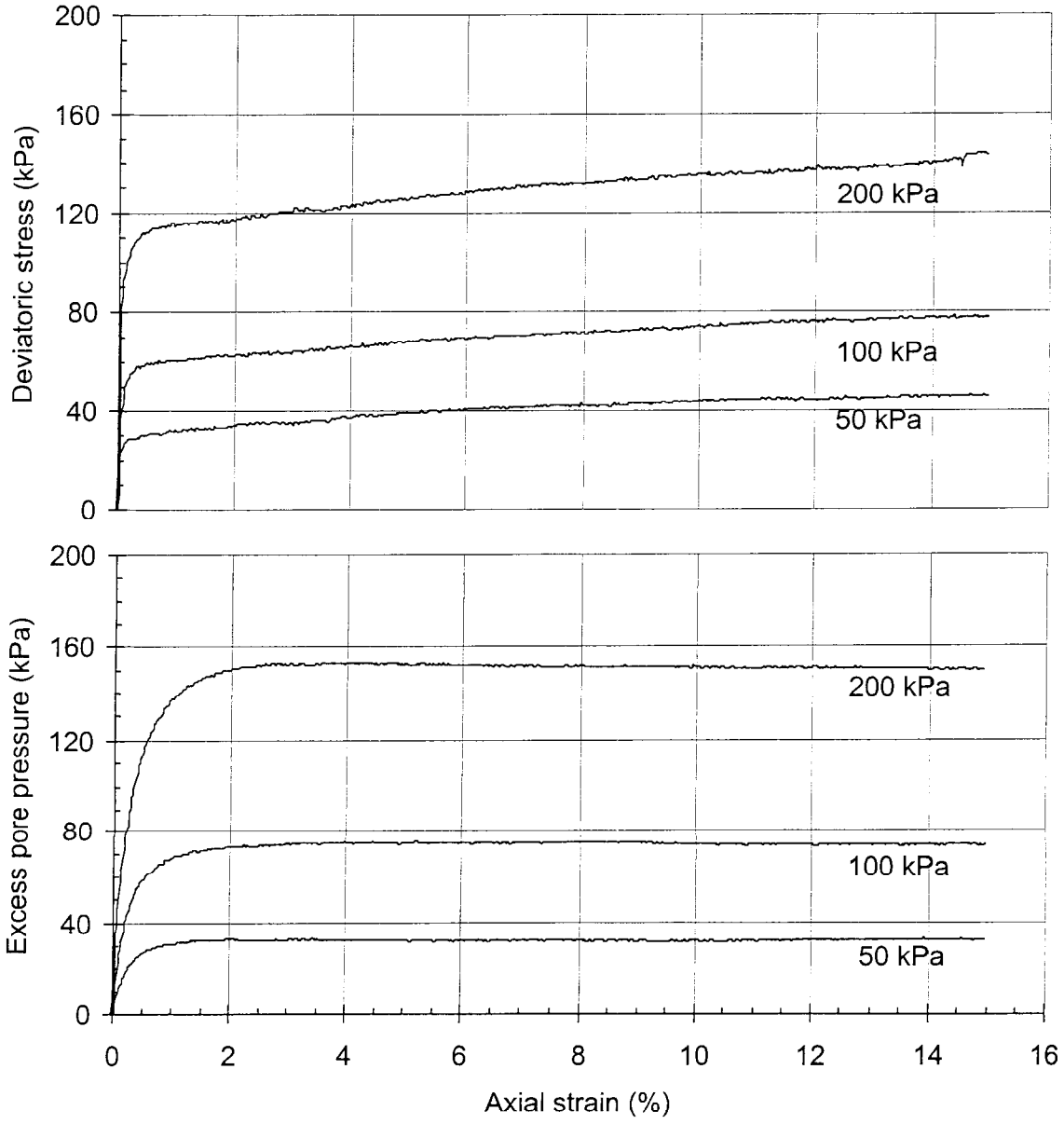

Figure 6. Kapolei Red silt, CIU strain-controlled strength tests: stress-strain behavior.

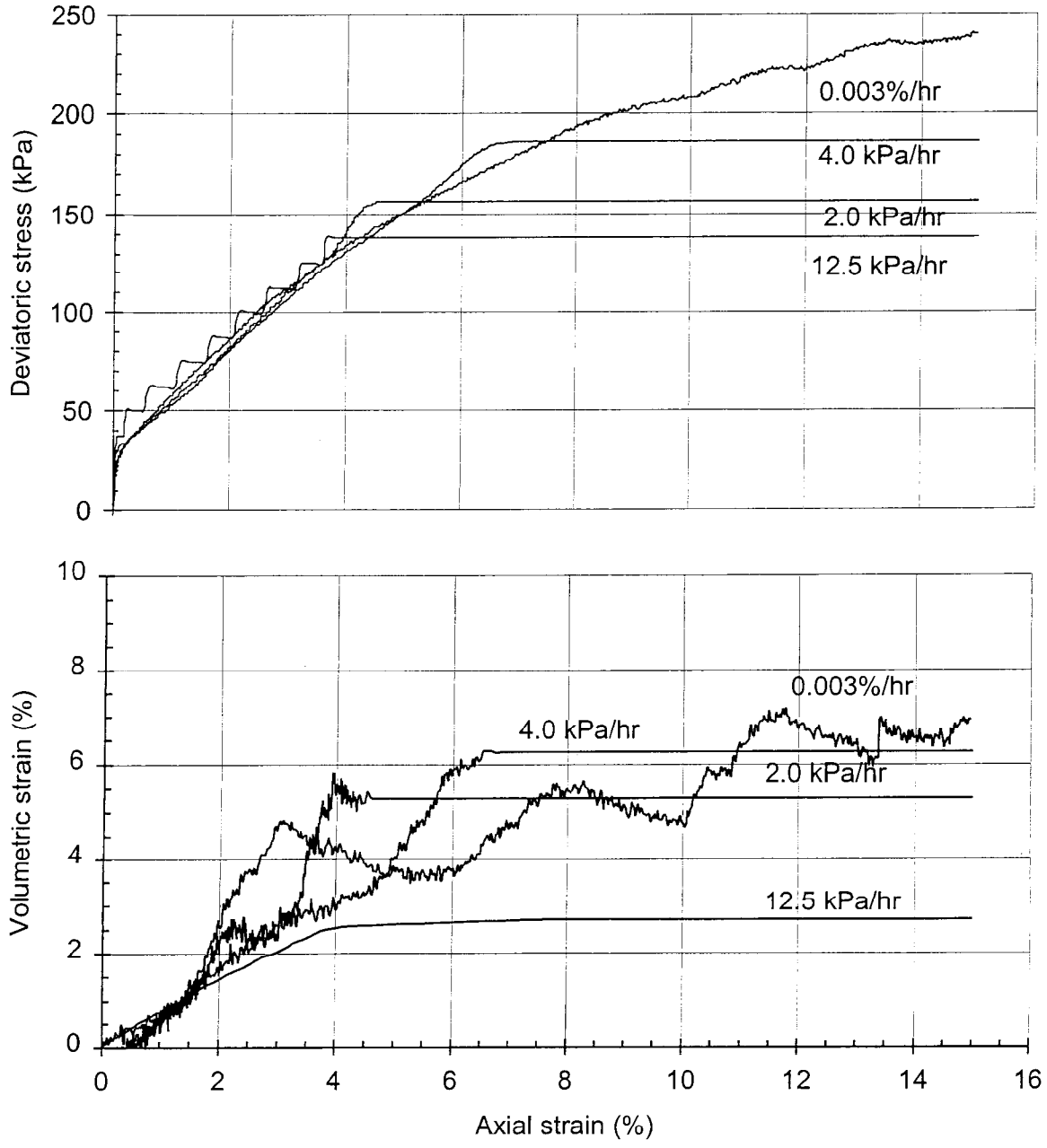

Figure 7. Kapolei Red silt, CID stress and strain-controlled strength tests: stress-strain behavior.

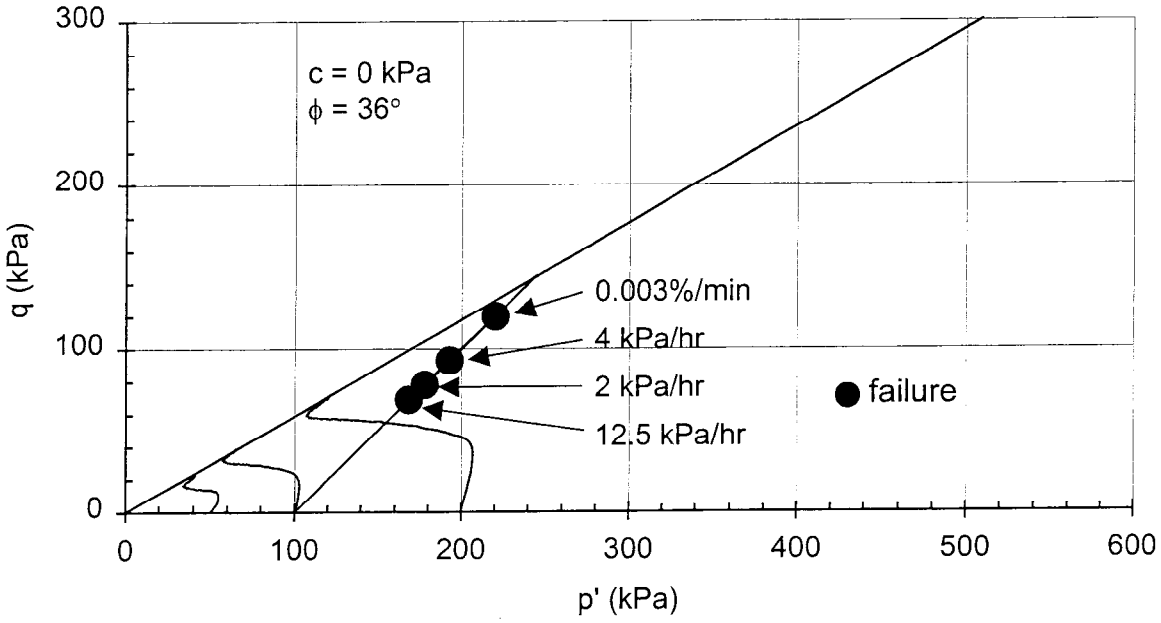

Figure 8. Kapolei Red silt, CIU and CID strength tests: stress paths.

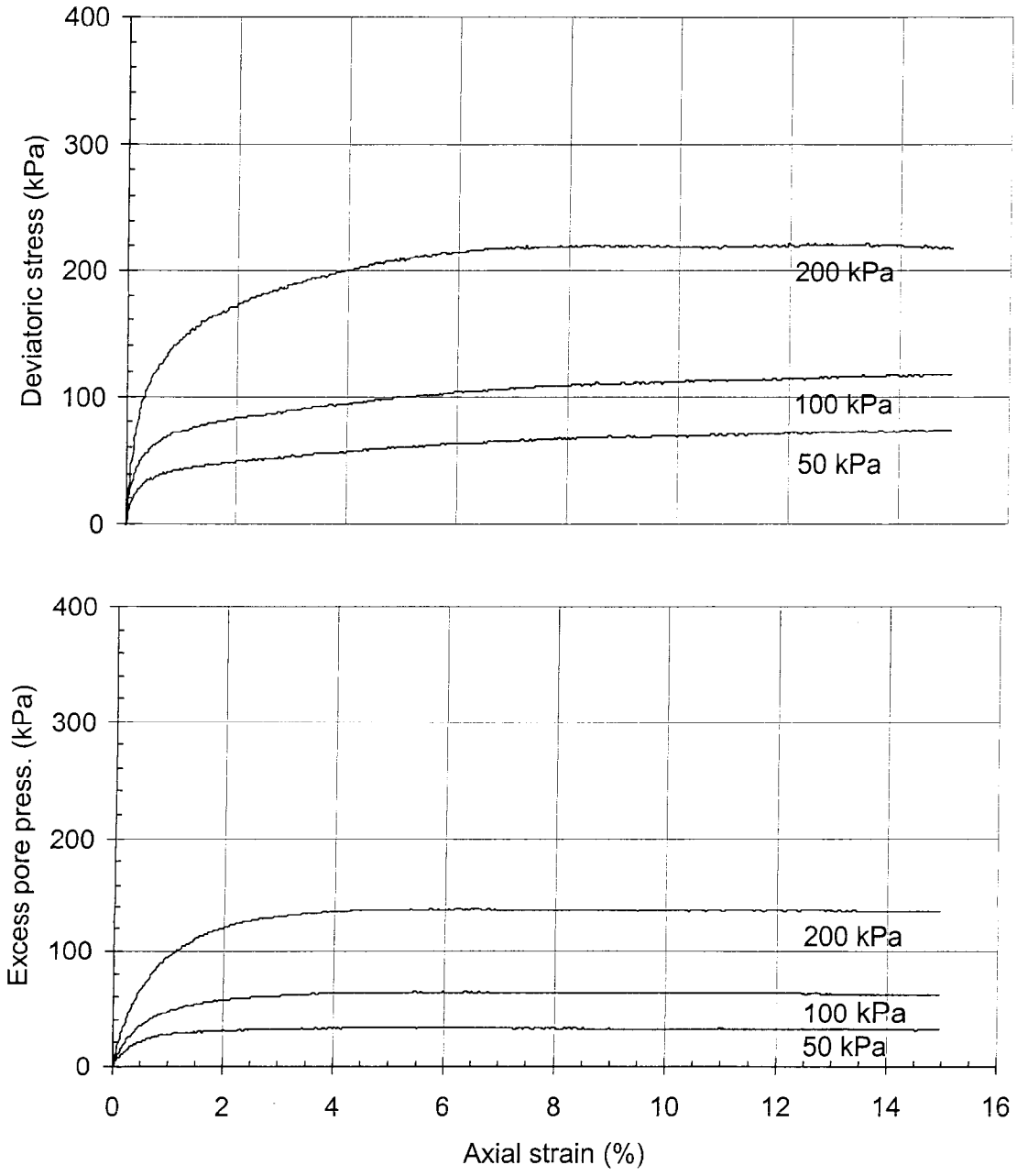

Figure 9. Hilo Ash soil, CIU strength tests: stress-strain behavior.

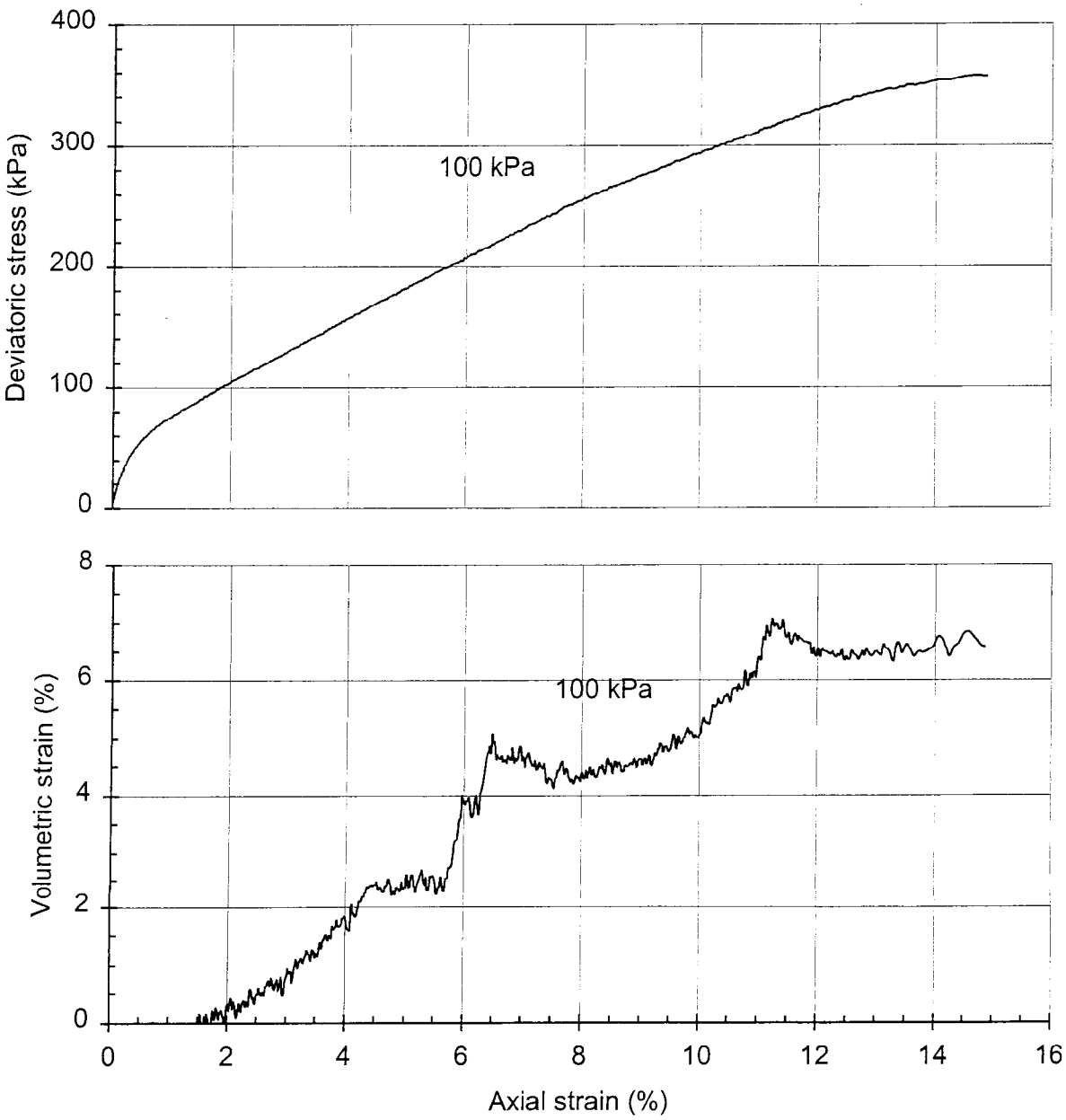

Figure 10. Hilo Ash soil, CID strength test: stress-strain behavior.

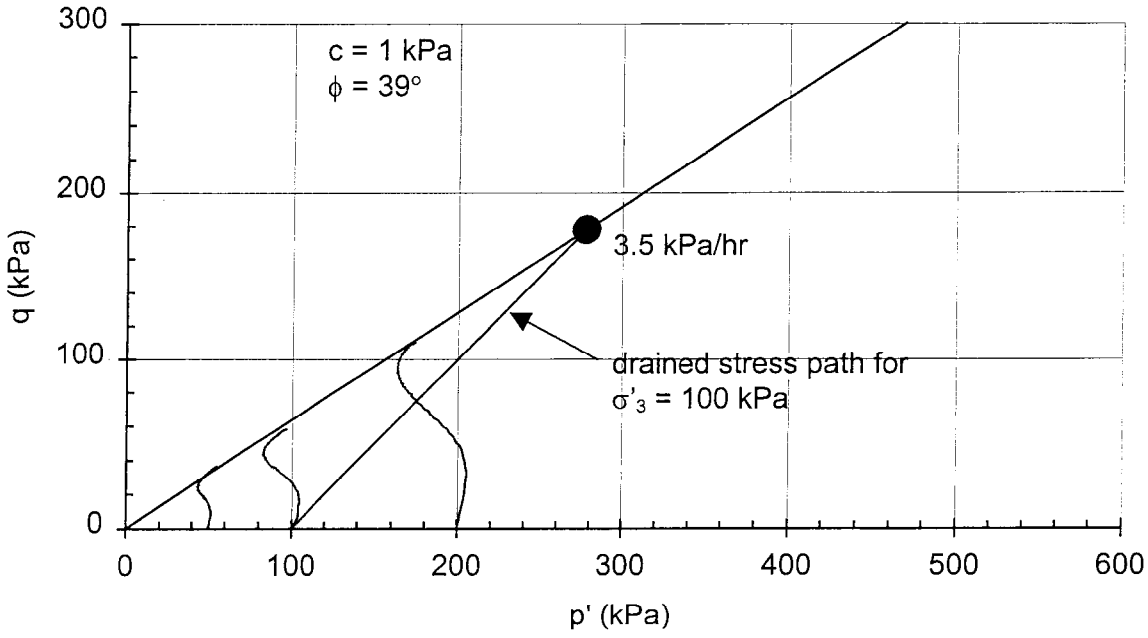

Figure 11. Hilo Ash soil, CIU and CID strength tests: stress paths.

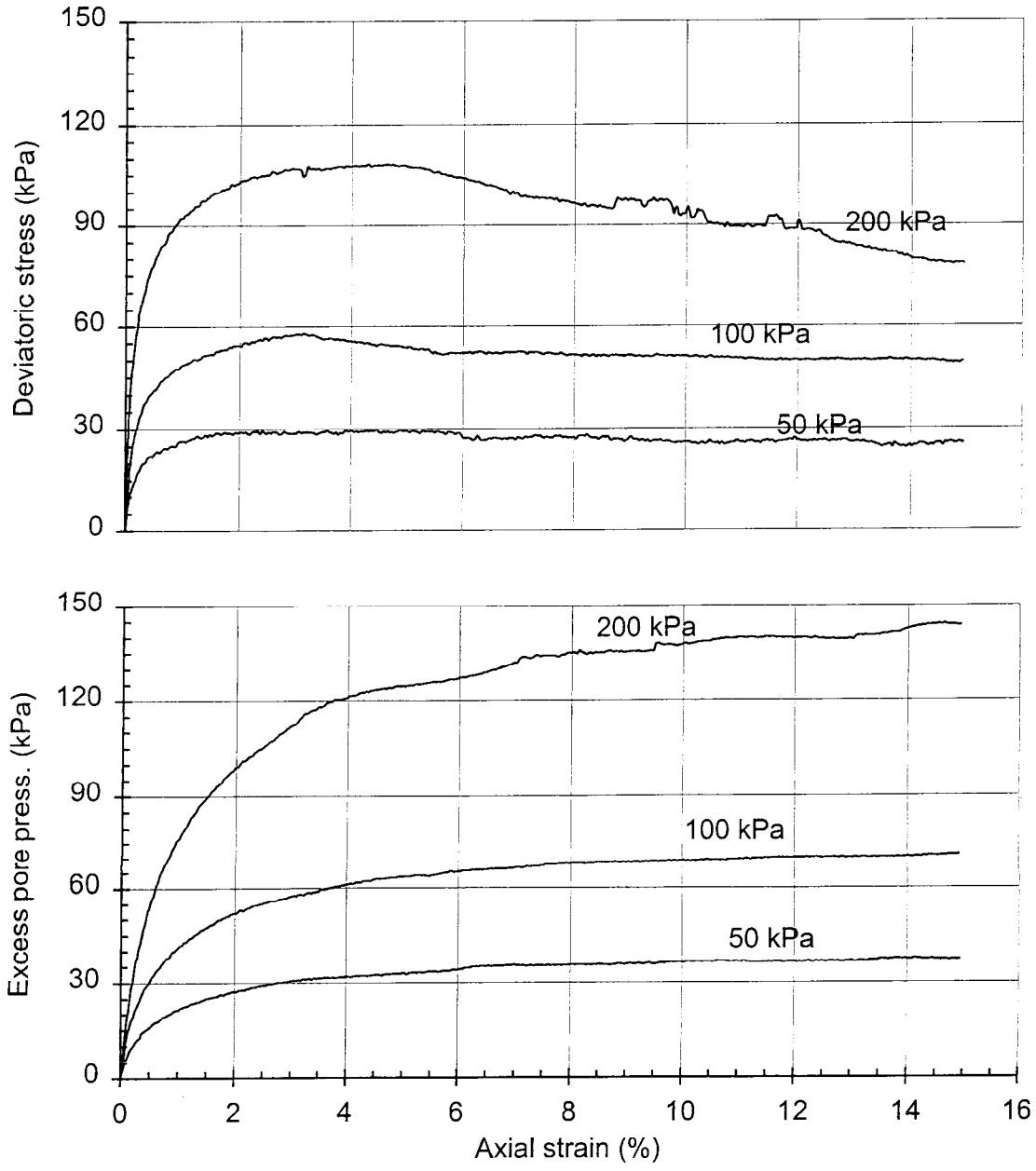

Figure 12. Kapolei Brown clay, CIU strength tests: stress-strain behavior.

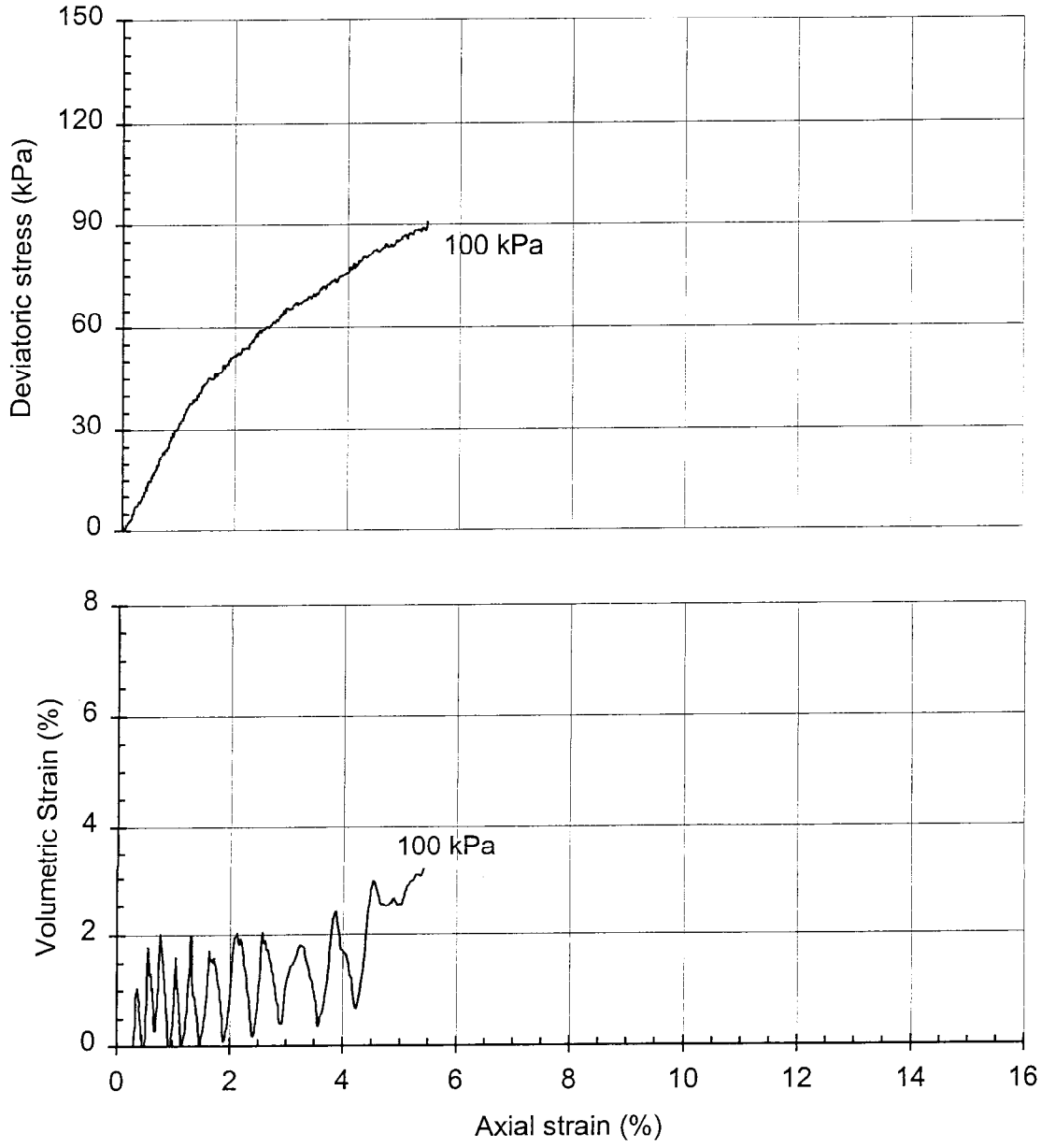

Figure 13. Kapolei Brown clay, CID strength tests: stress-strain behavior.

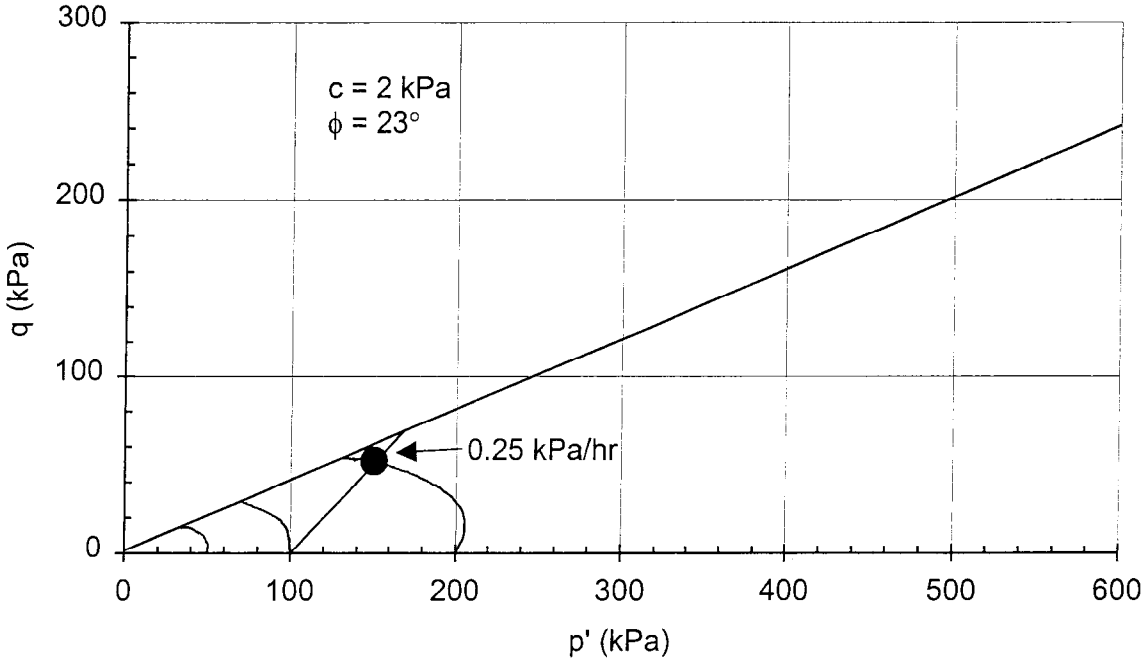

Figure 14. Kapolei Brown clay, CIU and CID strength tests: stress paths.

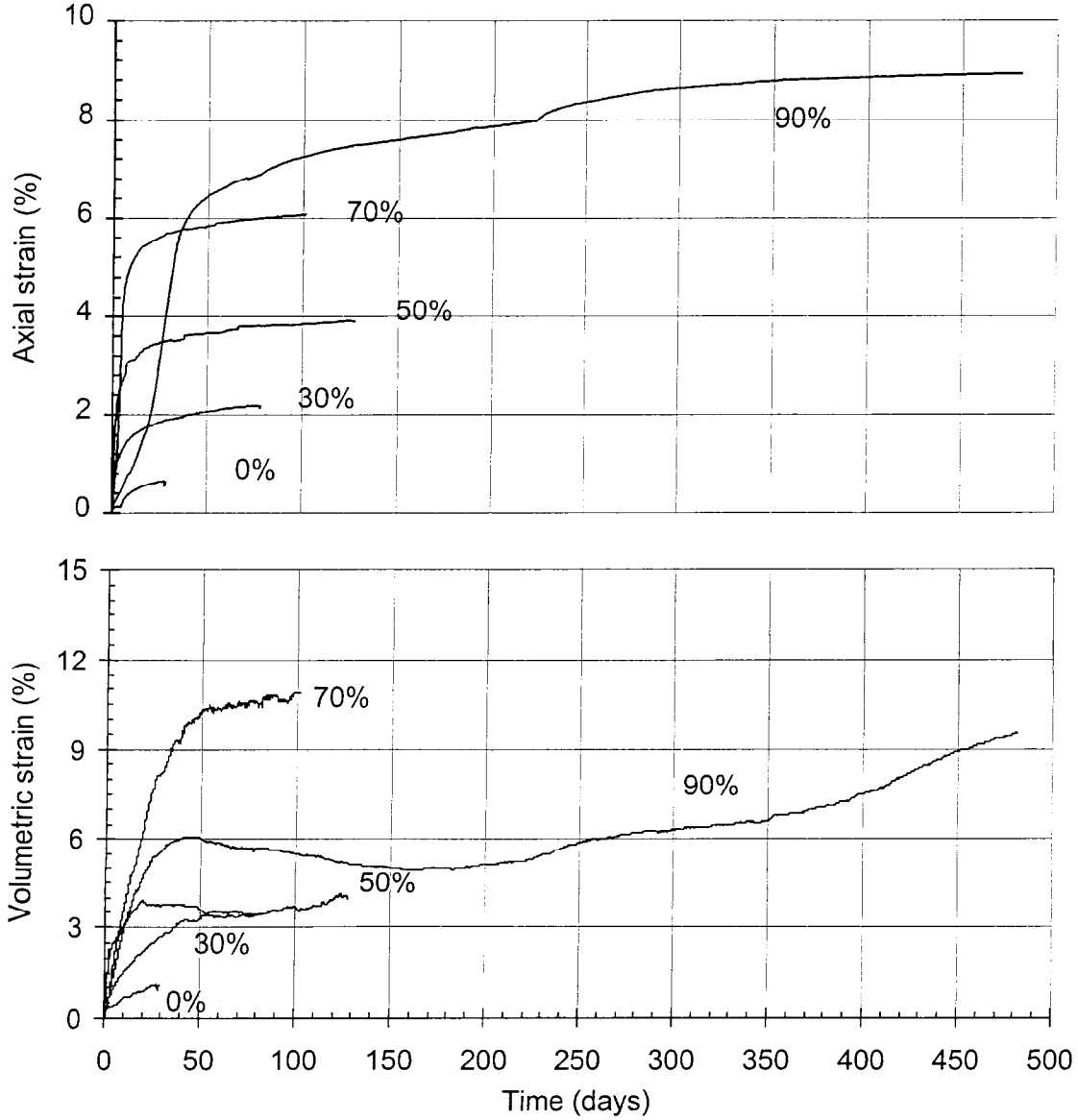

Figure 15. Manoa clay, creep axial and volumetric strains.

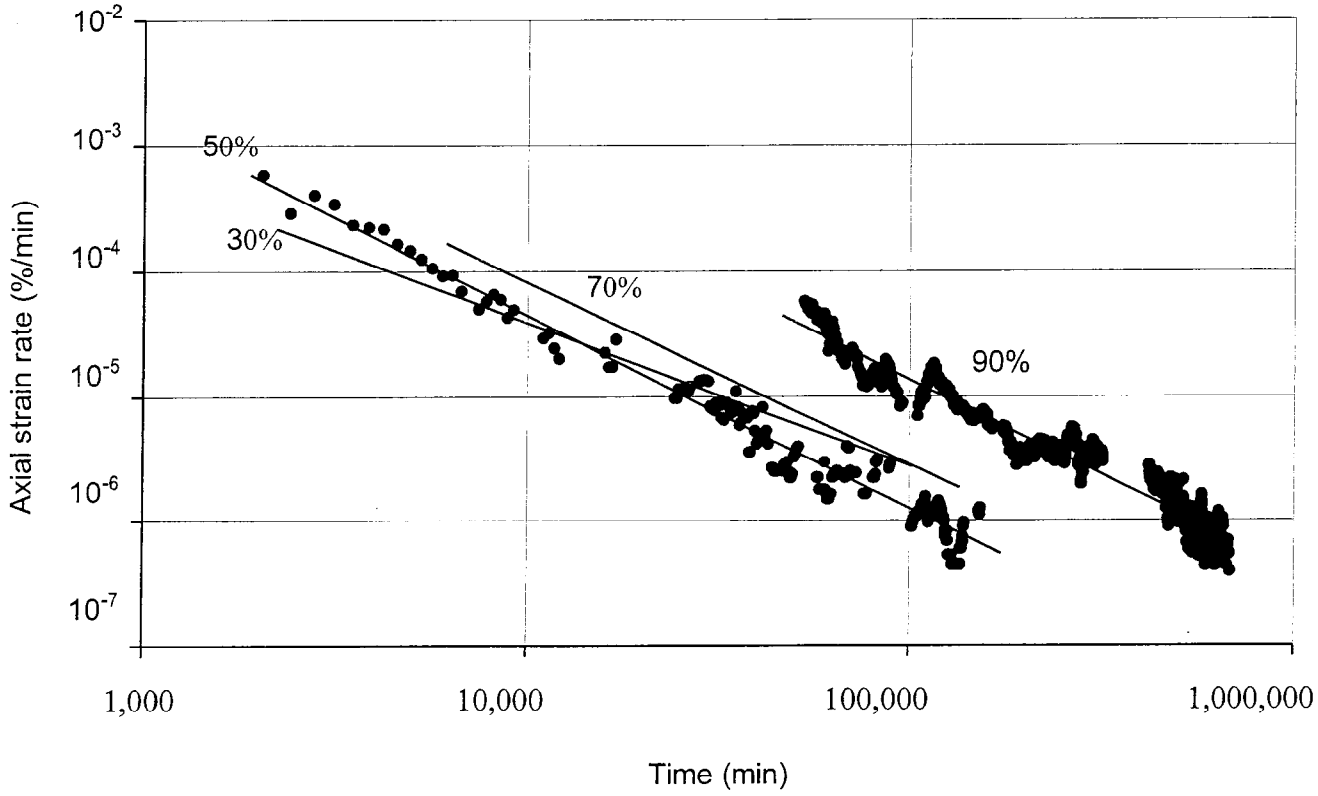

Figure 16. Manoa clay, creep axial strain rate behavior (data points are shown for 50% and 90% tests).

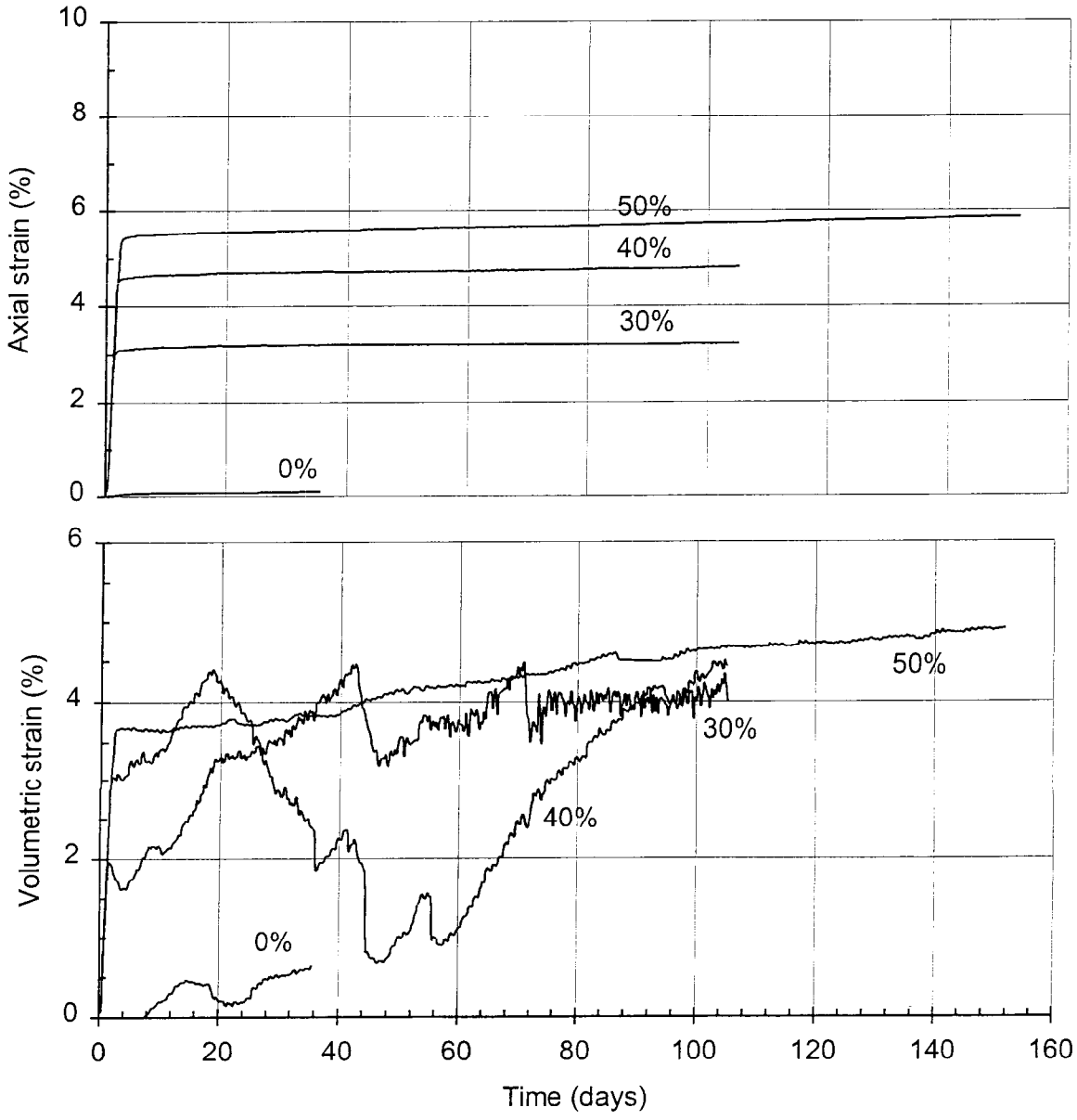

Figure 17. Kapolei Red silt, creep axial and volumetric strains.

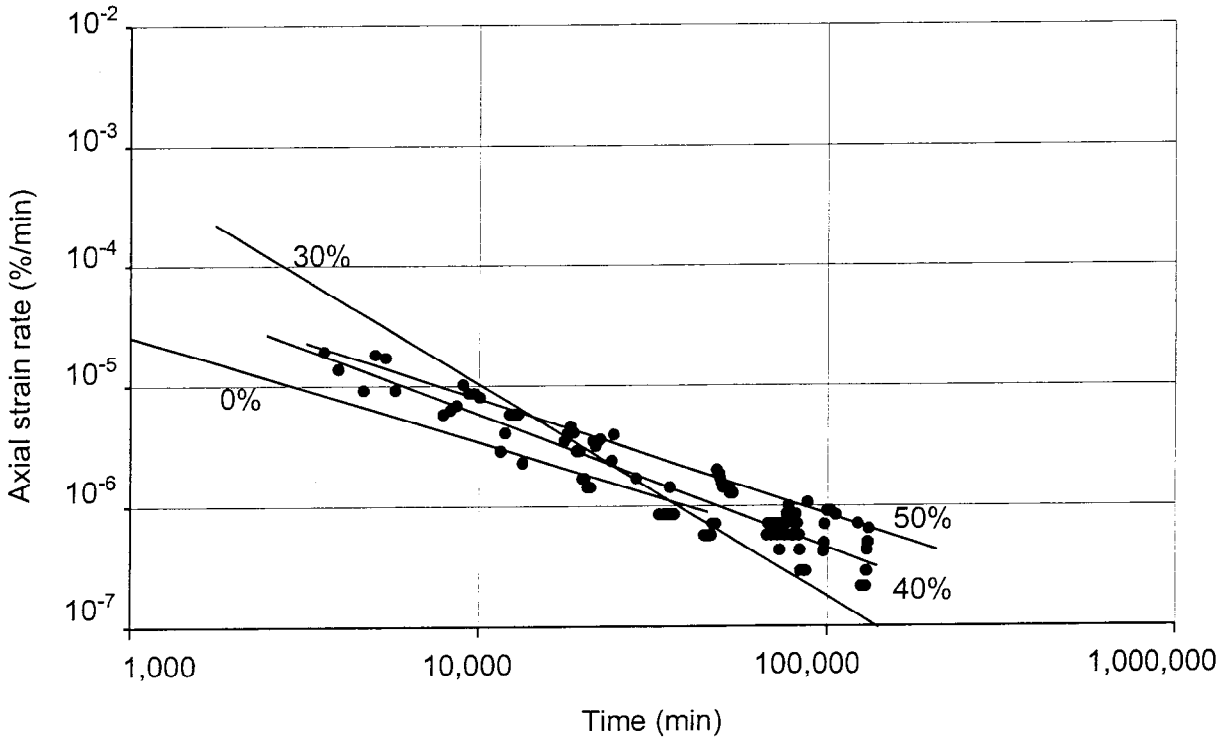

Figure 18. Kapolei Red silt, creep axial strain rate behavior (data points are shown for 40% test).

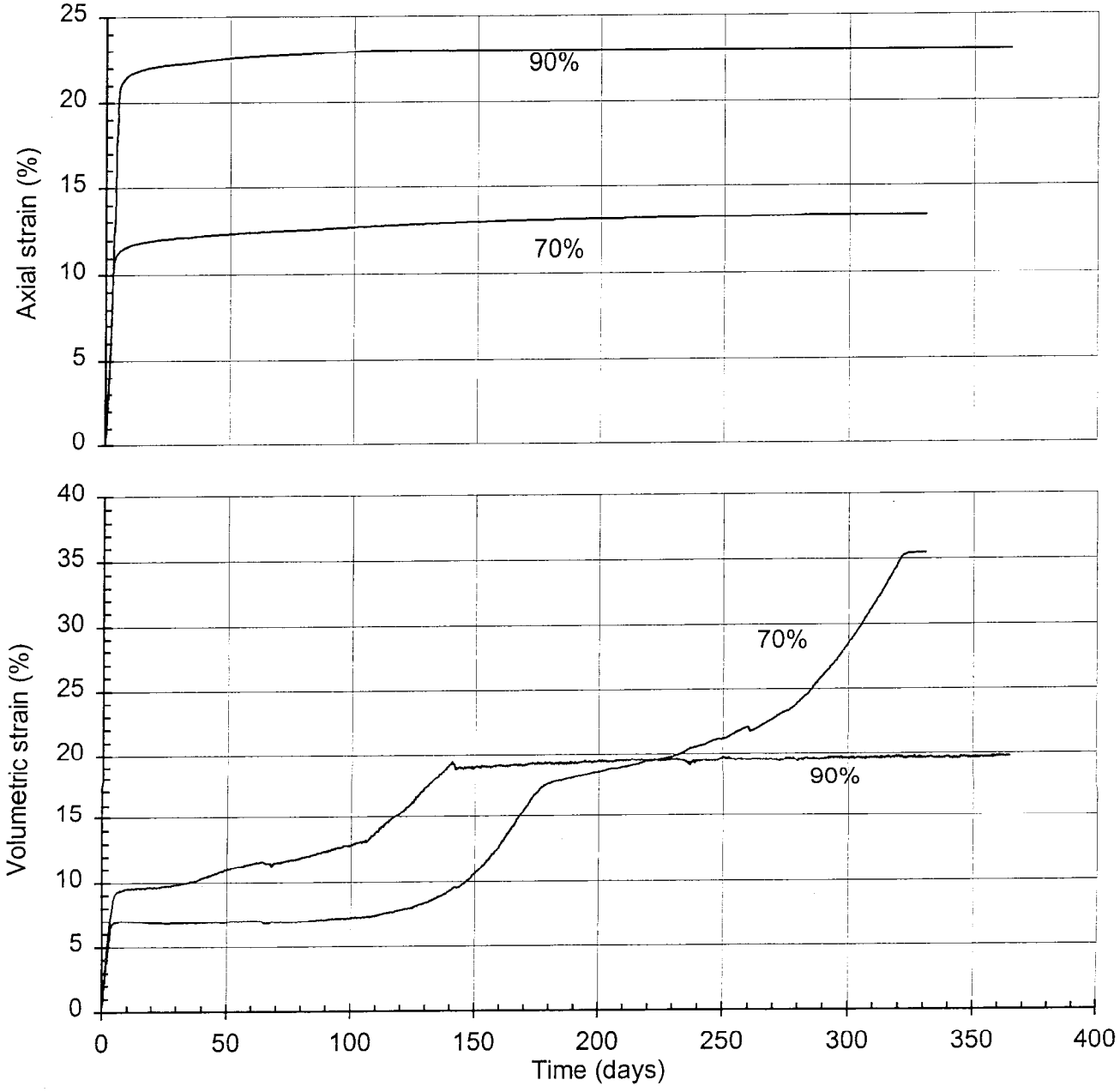

Figure 19. Hilo Ash soil, creep axial and volumetric strains.

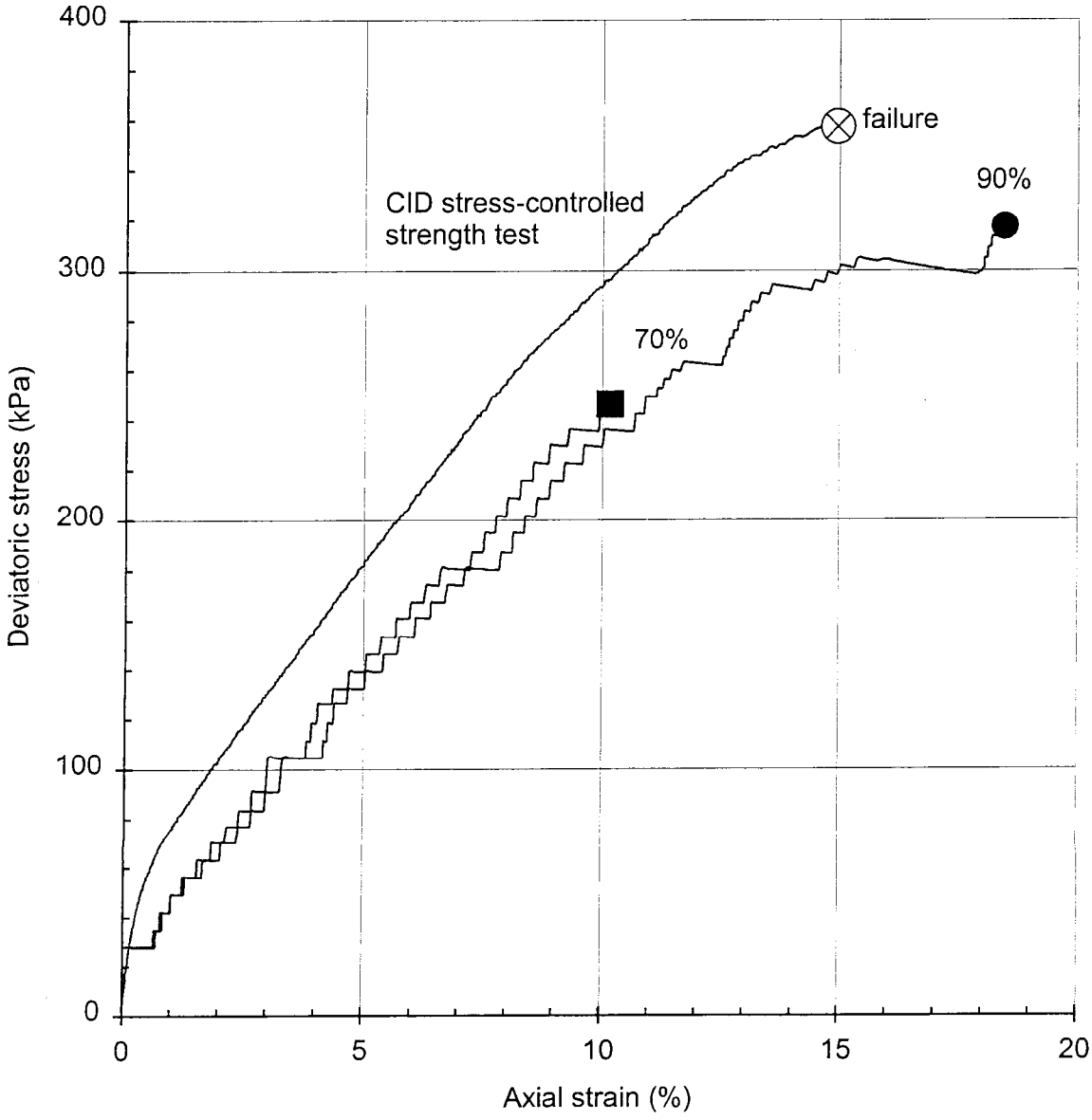

Figure 20. Hilo Ash soil, loading phase for creep and CID strength tests.

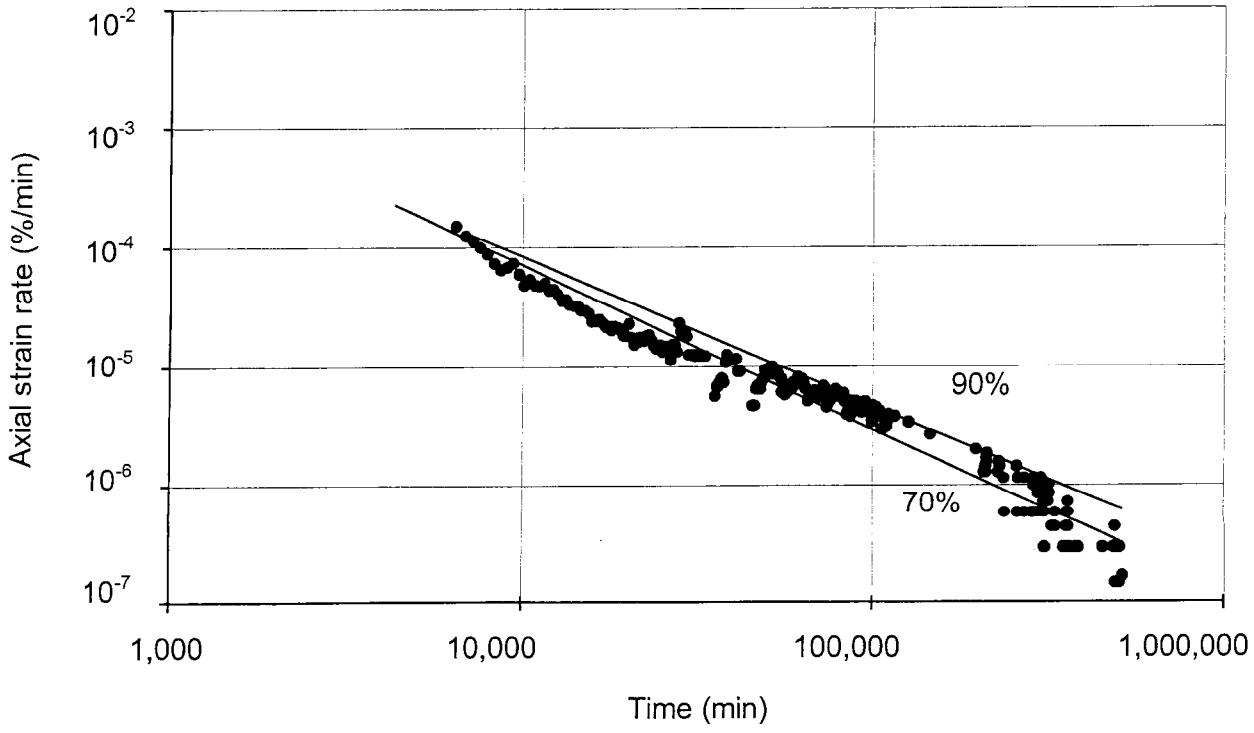

Figure 21. Hilo Ash soil, creep axial strain rate behavior (data points are shown for 70% test).

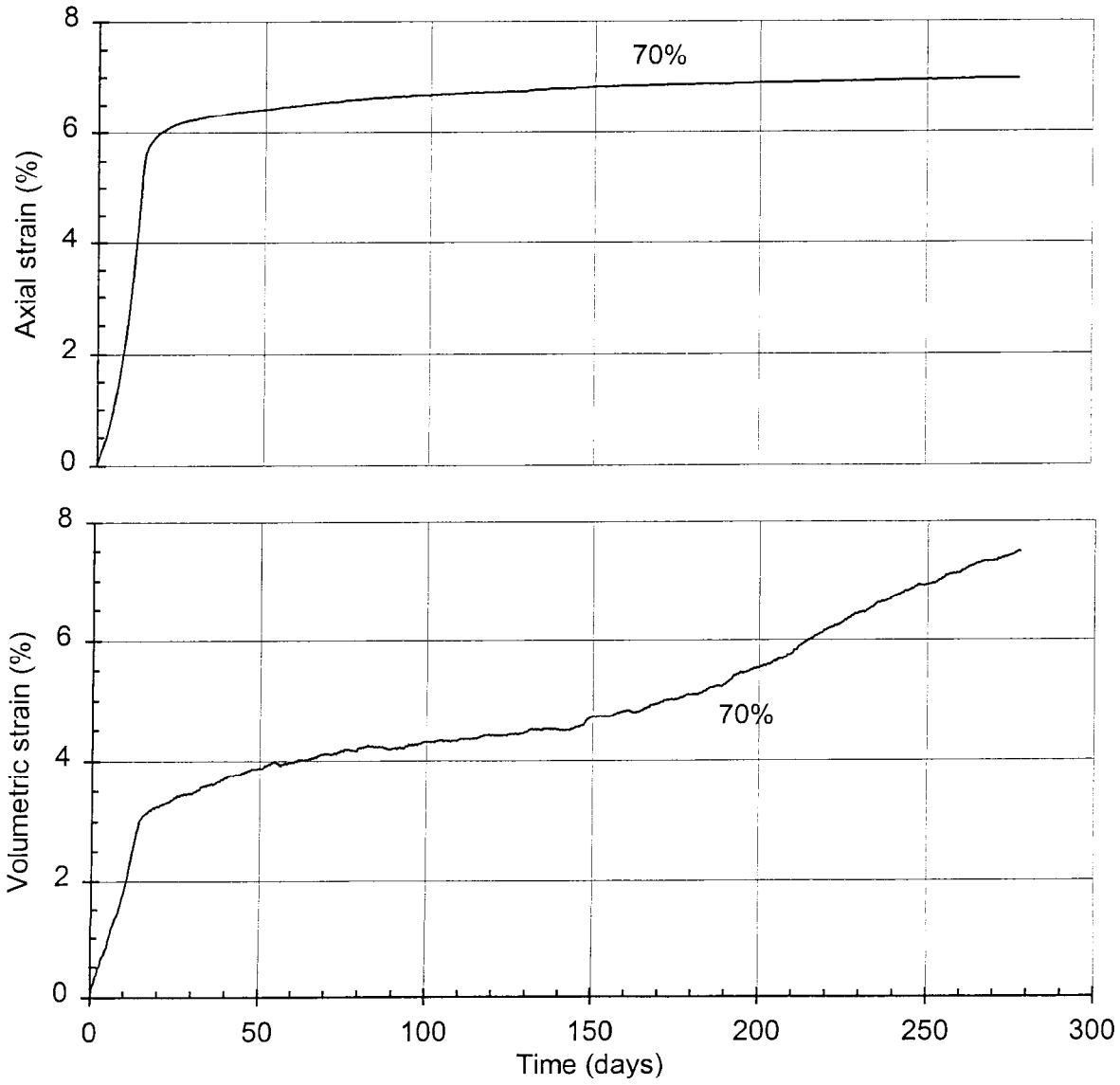

Figure 22. Kapolei Brown clay, creep axial and volumetric strains.

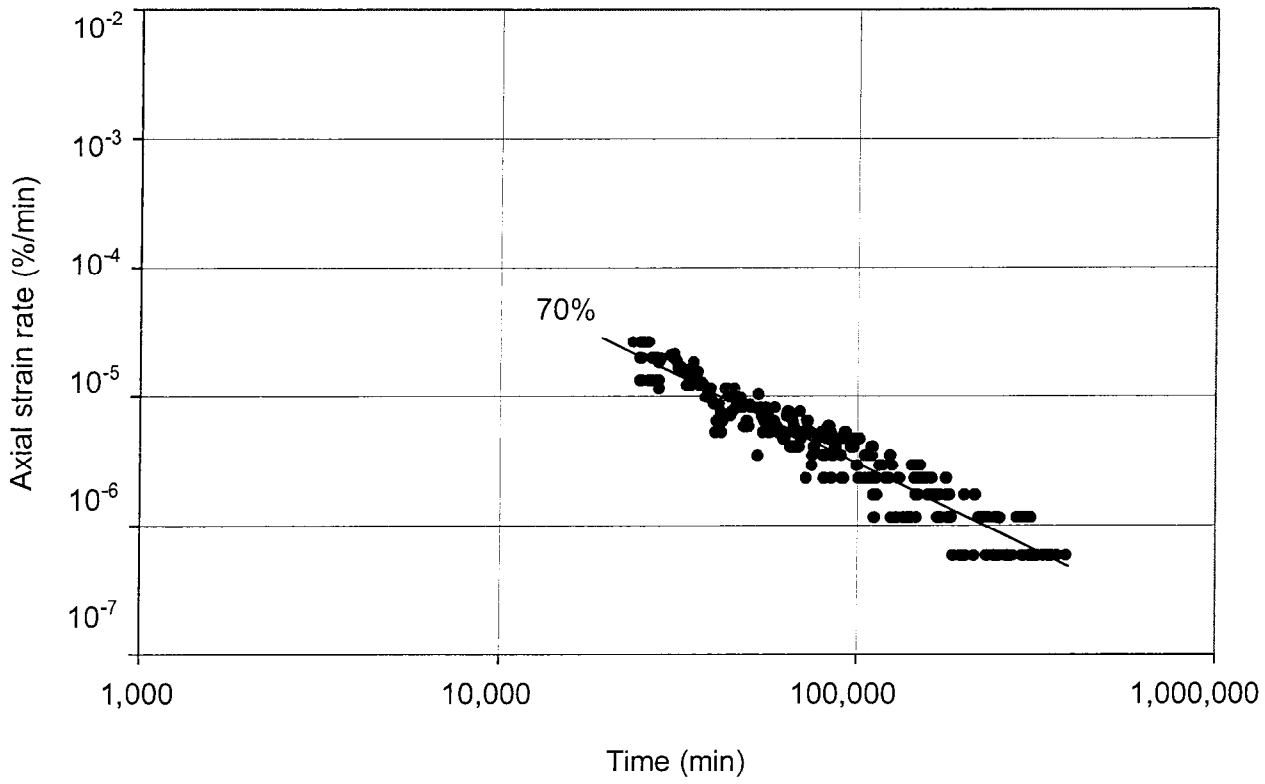

Figure 23. Kapolei Brown clay, creep axial strain rate behavior.

a. Axial strains.

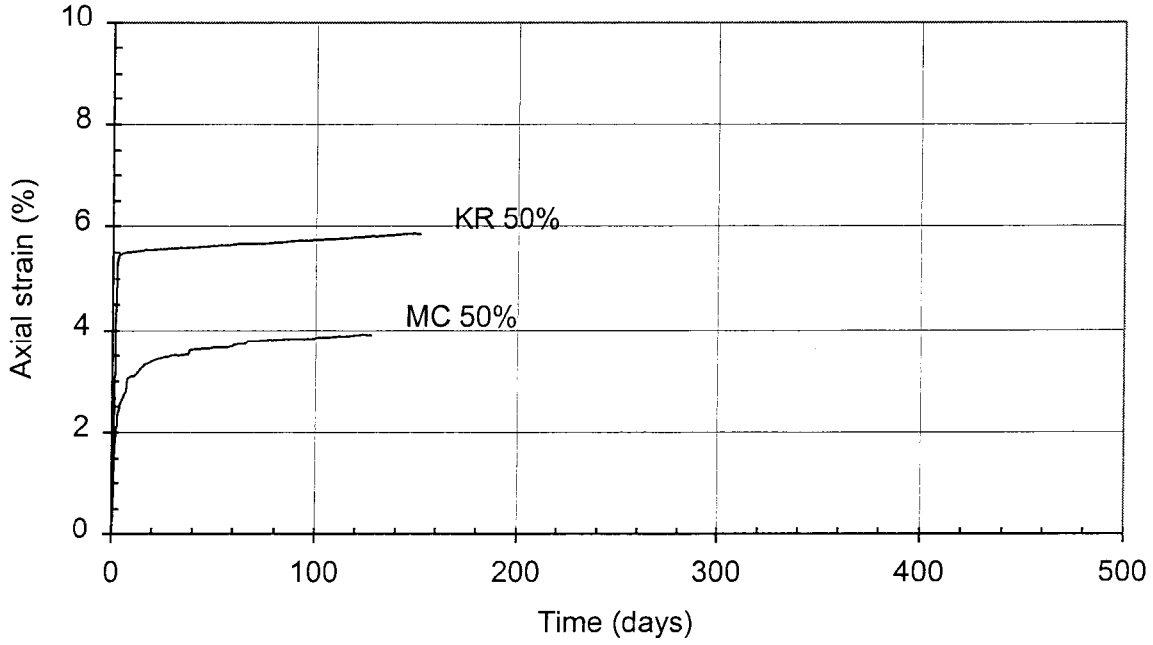

b. Axial strain rates.

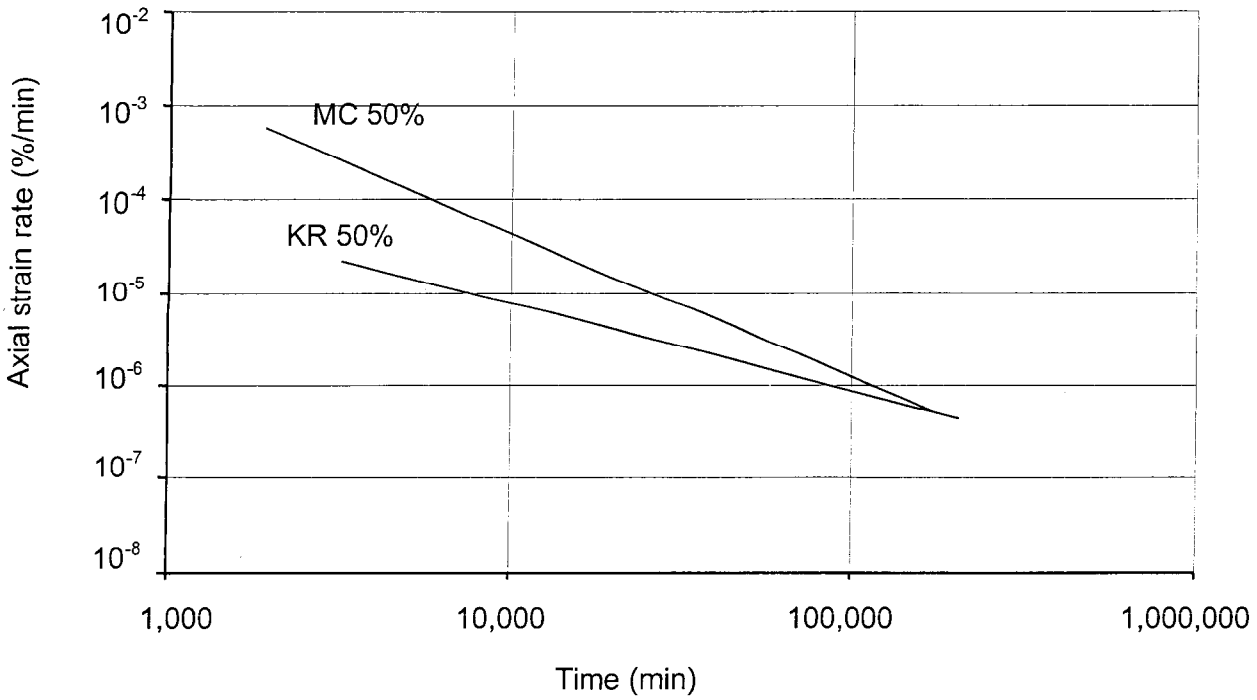

Figure 24. Comparison of creep behavior at 50% stress level among Manoa clay and Kapolei Red silt soils.

a. Axial strains.

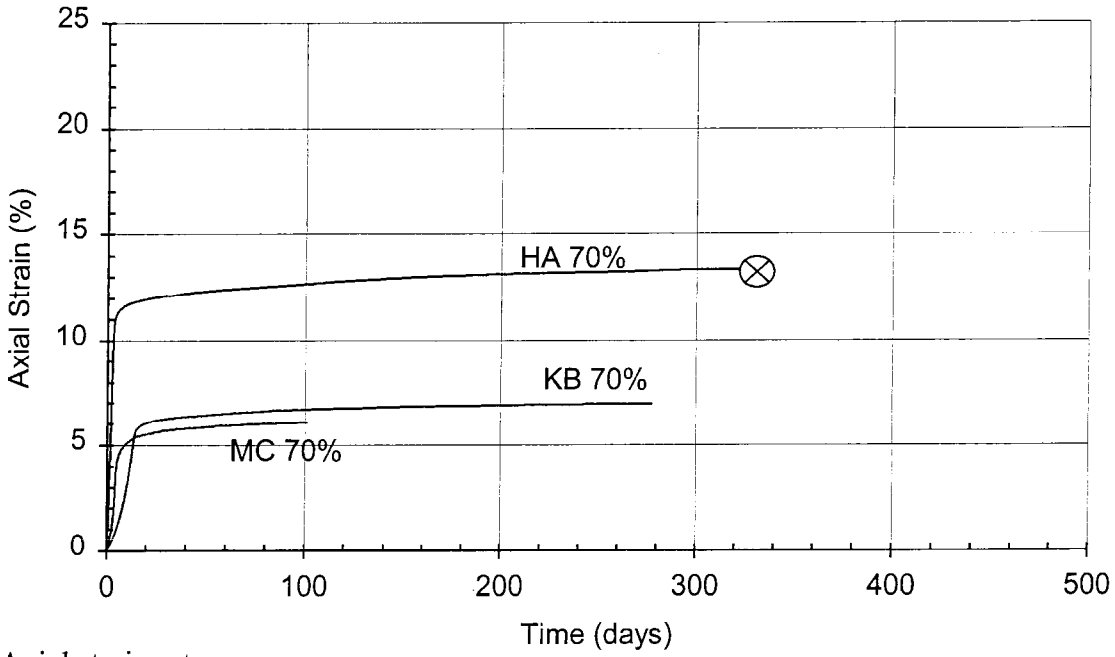

b. Axial strain rates.

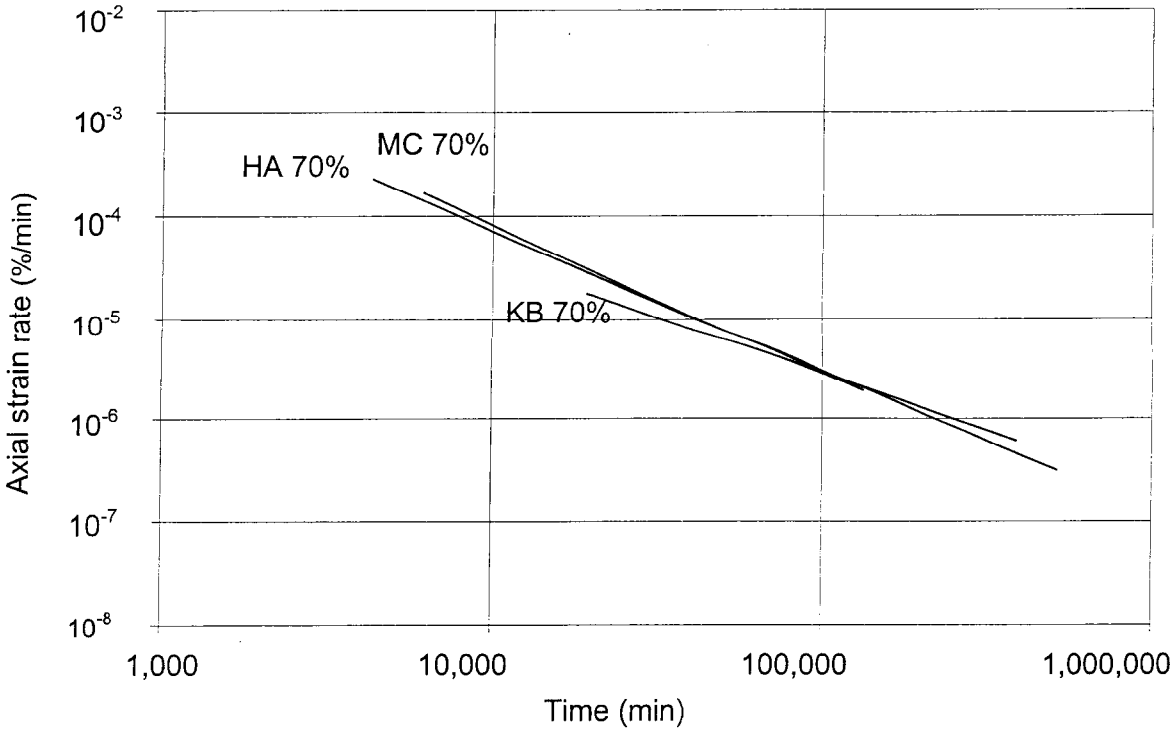

Figure 25. Comparison of creep behavior at 70% stress level among Manoa clay, Kapolei Brown clay and Hilo Ash soils.

a. Axial strains.

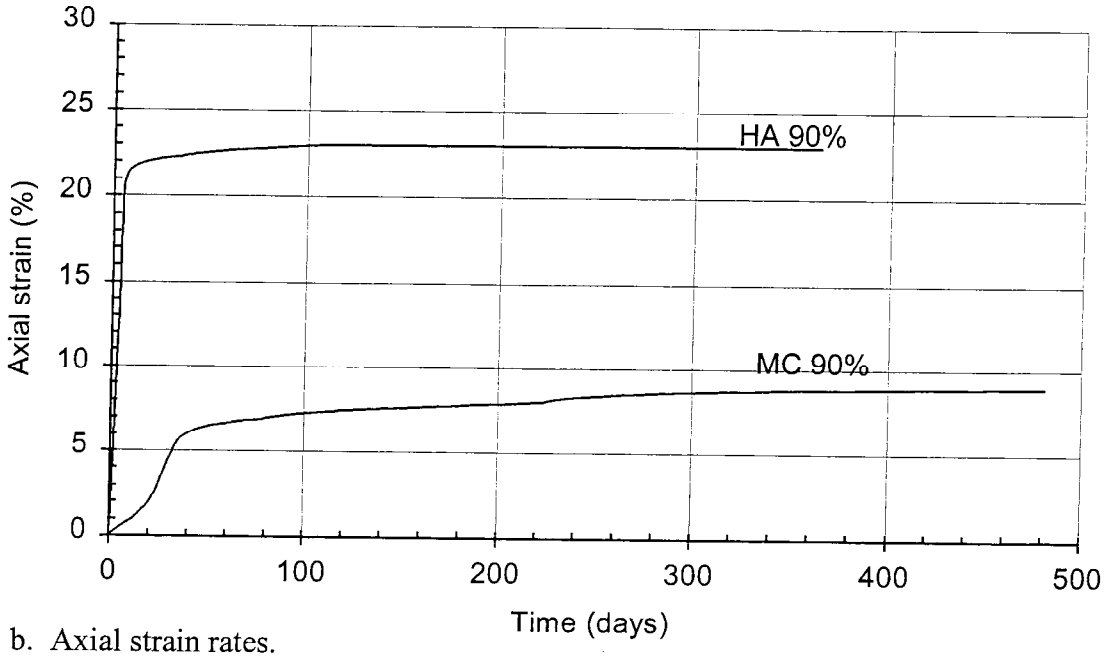

b. Axial strain rates.

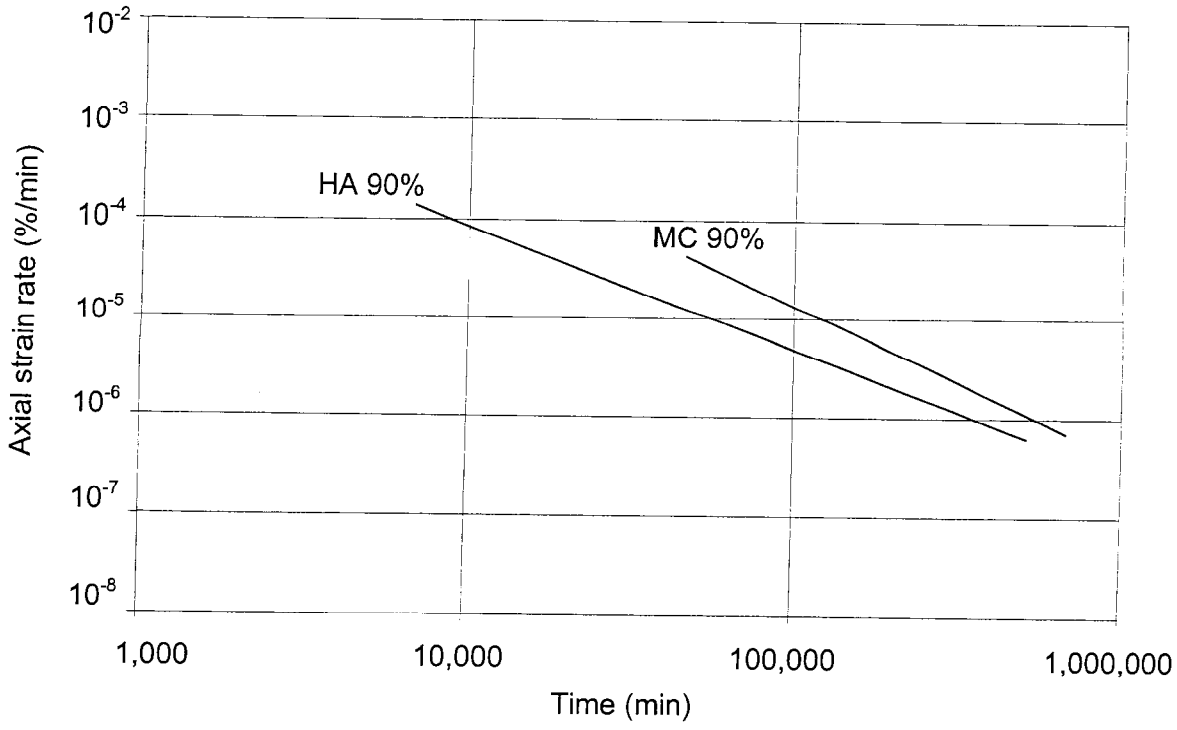

Figure 26. Comparison of creep behavior at 90% stress level among Manoa clay and Hilo Ash soils.

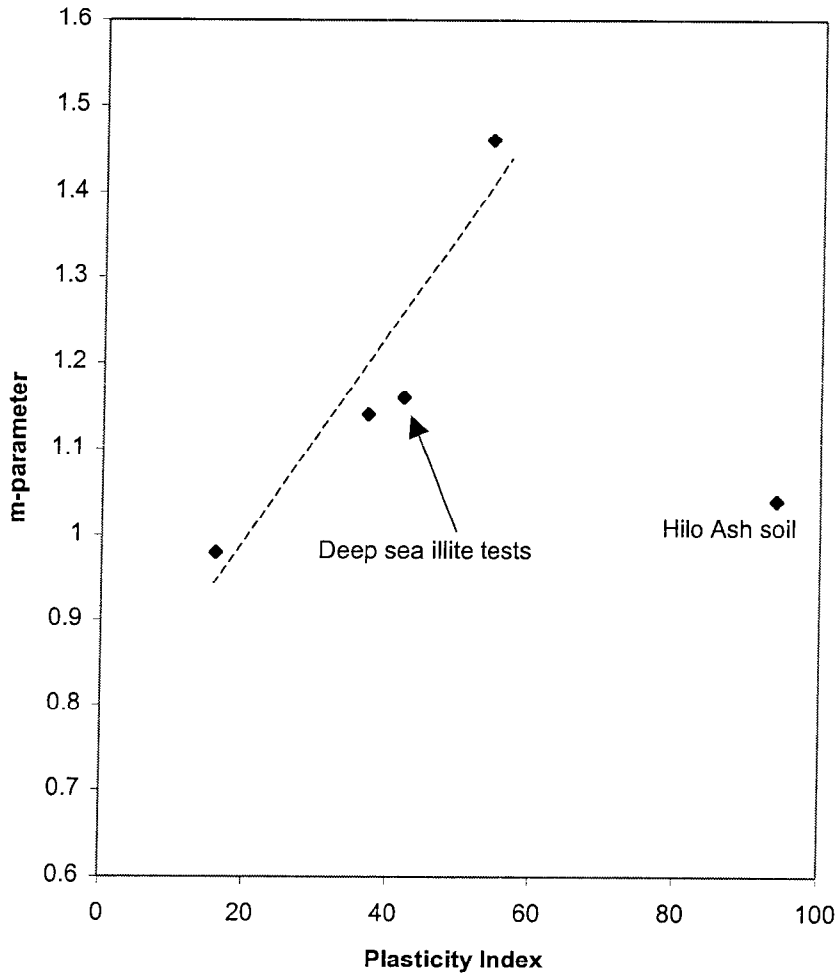

Figure 27. Creep strain rate attenuation versus plasticity index.

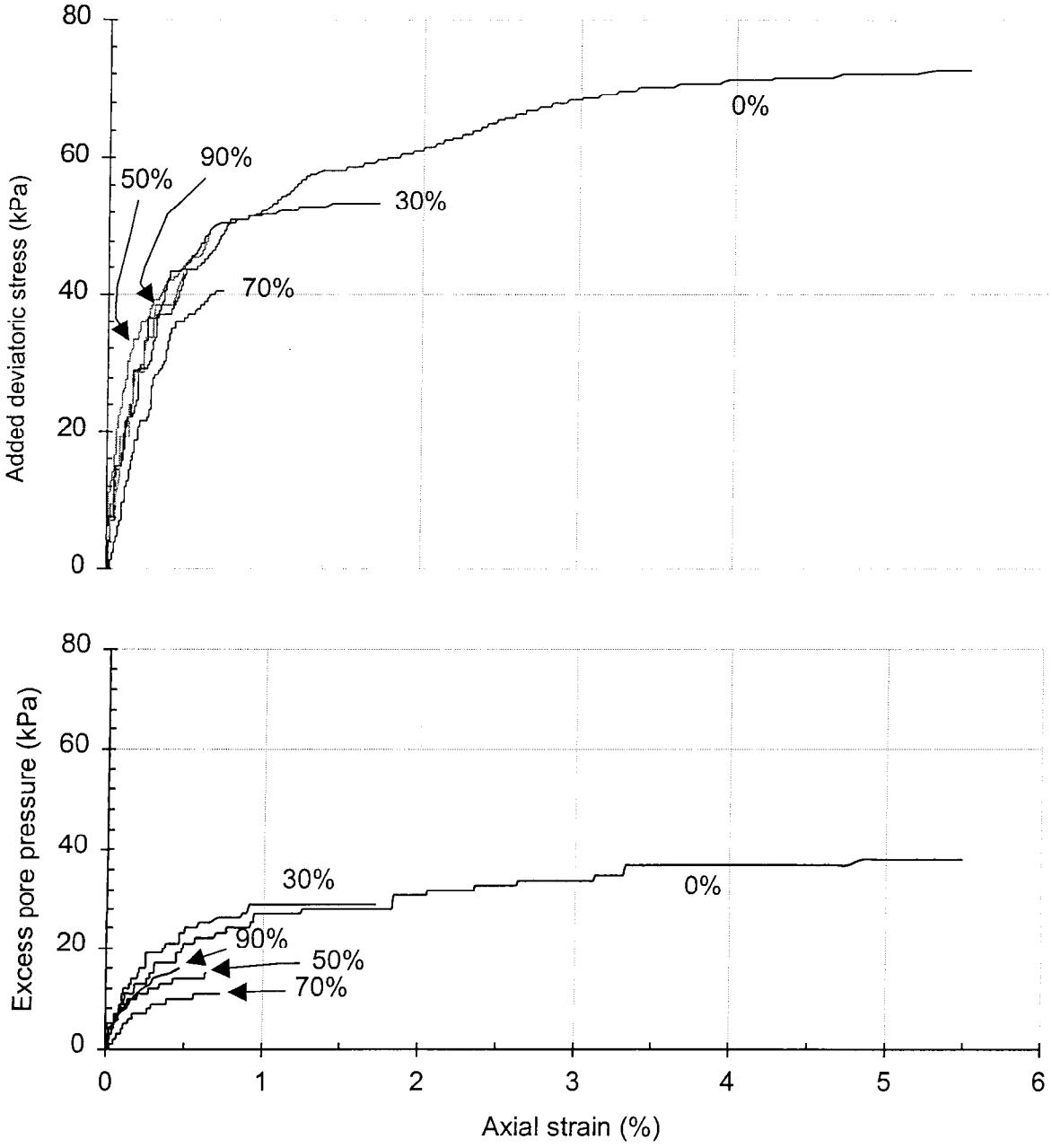

Figure 28. Manoa clay, post-creep undrained strength tests: stress-strain behavior.

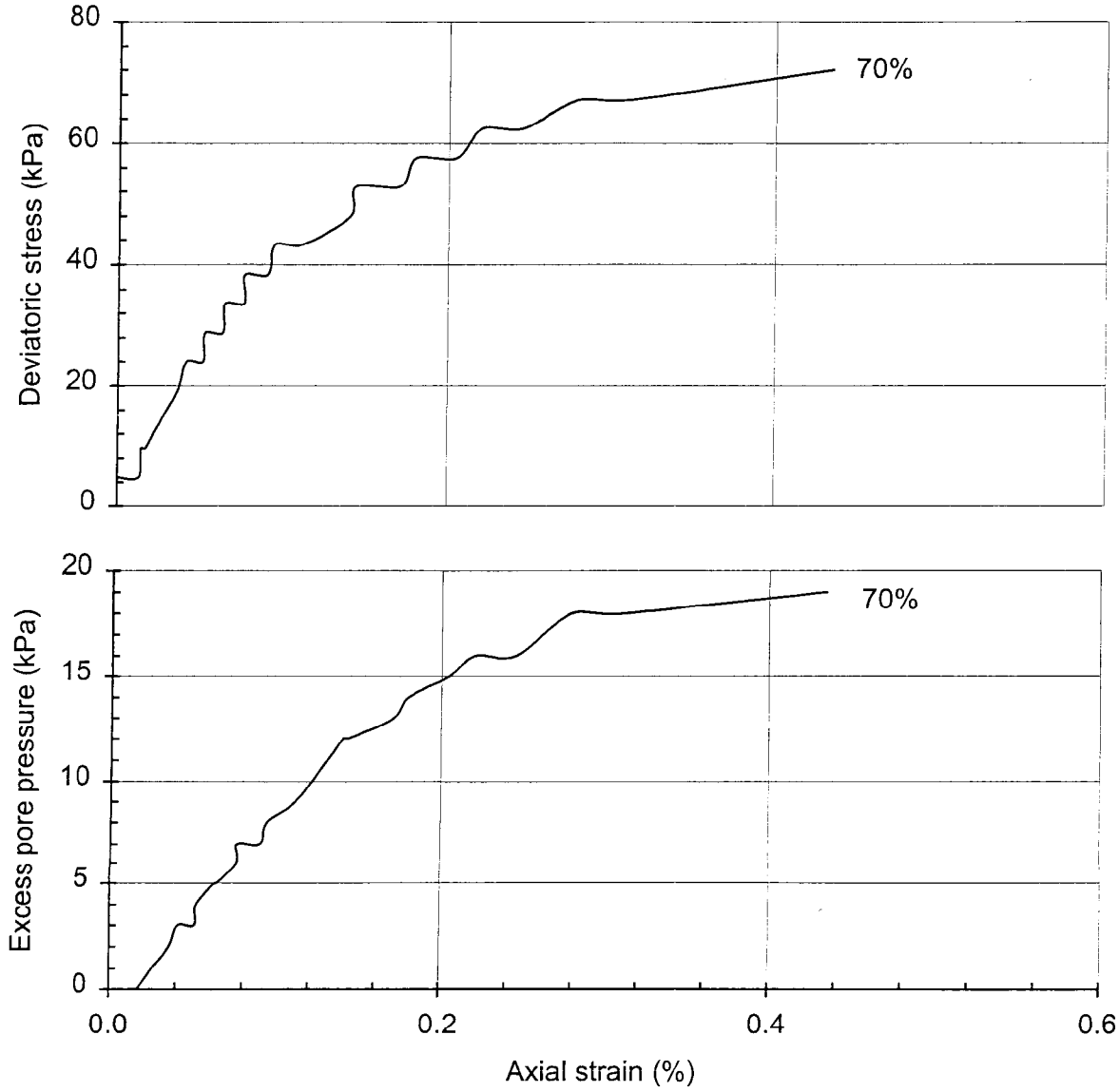

Figure 29. Kapolei Brown clay, post-creep undrained strength test: stress-strain behavior.

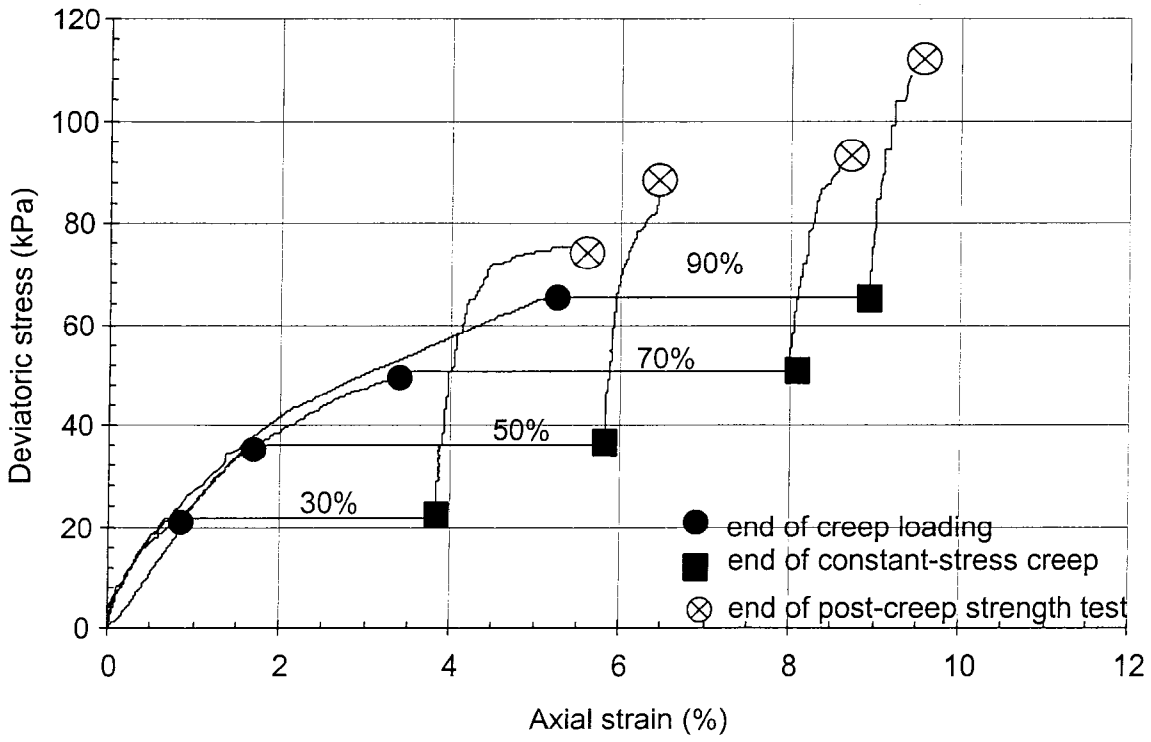

Figure 30. Manoa clay, composite creep and post-creep stress-strain curves.

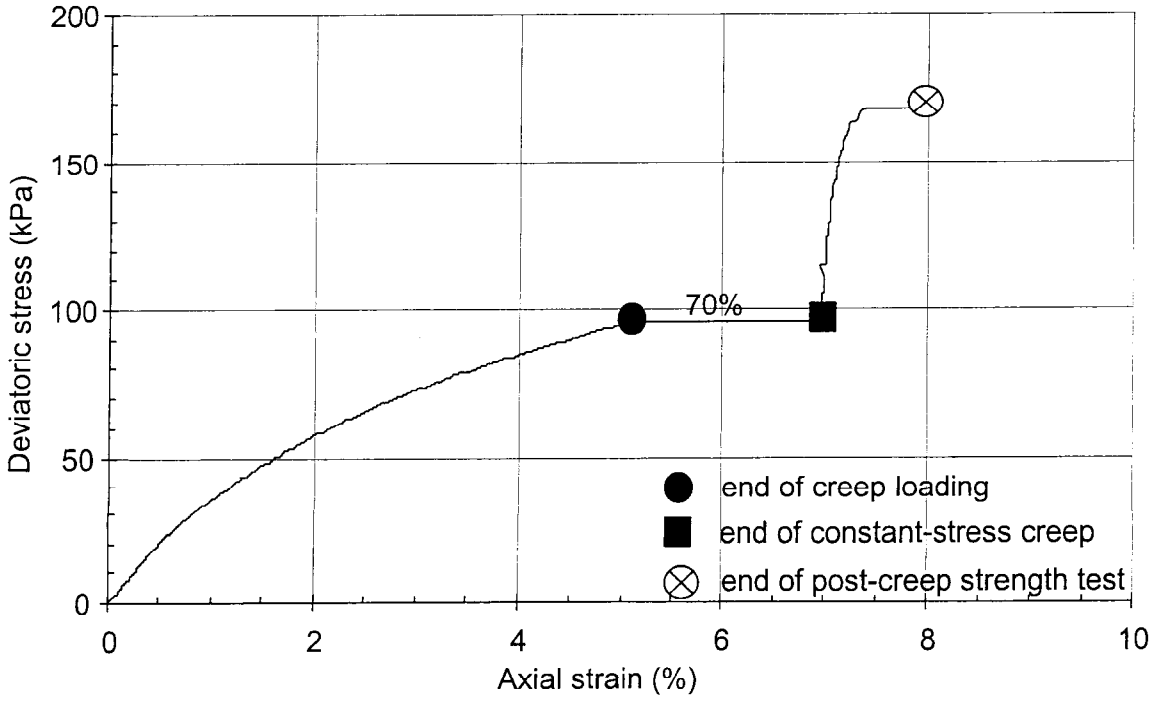

Figure 31. Kapolei Brown clay, composite creep and post-creep stress-strain curves.

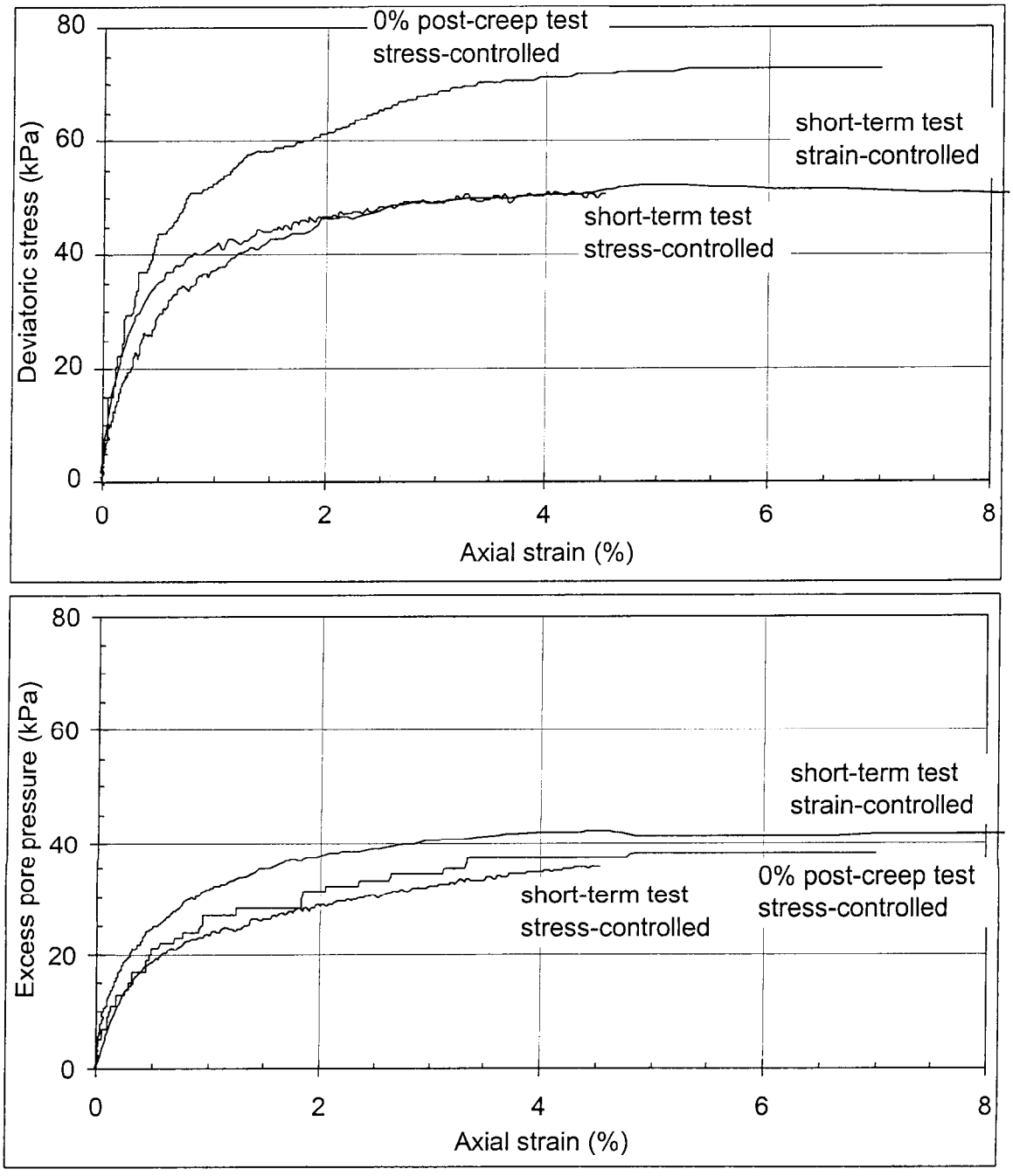

Figure 32. Manoa clay, post-creep stress-strain behavior.

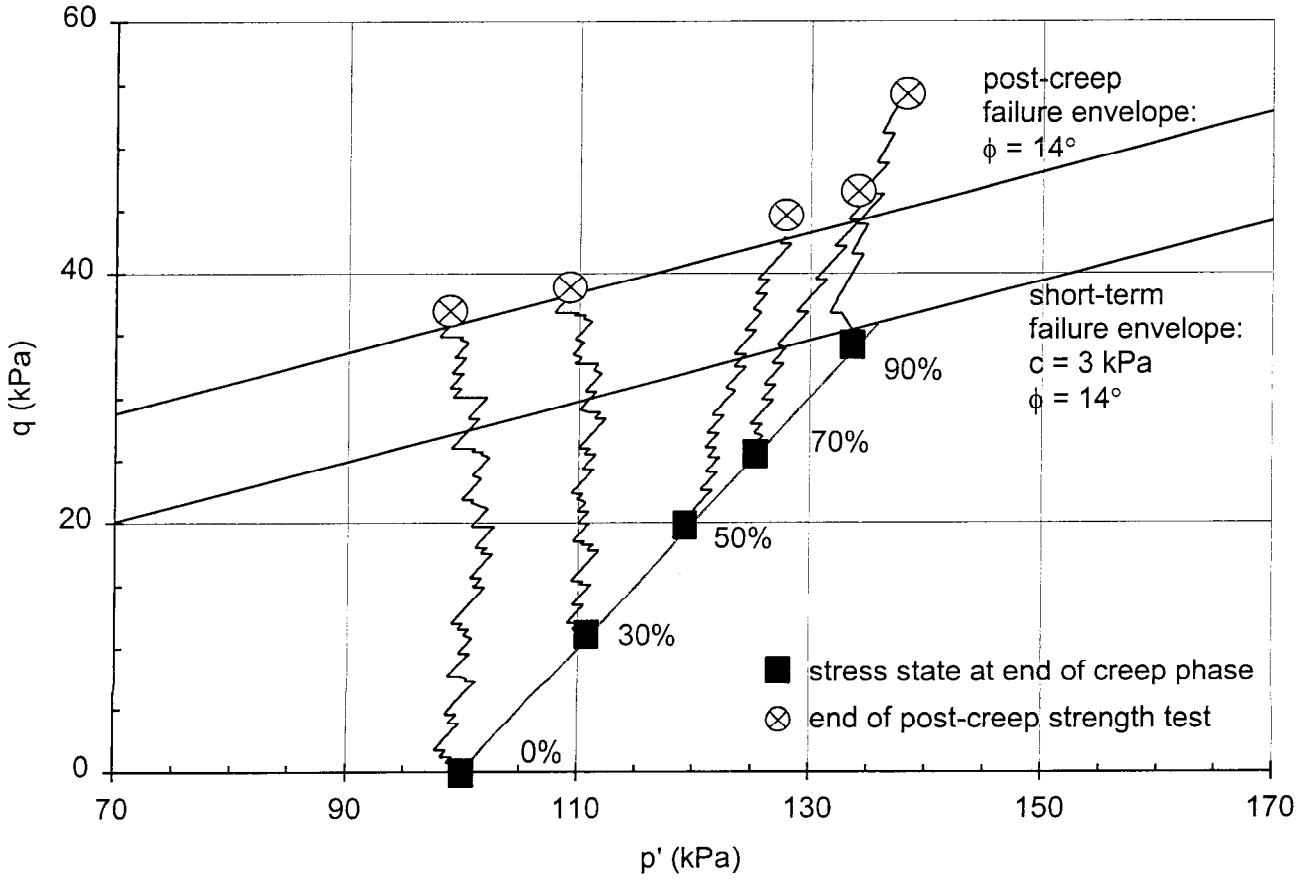

Figure 33. Manoa clay, post-creep stress paths.

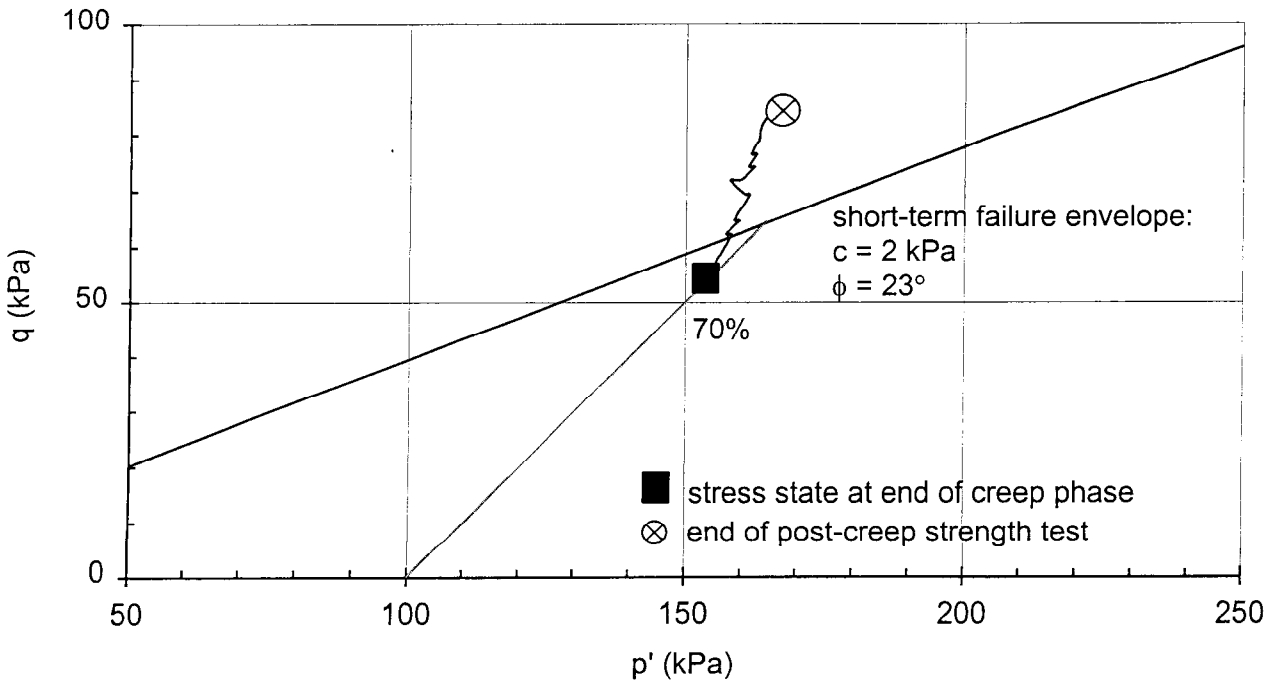

Figure 34. Kapolei Brown clay, post-creep stress paths.

4. Appendix A – Background

Background

Long-term strength and deformation behavior in soils has received considerable attention through the years. These strength loss and deformation characteristics can be significant, and can lead to structural damage and slope failures. Suklje (1961) investigated a landslide caused by possibly centuries of unequal creep deformation of the underlying cohesive strata. These creep deformations overcame the cohesion of the sandstone, conglomerate, and volcanic overburden. The shear strength of the over-consolidated cohesive lower strata was subsequently overcome by creep over a long period, thus leading to the eventual landslide.

Long-term creep deformations have led to structural damage or failure in retaining walls on London clay slopes (Henkel, 1957) and in a reinforced concrete viaduct at Klosters, Switzerland (Haefeli et al, 1953). Some of the downhill displacements occurring on the slopes of Manoa Valley, Aina Haina Valley, and upper Palolo Valley in Hawaii are attributed to creep deformations. These downhill displacements result in significant structural damage to residential homes and streets.

Often, long-term slope failures can be avoided through more thorough investigations of the long-term strength and deformation behavior of the soil. However, the tests required to investigate these characteristics are time consuming and cumbersome. Instead, short-term tests are conducted with a large safety factor to compensate for an overestimation of the long-term strength. This can be a potentially flawed procedure, as it overlooks some of the more specific characteristics of creep behavior. In addition, while many studies have been done on long-term strength and creep behavior, relatively few have been done on tropical soils, and more specifically, Hawaiian soils. Clearly, more investigations must be done to understand the creep behavior of these soils.

The long-term deformation of a soil is the result of several factors, including wet-dry cycles, freeze-thaw cycles, secondary consolidation, and creep. Wetting or freezing will cause the soil layer to expand in a direction perpendicular to the slope. Drying or thawing will cause the soil layer to shrink in a vertical direction. This cycle will result in a gradual zigzag movement down the slope.

Immediate settlement is the elastic deformation of soils with no change in the moisture content. Primary consolidation refers to the dissipation of excess pore pressure through pore water drainage, resulting in a reduction of volume of the soil mass. Secondary consolidation refers to the specific case of volumetric strain that follows primary consolidation, after pore pressures have dissipated. It is the result of the plastic adjustment of soil fabrics while under a constant effective stress. Secondary consolidation can continue long after primary consolidation has ceased, and can be a major contributor to the overall settlement of a structure in the long-term.

Creep is commonly defined as a continuing deformation under a constant state of stress. Most natural and man-made materials creep, but it is of particular concern in fine-grained soils, whose microstructural arrangements and electro-chemical interparticle bonding allow for significant shearing and volumetric compression or swelling over time. Like secondary consolidation, creep

under completely drained conditions involves the adjustment of soil fabrics under a constant effective stress. However, this adjustment will result in time-dependent shear strains in addition to volumetric strains. For the case of creep under limited or non-existent drainage conditions, volume change will also be limited or non-existent. Instead, there can be a change in pore pressures and the sample will be subjected to a change in the effective stresses. Thus, undrained creep involves the adjustment of soil fabrics under a constant total stress, rather than a constant effective stress. This adjustment of soil fabrics results in time-dependent shear strains, but not volumetric strains. For the purposes of this investigation, creep will refer to the specific case of long-term deformation under a constant deviatoric stress.

Long-term strength loss and creep deformations are most prevalent in soft, saturated clays under undrained conditions and overconsolidated clays in drained conditions. Short-term undrained strength tests can overestimate the long-term strength through insufficient pore pressure dissipation within the sample. The use of these short-term strengths can lead to undesirable deformations or eventual failure of the excavation wall. Drained tests can also overestimate the long-term strength of a soil if the dilative effects of an overconsolidated soil are not considered. Over a long period, an overconsolidated soil will tend to dilate, increasing its moisture content and thus weakening the soil. The obvious remedy to avoid these long-term deformations is to perform longer strength tests. However, practicality and cost-efficiency will often override the desire to conduct cumbersome and time-consuming long-term tests in favor of quicker and less expensive short-term tests with an adequate safety factor for compensation.

A.1. General Characteristics

Time-dependent deformations and stress relaxation in soils are important whenever long-term behavior is of concern. Typical time-dependent deformations and stress relaxations are presented in Figure 1.1.

Time-dependent responses may assume a variety of forms depending on soil type, soil structure, stress history, stress system, drainage conditions, and other factors. The result of such effects are sets of randomly appearing creep curves such as those presented in Figure 1.2. However, studies have shown that the fundamental behavior of creep in soils follows a set of logical and often predictable patterns.

Creep typically consists of the three stages shown in Figure 1.3. The transient or primary stage consists of decreasing strain rates over time after the application of stress. This is followed by a period of relatively constant strain rate, termed the steady state or secondary stage. For those soils susceptible to creep rupture, strain rates will increase and the soil will eventually fail. This final stage is termed the tertiary stage.

A true steady between strain and time does not exist, although for some soils part of the strain vs. time curve can be approximated as a straight line. However, a characteristic relationship between strain rate and time does exist for most soils, as presented in Figure 1.4 for undrained creep of Haney clay. At any stress intensity, the logarithm of the strain rate decreases linearly with the logarithm of time. Increases in stress intensities shift the line vertically upwards, but the slope remains essentially independent. This relationship is applicable for undisturbed and

remolded clay, wet clay and dry clay, normally consolidated and overconsolidated soil, and sand. The onset of failure, or creep rupture, is signaled by a reversal in the slope of the relationship as shown by the topmost curves in Figure 1.4. Some soils experience a strength gain during a sustained creep stress. Deformation under a sustained stress can produce an increase in stiffness under both drained and undrained conditions.

The creep strain rate of a specific soil is largely influenced by the creep stress intensity applied to it. Figure 1.5 presents the variation of strain rate with stress intensity at different elapsed times for undrained creep of remolded illite. At low stress intensities the strain rates are small. At the midrange of stress intensities, the relationship between the logarithm of strain rates and stress intensity is nearly linear. At very high stress intensities approaching the strength of the material, strain rates become very large and signal the onset of failure.

A.2 Factors that Influence Creep

Typically, creep effects increase with the plasticity, activity, and water content of the soil. Other factors that can influence the creep effects of a soil are clay type, clay content, aging, and thixotropic hardening. Figures 1.6.a and 1.6.b illustrates how steady state creep rates are influenced by the type of clay, and increase with higher clay contents and plasticity indices. Creep effects are more important for higher water contents than lower water contents. For stresses greater than the preconsolidation pressure, creep effects are greater for sensitive soils than insensitive, remolded soils.

Increases in temperature leads to increases in pore pressure, reduction in effective stress, and subsequent weakening of the soil structure. In creep tests, this can lead to increases in creep rates, as presented in Figure 1.7. In stress relaxation tests, this can lead to decreases in stresses.

The majority of studies done on long-term deformations have been done on isotropically consolidated triaxial samples. In contrast, the majority of soils found in nature are anisotropically consolidated with K_o values ranging from 0.5 or less for normally consolidated clays to values approaching 3.0 for heavily overconsolidated clays. Additionally, deformation conditions in the field often resemble plane strain more closely than triaxial compression. Campanella and Vaid (1974) tested undisturbed Haney clay under different pre-stress histories. Samples were tested in triaxial compression consolidated under isotropic and anisotropic conditions, as well as in plane strain consolidated under anisotropic conditions. Creep behavior varied significantly due to the pre-stress history, as presented in Figure 1.8.

Rapid application of a stress or a strain will lead to pore pressure changes in a saturated soil. During creep, the pore pressures will change slowly if the sample is undrained, or will dissipate with accompanying volume change if the sample is drained. Figure 1.10 shows an increase in pore pressure over time for undrained creep of San Francisco Bay mud. Some samples will display a decrease in pore pressure over time. For a constant total minor principal stress, the magnitude of the pore pressure depends on the volume change tendencies of the soil when subjected to shear distortions. These tendencies are controlled by the void ratio, structure, and effective stress. Soil strength in terms of effective stress does not change during creep. Changes in soil strength during creep in the absence of chemical effects can be attributed to changes in

effective stress due to pore pressure changes in undrained tests and changes in water content due to drainage in drained tests.

Effects of secondary consolidation can complicate the interpretation of pore pressure measurements during creep tests. All tests in Figure 1.9 were allowed to consolidate under an effective confining pressure of 1.0 kg/cm^2 for 1800 minutes before the cessation of drainage and start of the undrained creep test. The test labeled 0 percent refers to a test that was maintained undrained but not subjected to a deviator stress. Inspection of the curves shows that there was a significant amount of pore pressure change 0 percent test. This curve indicates that each of the other tests was influenced by a residual effect from the previous consolidation history. More specifically, this residual effect is reflective of the amount of time allowed for secondary consolidation. Neglecting to allow adequate time for this secondary consolidation will result in pore pressure changes due to this residual effect during all creep tests.

A.3 Creep Rupture

Creep rupture can occur at a sustained creep stress as much as 50 percent less than the peak stress measured in an undrained test where a sample is loaded to failure in a few minutes or hours (Casagrande and Wilson, 1951; Hirst and Mitchell, 1968). Some soils experience a strength gain from deformation under a sustained stress, which can produce an increase in stiffness under both drained and undrained conditions. For soils susceptible to rupture, there is a limiting value of creep stress intensity below which failure does not occur. At stresses above this value, the time to failure increases logarithmically with decrease in the stress level. This long-term strength loss is most prevalent in soft, saturated clays under undrained conditions and overconsolidated clays in drained conditions. Strength loss in soft saturated clays present stability problems immediately after construction. Strength loss in overconsolidated clays present problems in long-term stability.

Mitchell (1976) listed several factors that can lead to the loss of strength during creep:

1. If a significant portion of the strength of the soil is due to cementation and creep deformations lead to the failure of these cemented bonds, then strength will be lost.
2. In the absence of chemical or mineralogical changes, the strength of a soil is dependent on the effective stresses at failure. If these effective stresses changes during creep then the strength will also change.
3. Changes in water content cause changes in strength.
4. In almost all soils, shear causes changes in pore pressures, and thus effective stresses, in undrained deformation and changes in volume, and thus water content, in drained deformation.

In the absence of cementation, for both strength gain and strength loss, the post-creep strength plots on the same effective stress envelope prior to creep (Hirst and Mitchell, 1968, Campanella and Vaid, 1972). If cementation bonds are broken then there will be a change to a different effective stress envelope.

In undrained creep on heavily overconsolidated saturated clays, application of creep stresses will induce negative pore pressures within the sample. Rather than developing uniformly throughout the sample, these negative pore pressures tend to accumulate along planes where high shear strains occur. Over time, there will be a migration of water into the shear plane areas of negative pore pressures. This will lead to softening and a strength decrease of the sample as compared to normal strength tests prior to creep.

In drained creep, the dissipation of negative pore pressures resulting from application of creep stresses will cause dilation within the sample. This dilation will result in a higher water content and thus a lower strength of the sample as compared to normal strength tests prior to creep.

A.4 Rheological Models and Stress-Strain-Time Functions

Rheological models consist of a combination of linear springs, linear and non-linear dashpots, and sliders that provide a reasonable approximation of behavior for certain soils and loading conditions. They are useful conceptually to aid in recognition of elastic and plastic components of deformation. They are also helpful for visualization by analogy of viscous flow that accompanies time-dependent change of structure to a more stable state. Mathematical relationships can be developed using these models to describe creep and stress relaxation. In most cases, these relationships are complex and necessitate the evaluation of several parameters that may not be valid for different stress intensities (Mitchell, 1976). Moreover, none has been proposed that yield relationships as simple as those given by the following equations for stress-strain-time relationships, which depend on only three parameters and the strain at one known time.

The simplicity and uniqueness of the stress-strain-time relationships allow the use of simplified expressions to characterize the behavior of creep. One such relationship, relating the strain rate $\dot{\varepsilon}$ as a function of stress intensity and time, is presented here.

$$\dot{\varepsilon} = Ae^{\alpha D}\left(\frac{t_1}{t}\right)^m \qquad (1.1)$$

where

- A = the value of strain rate $\dot{\varepsilon}$ obtained by projecting the linear portion of the log strain rate vs. creep stress intensity plot at reference unit time t_1 to a value of D = 0, as presented in Figure 1.10.
- α = slope of the linear portion of the log strain rate vs. creep stress intensity plot, as presented in Figure 1.10.
- D = deviatoric stress intensity, which can be taken as the applied deviatoric stress.
- t_1 = a reference unit, for example, 1 minute.
- t = time
- m = absolute value of the slope of the linear portion of the log strain rate vs. log time plot, as presented in Figure 1.4.

Therefore, two plots are needed to complete equation 1.1; the log strain rate vs. log time plot, which can be obtained from one creep test, and the log strain rate vs. stress intensity, which can be obtained from at least two creep tests. A minimum of one creep test is needed to find the value of m for a soil. A minimum of two creep tests at different creep stress intensities are needed to establish values of A, and α for a soil. Using this equation, the creep rate behavior for different creep stress intensities can be found. This simple three-parameter relationship has been found suitable for a variety of soils.

Integration of equation 1.1 gives the general relationship between strain ε and time. Two solutions are obtained, depending on the value of m. If $\varepsilon = \varepsilon_1$ at $t = 1$ and $t_1 = 1$, then

$$\varepsilon = \varepsilon_1 + \frac{A}{1-m} e^{\alpha D}\left(t^{1-m} - 1\right) \qquad (m \neq 1) \qquad (1.2)$$

and

$$\varepsilon = \varepsilon_1 + A e^{\alpha D} \ln t \qquad (m = 1, t = 1) \qquad (1.3)$$

Equations 1.2 and 1.3 have been shown to fit actual creep data well (Singh and Mitchell, 1968).

Soils with values of the parameter m less than 1.0 in equations 1.1 to 1.3 are indicative of a high potential strength loss during creep and eventual creep rupture (Singh and Mitchell, 1969). Examples of creep rupture are presented in the topmost curves in Figure 1.4. The onset of creep rupture is marked by the minimum strain rate $\dot{\varepsilon}_{min}$. Strain rates then increases until rupture. The minimum strain rate $\dot{\varepsilon}_{min}$ decreases and the time to failure increases as the creep stress intensity decreases, as shown in Figure 1.4.

This relationship between the minimum strain rate $\dot{\varepsilon}_{min}$ and the time to failure t_f is unique, as presented in Figure 1.11, and can be expressed by the equation

$$t_f = \frac{C}{\dot{\varepsilon}_{min}} \qquad (1.4)$$

where

$$C = (1-m)\varepsilon_f \qquad (1.5)$$

ε_f = strain at failure

Equations 1.1 to 1.3 describe the strain rate-time behavior until $\dot{\varepsilon}_{min}$ is reached. The time to failure t_f can be expressed as

$$\ln t_f = \frac{1}{(1-m)}\left[\ln\left(\frac{C}{A}\right) - \alpha D\right] \qquad (1.6)$$

The strain at failure, taken as corresponding to the minimum strain rate, is a constant independent of the creep stress intensity and the strain rate. It can be determined be either a creep rupture test or by a constant rate of strain test, as strain at failure is independent of test type. Parameter m can be determined by a creep test, and parameters A, and α can be determined from two creep tests at different creep stress intensities, as discussed earlier.

A.5 PROJECT OBJECTIVES

While there have been numerous studies on soil creep, relatively few have been conducted on tropical soils, and more specifically, Hawaiian soils. In addition, the majority of the creep studies have concentrated on creep under undrained conditions, with the tests lasting for about a week. Nicholson, Fujiii, and Russell (1995) studied the creep effects and deformation characteristics of Manoa clay, Waianae clay, and Kaneohe clay. Both drained and undrained tests were conducted on compacted soil samples for an average of three months each. The soils were of moderate to high plasticity and displayed time dependent stress-strain characteristics. The study indicated that all three soils showed m-values less than 1, indicative of significant creep potential and strength loss potential over time.

The majority of the creep tests were undrained. Nicholson et al concluded that drained creep tests would be more useful for the following reasons:

1. The soil samples were likely overconsolidated and potentially dilative.
2. A combination of testing results and theoretical mechanics indicate the creep is not generally a function of pore pressure build-up from undrained conditions but a rearrangement of clay particles and structure under drained conditions.
3. Creep is a long-term process that is conventionally considered best represented by drained conditions.

The objective of this study is to build on the research done by Nicholson et al by conducting long term creep tests on common tropical Hawaiian soils under drained conditions. The majority of creep tests should be conducted for at least 3 months each, unless the soil undergoes creep rupture first. Drained conditions will allow for possible particle rearrangement that may lead to strength loss over time. Creep tests are time-consuming and expensive. For this reason, this study will concentrate on investigating creep potential and time-dependent stress-strain behavior and correlating these characteristics with soil physical properties such as plasticity indices. Data obtained from this study can also be used for constitutive models for accurate analysis of generic geotechnical problems through the use of appropriate numerical formulations.

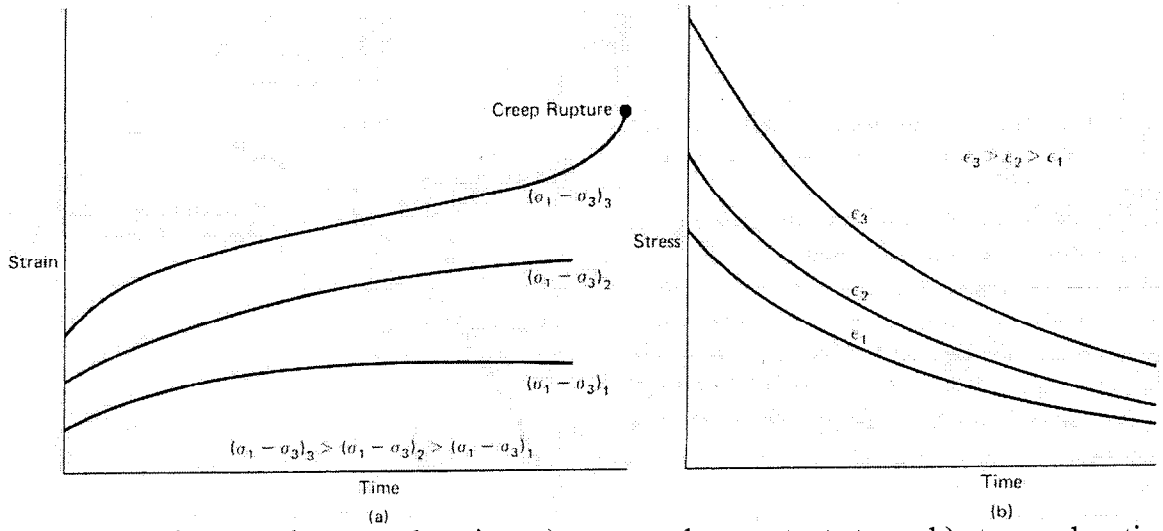

Figure 1.1. Creep and stress relaxation: a) creep under constant stress, b) stress relaxation under constant strain (Mitchell, 1976)

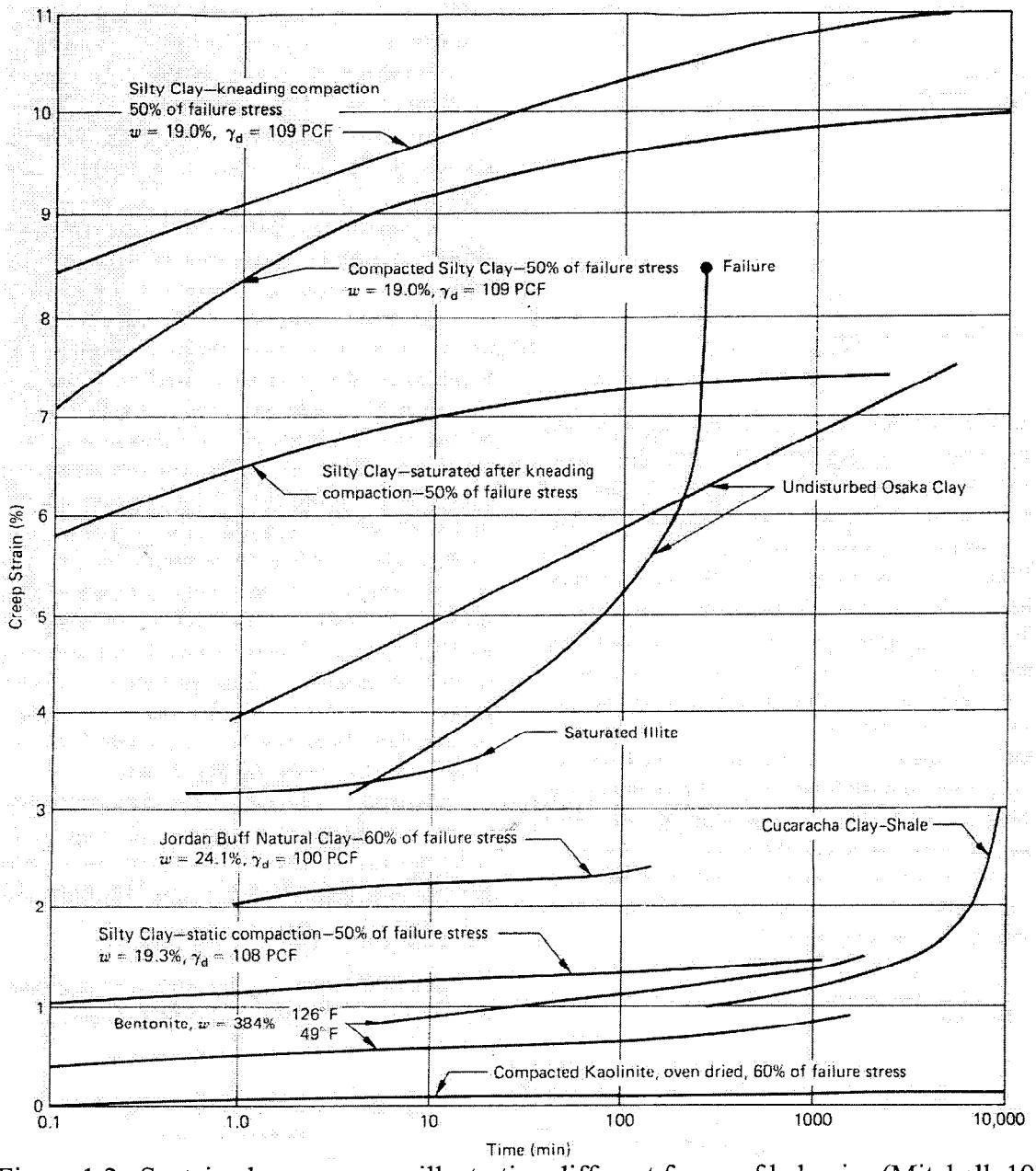

Figure 1.2. Sustained creep curves illustrating different forms of behavior (Mitchell, 1976)

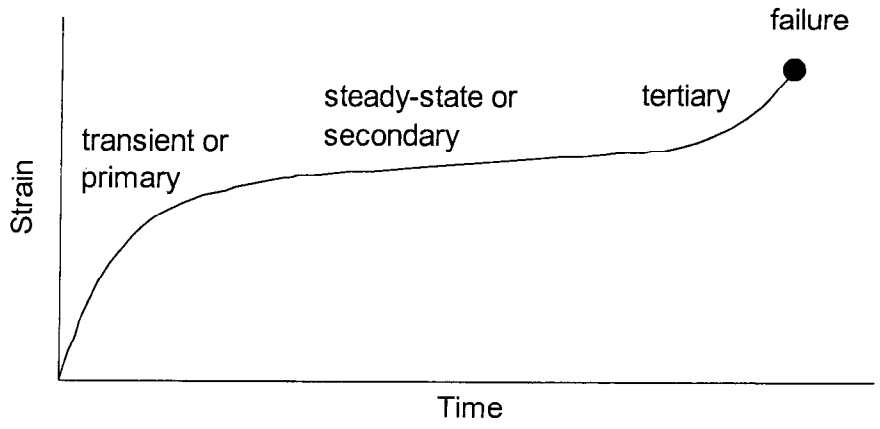

Figure 1.3. Stages of creep

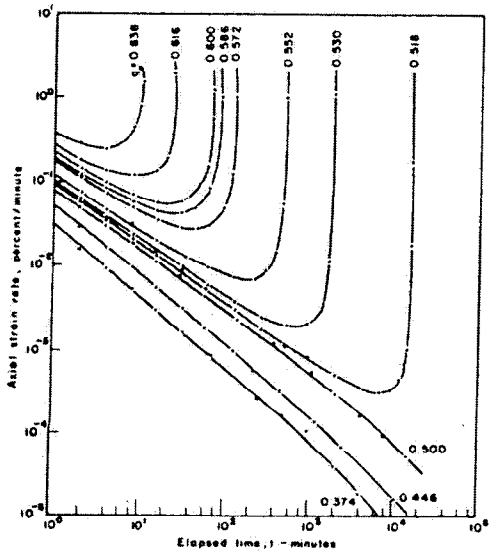

Figure 1.4. Strain rate vs. time for undrained creep of Haney clay (Campanella and Vaid, 1974)

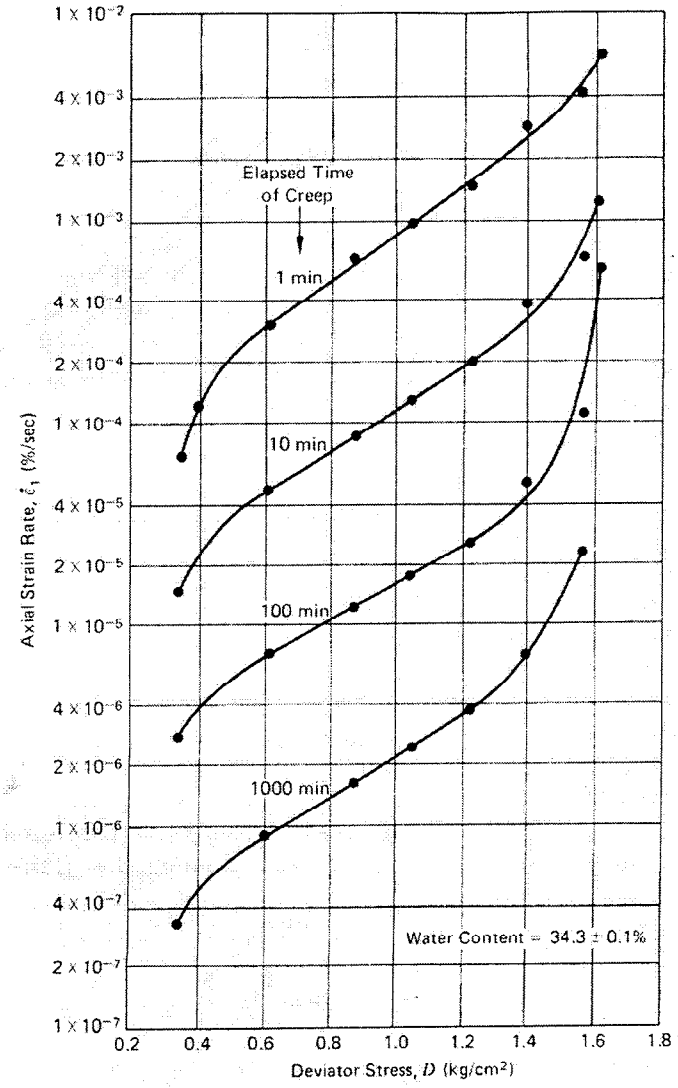

Figure 1.5. Strain rate vs. deviator stress for undrained creep of remolded illite (Mitchell, 1976)

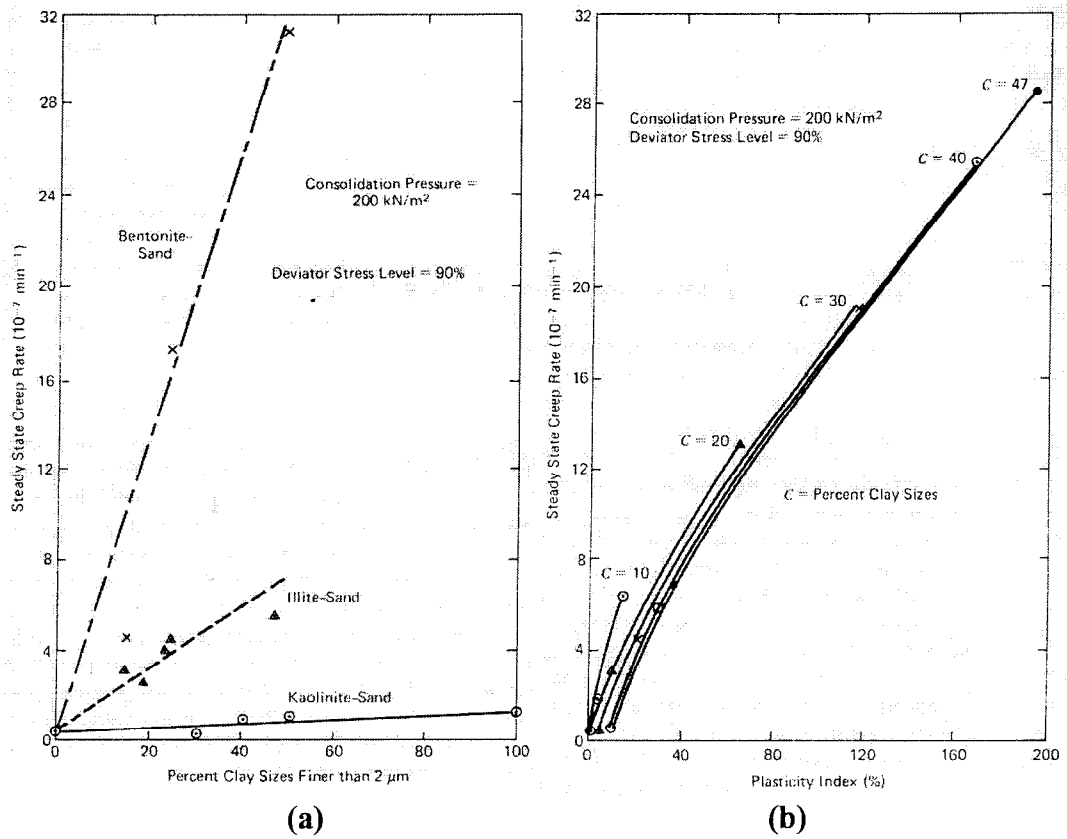

Figure 1.6. Relationship between steady-state creep rate and a) amount and type of clay, b) clay content and plasticity index (Mitchell, 1976)

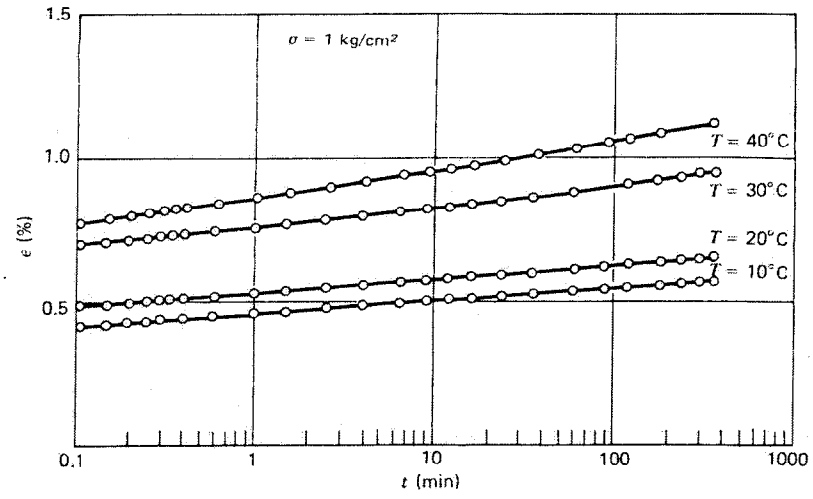

Figure 1.7. Creep curves for Osaka clay tested at different temperatures, undrained triaxial compression (Muruyama, 1969, reprinted from Mitchell, 1976)

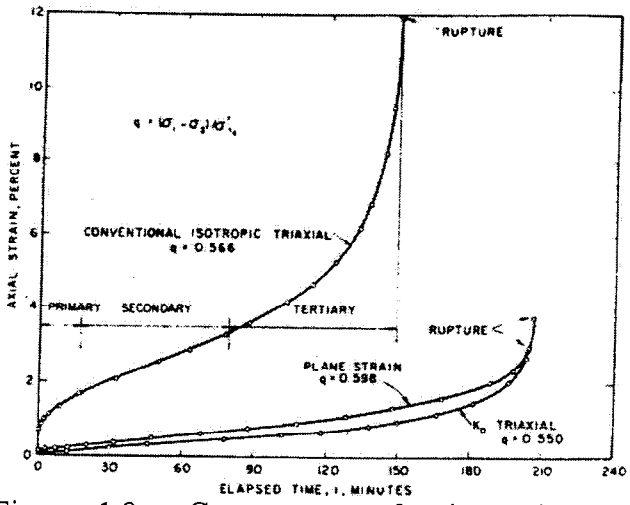

Figure 1.8. Creep curves for isotropically and anisotropically consolidated samples of undisturbed Haney clay tested in triaxial and plane strain compression (Campanella and Vaid, 1974)

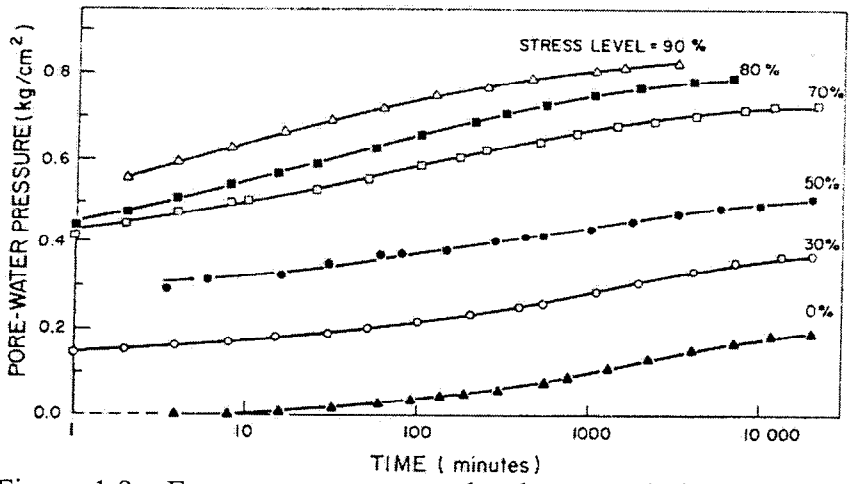

Figure 1.9. Excess pore pressure development during undrained creep of San Francisco Bay mud (Holzer, Hoeg, and Arulanandan, 1973)

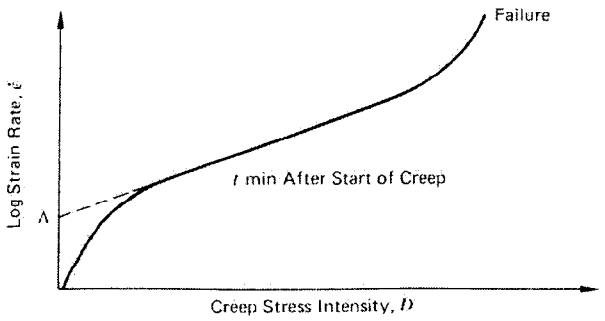

Figure 1.10. Influence of creep stress intensity on creep rate (Mitchell, 1976)

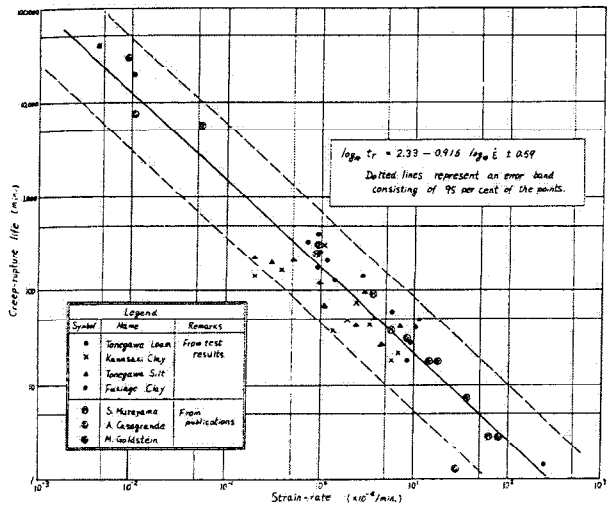

Figure 1.11. Relationship between time to failure and minimum strain rate (Saito and Uezawa, 1961)

5. Appendix B – Index Properties and Strength Tests

Index Properties and Strength Tests

Included in this appendix are miscellaneous results from the soil characterization program, one-dimensional consolidation tests, and strength tests. These figures are presented here for general reference and are discussed in some detail in Nakayama (2000).

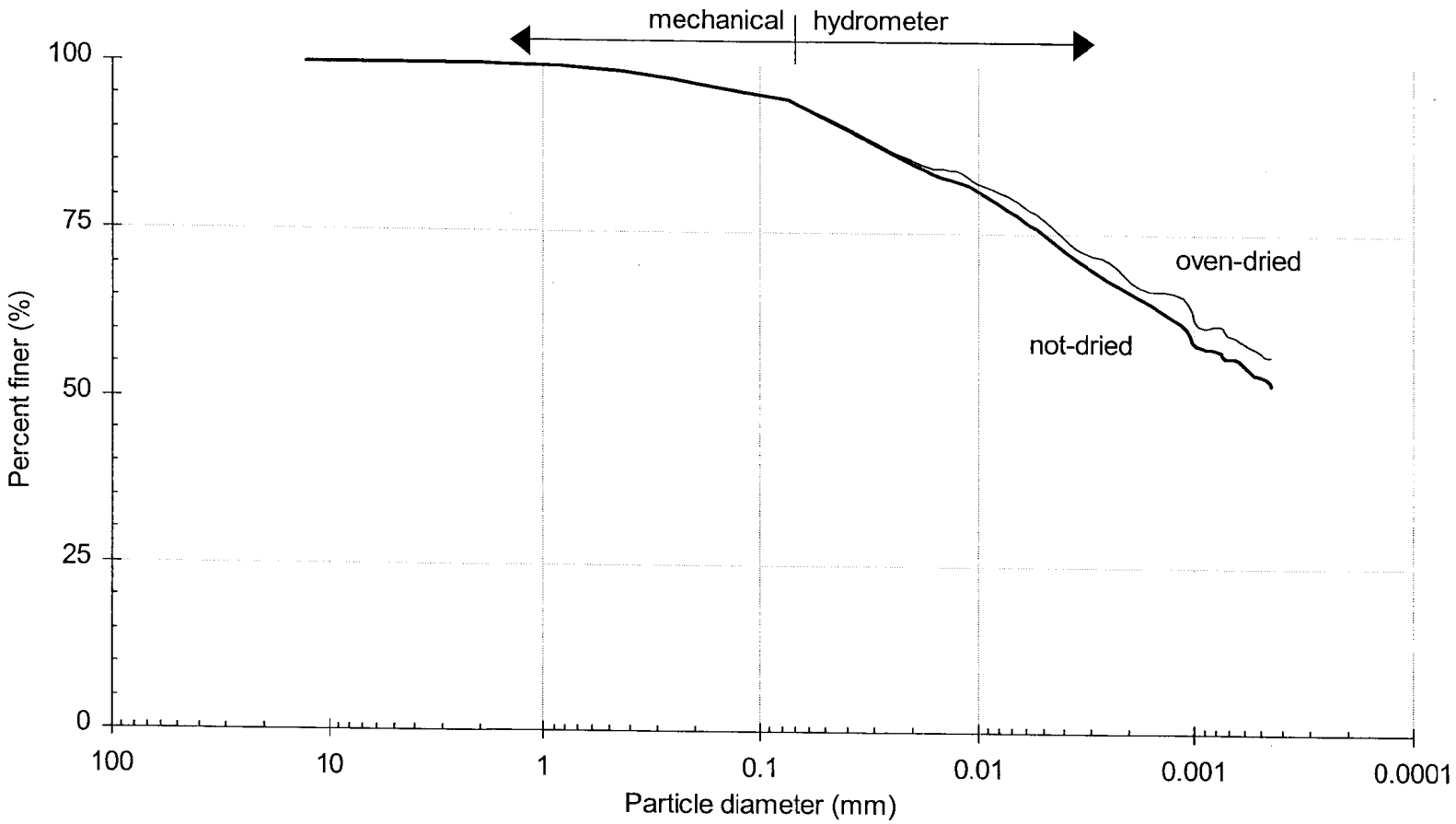

Figure B1. Manoa Clay – consolidation test: Grain size distribution.

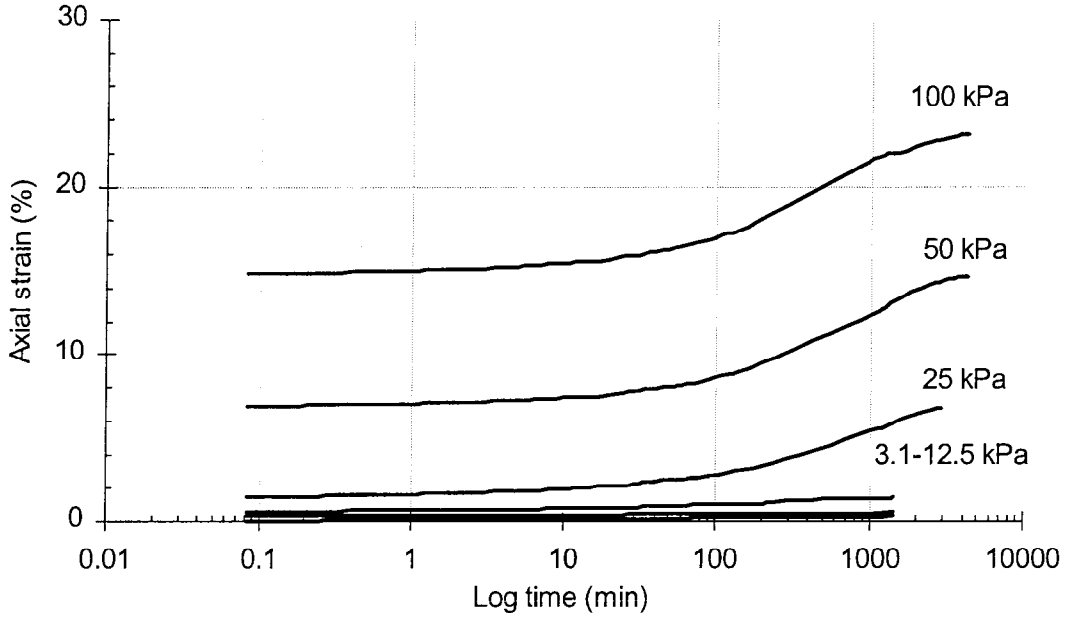

Figure B2. Manoa clay – consolidation test: Axial strain vs. time.

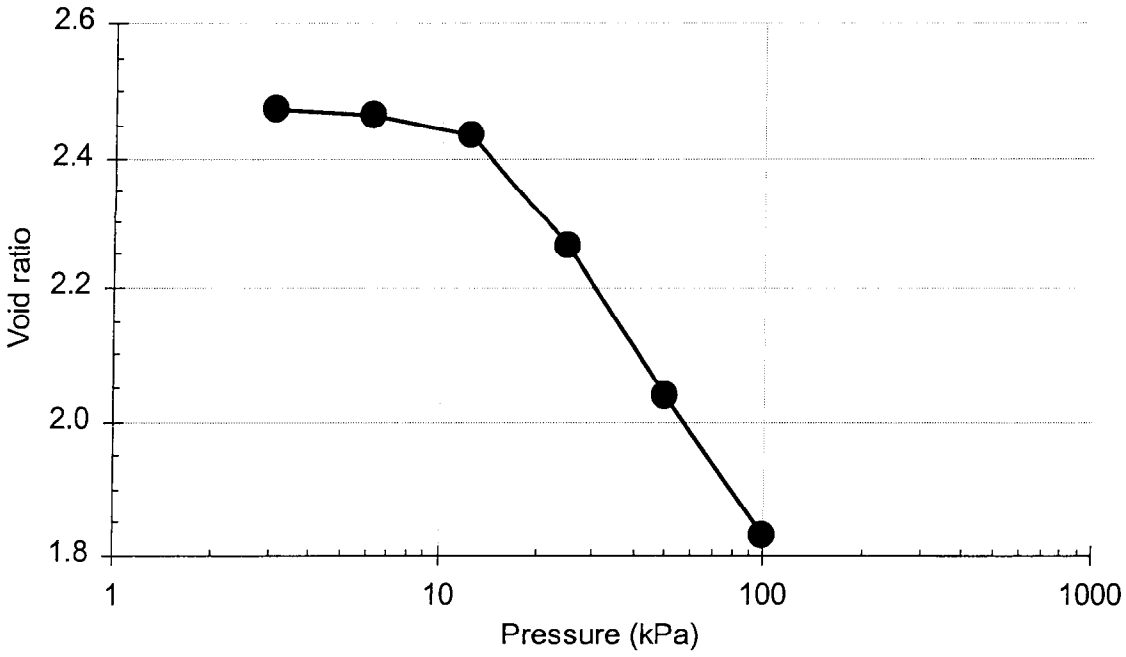

Figure B3. Manoa clay – consolidation test: Void ratio vs. pressure.

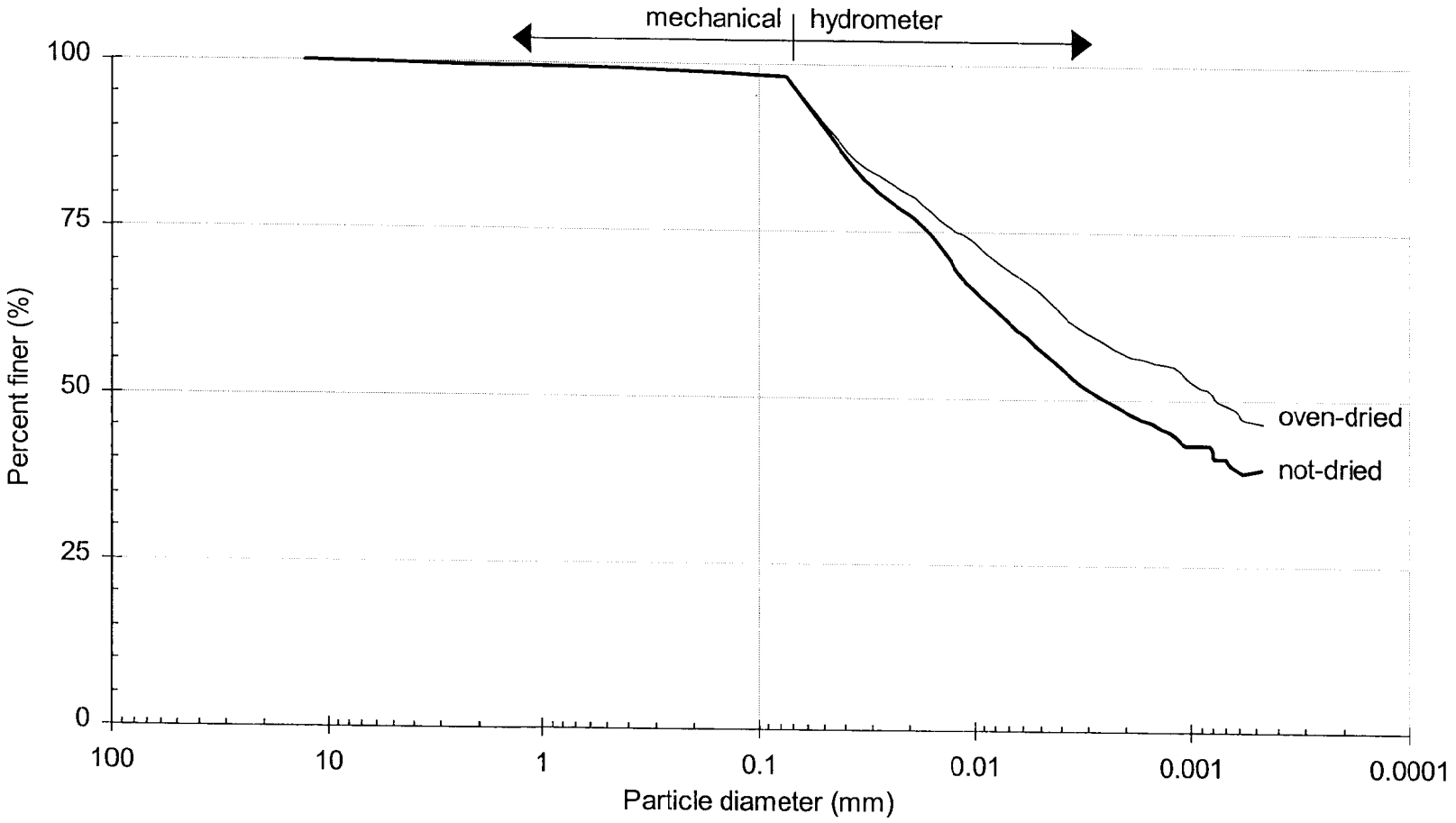

Figure B4. Kapolei Red silt – consolidation test: Grain size distribution.

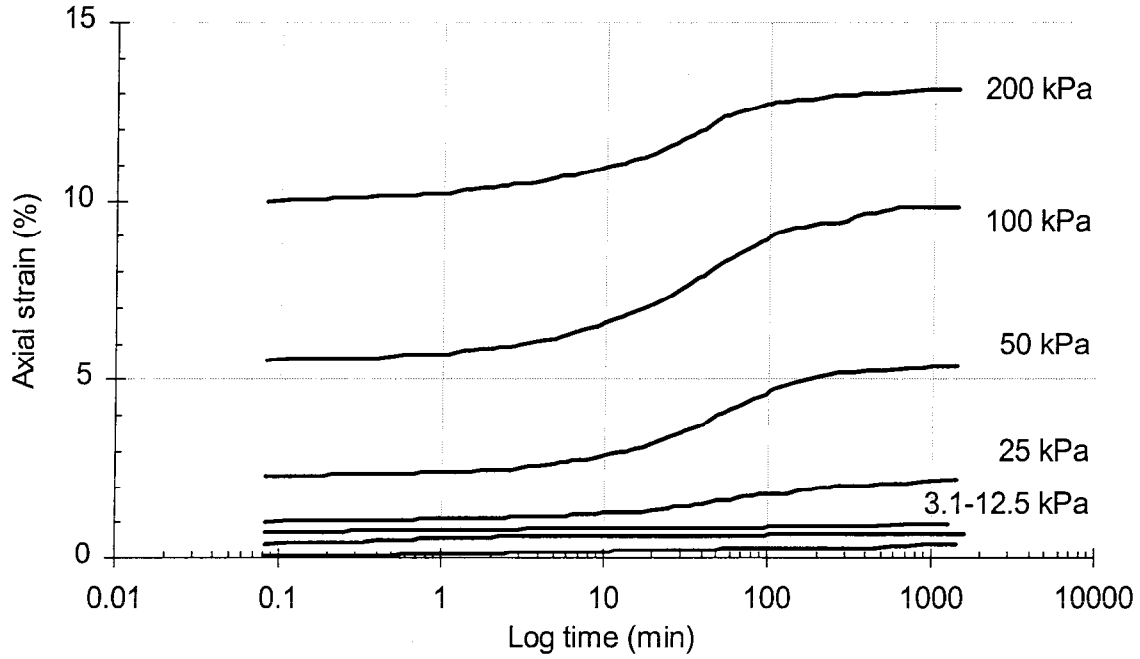

Figure B5. Kapolei Red silt – consolidation test: axial strain vs. time.

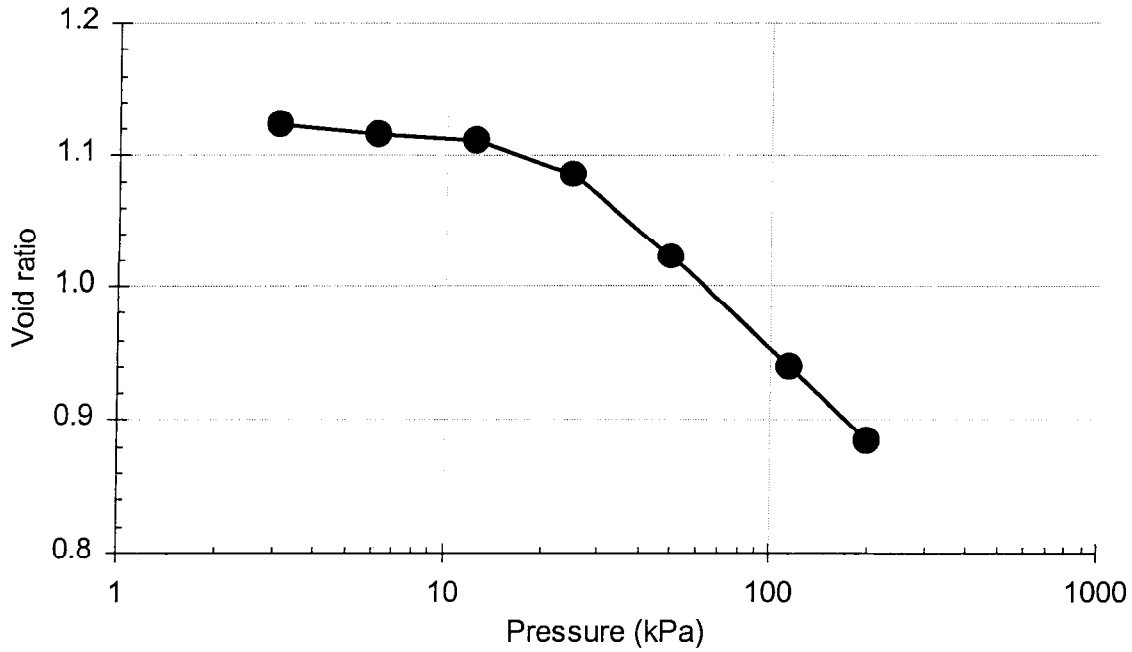

Figure B6. Kapolei Red silt – consolidation test: void ratio vs. pressure.

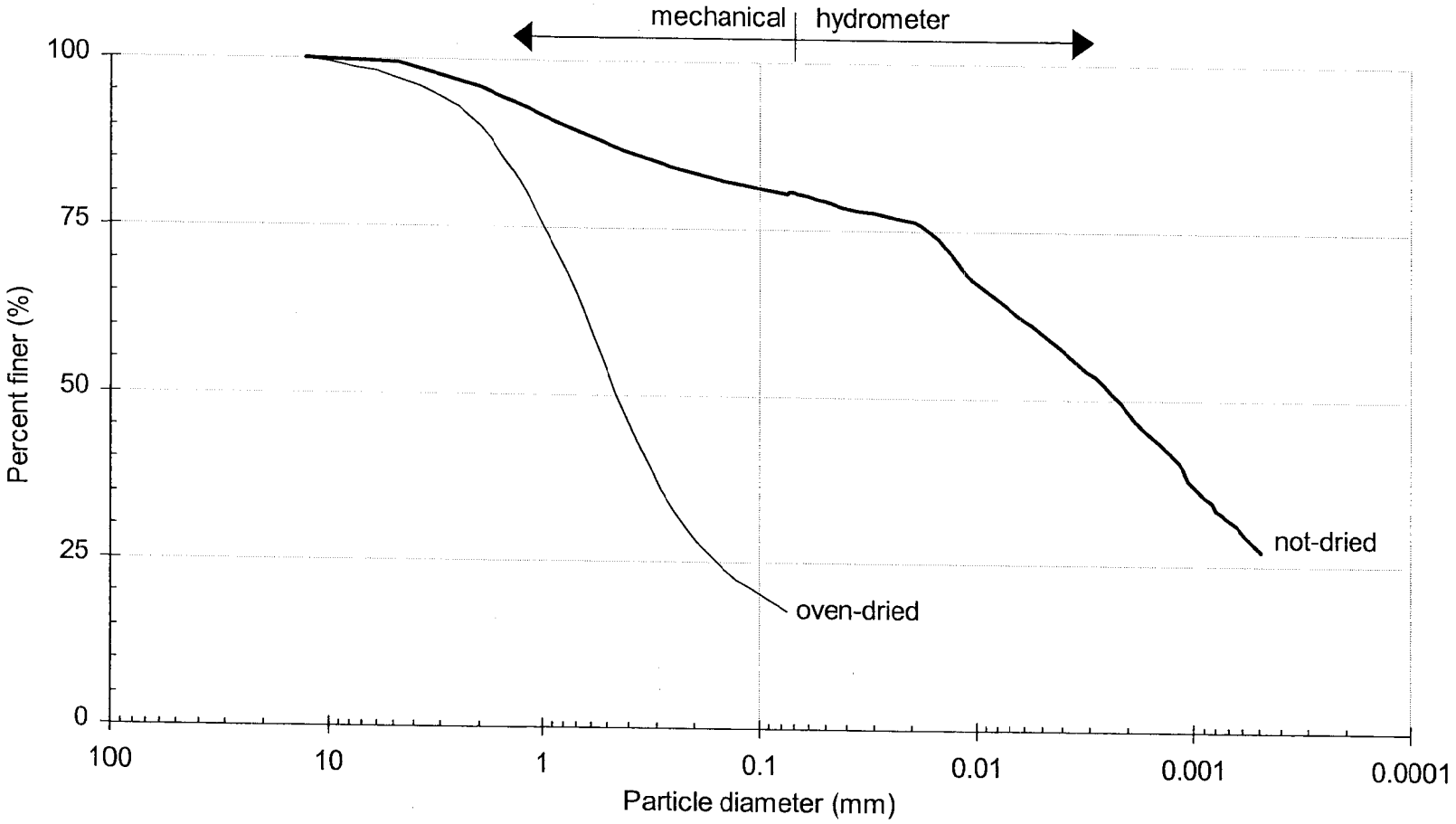

Figure B7. Hilo Ash soil – consolidation test: grain size distribution.

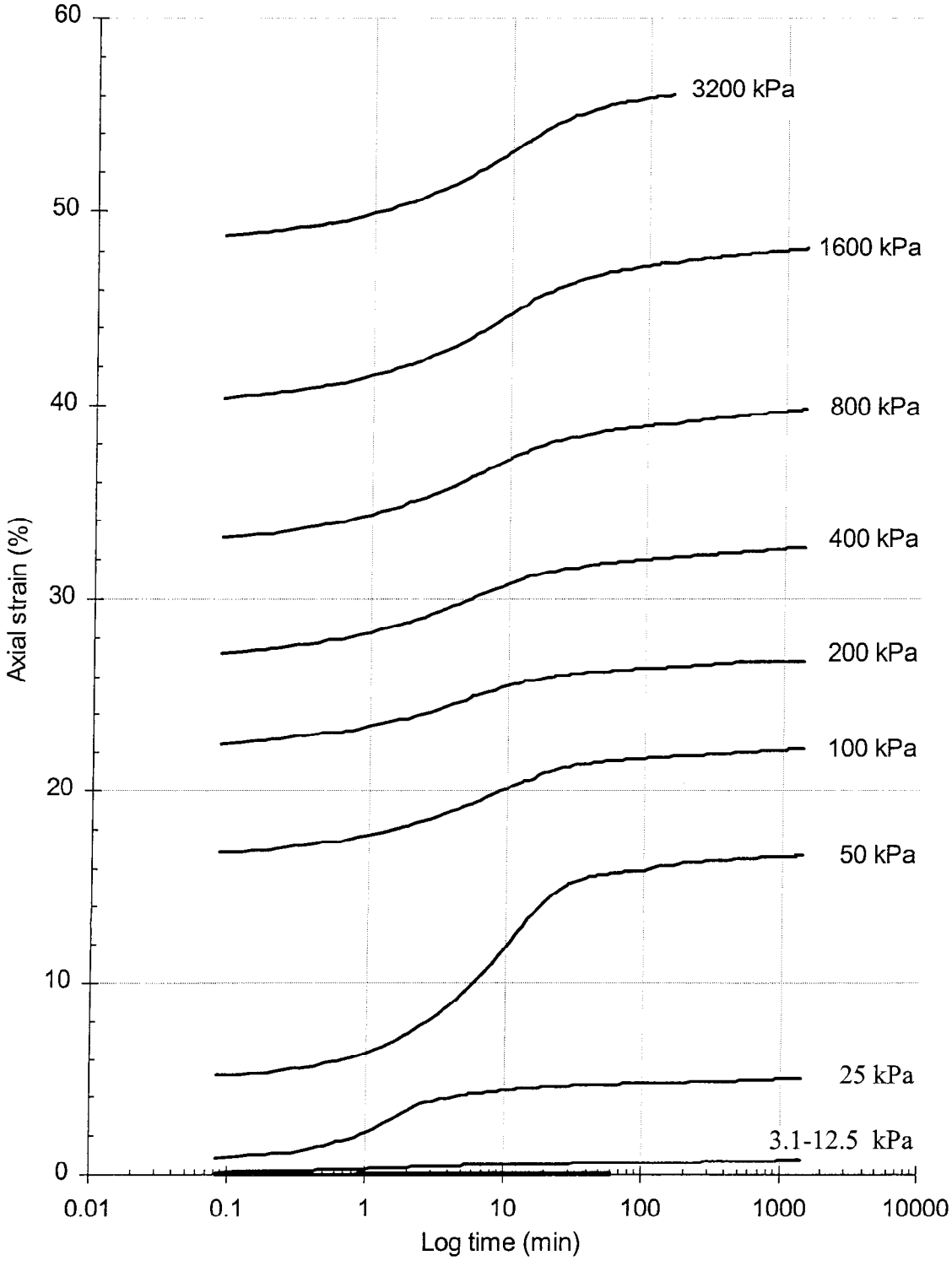

Figure B8. Hilo Ash soil – consolidation test: Axial strain vs. time

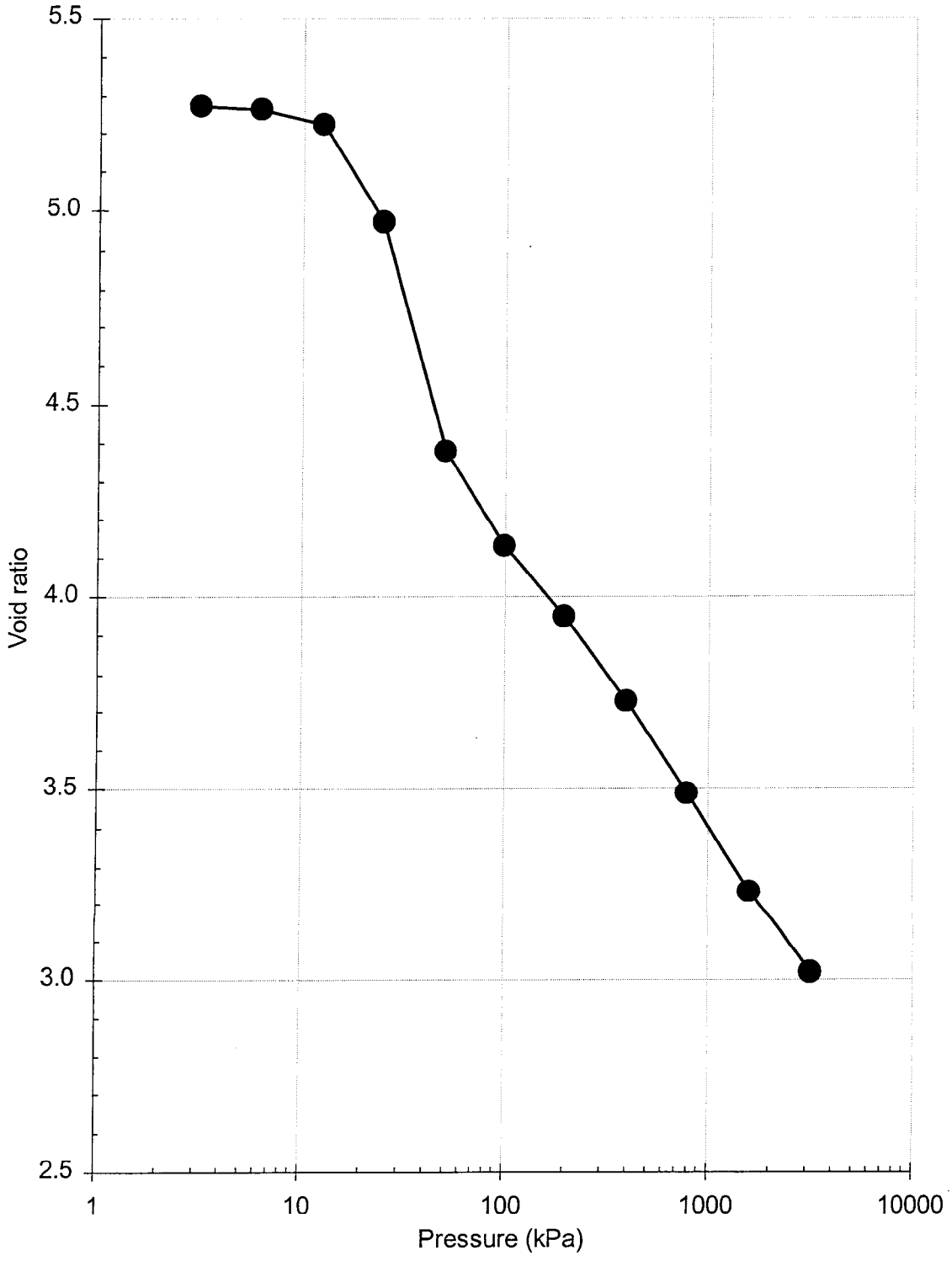

Figure B9. Hilo Ash soil – consolidation test: Void ratio vs. pressure

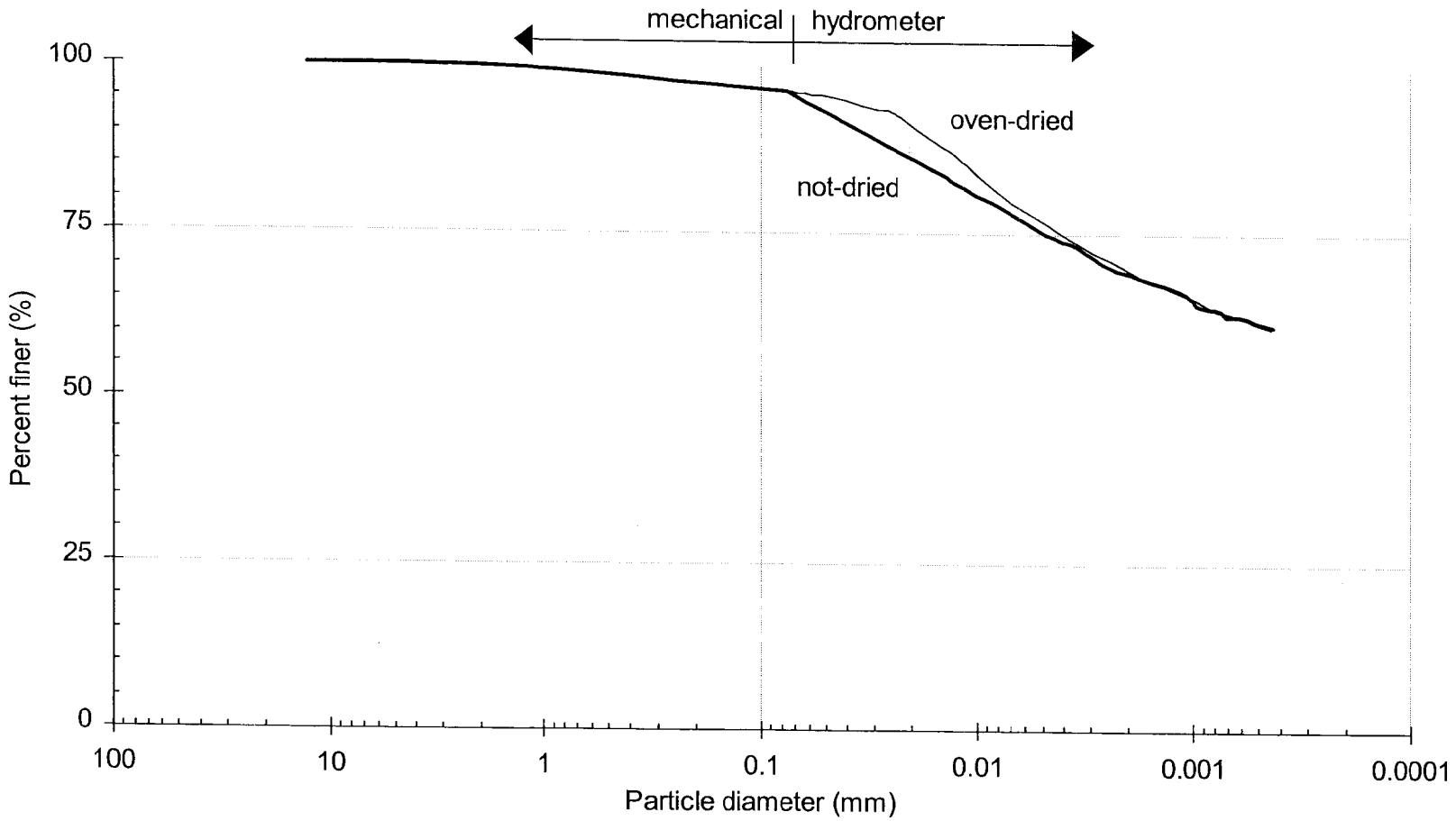

Figure B10. Kapolei Brown clay – consolidation test: Grain size distribution

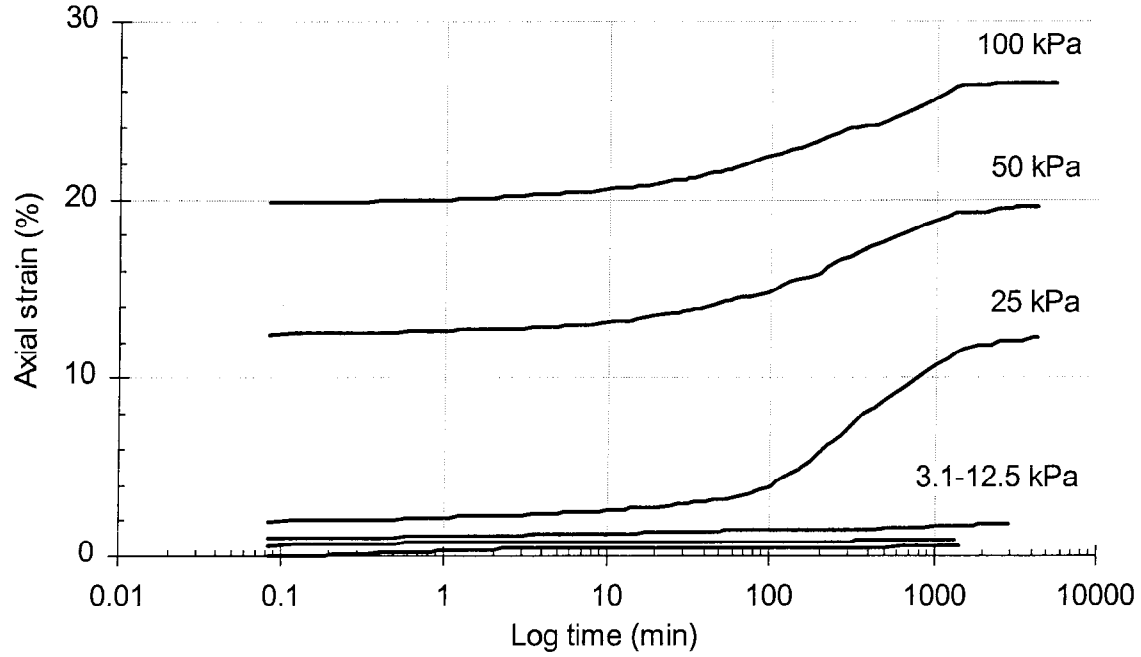

Figure B11. Kapolei Brown clay – consolidation test: Axial strain vs. time

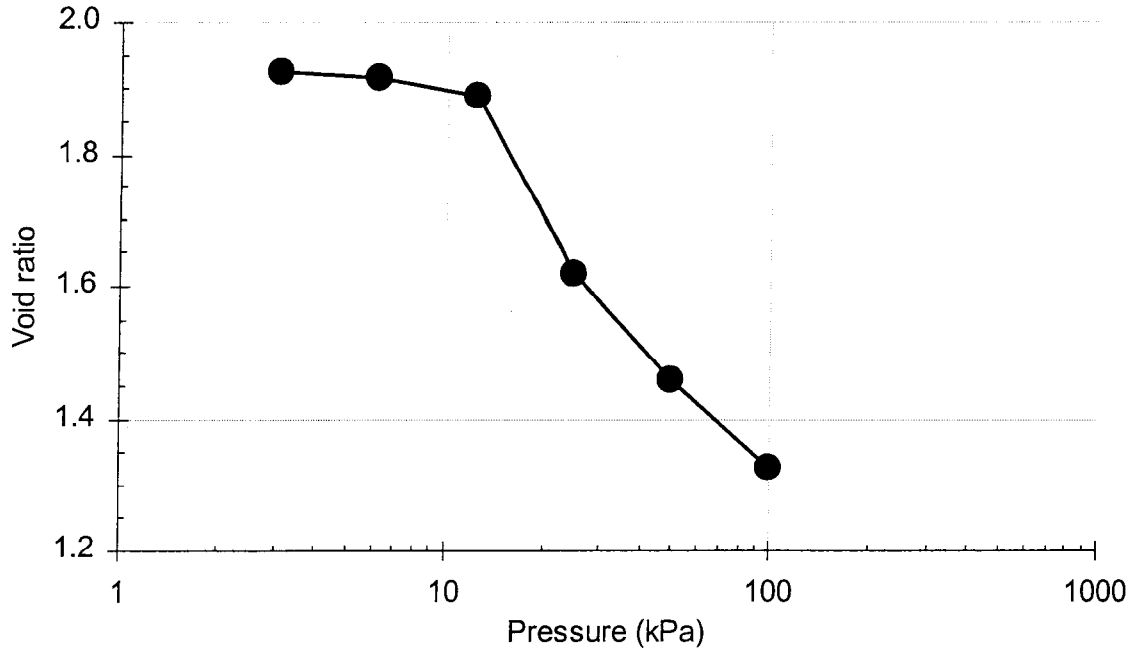

Figure B12. Kapolei Brown clay – consolidation test: Void ratio vs. pressure

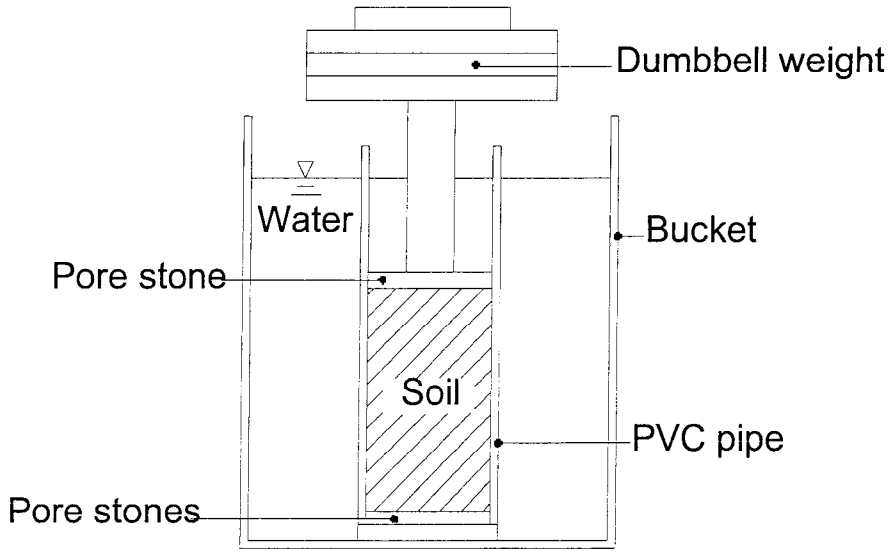

Figure B13. PVC pipe sample consolidation set-up (not drawn to scale)

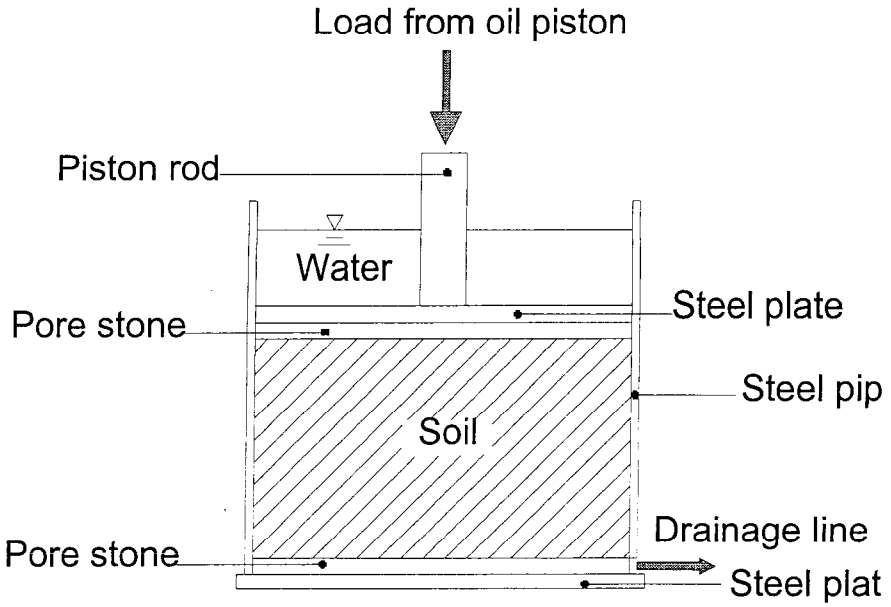

Figure B14. Steel pipe sample consolidation set-up (not drawn to scale)

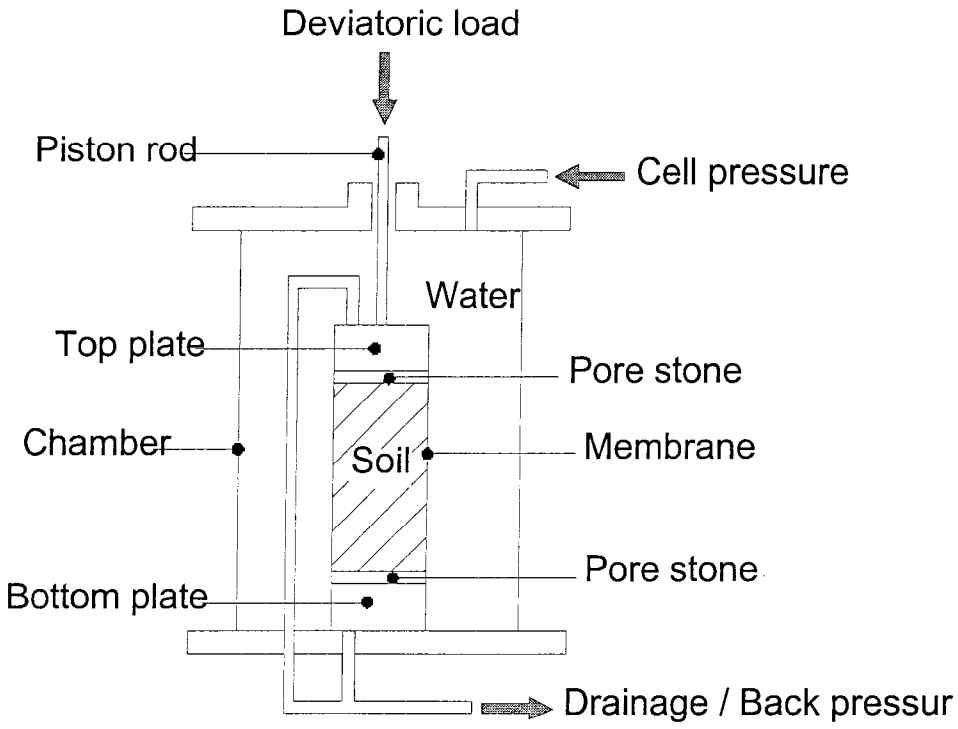

Figure B15 Triaxial cell (not drawn to scale)

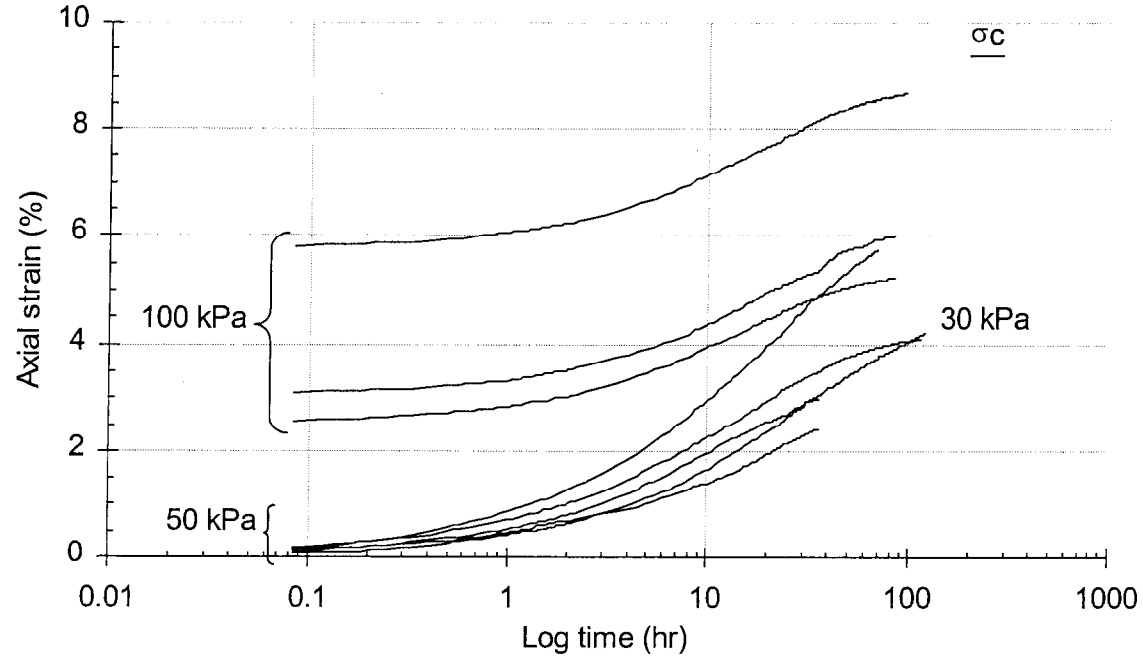

Figure B16 Manoa clay, isotropic consolidation for CU strength tests: Axial strain vs. log time.

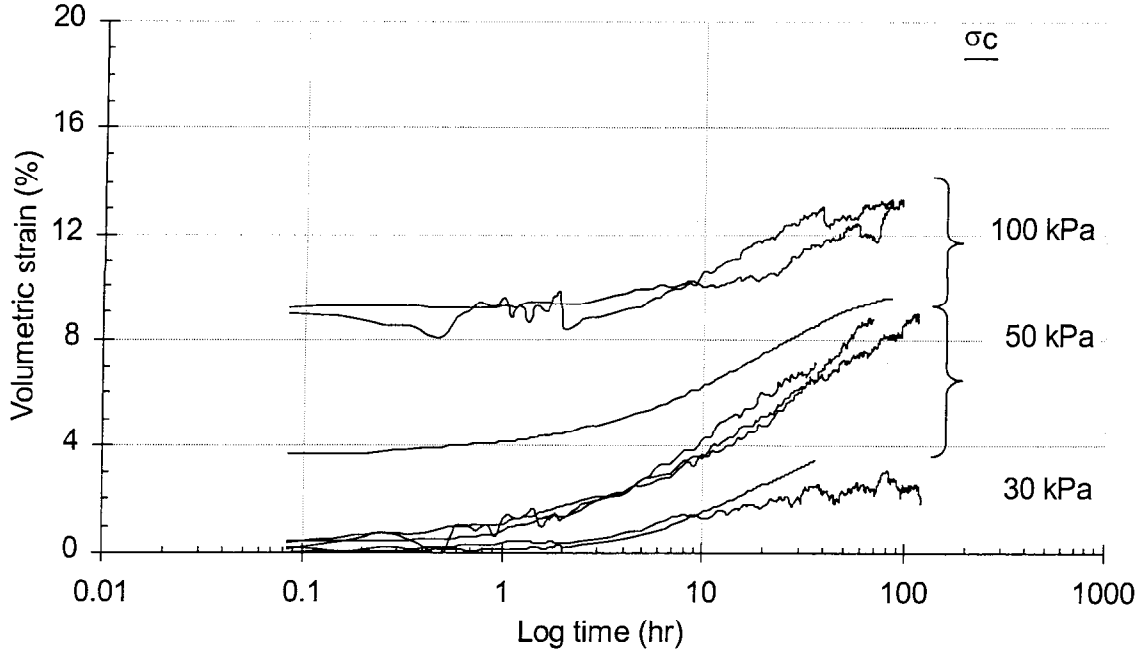

Figure B17 Manoa clay, isotropic consolidation for CU strength tests: Volumetric strain vs. log time.

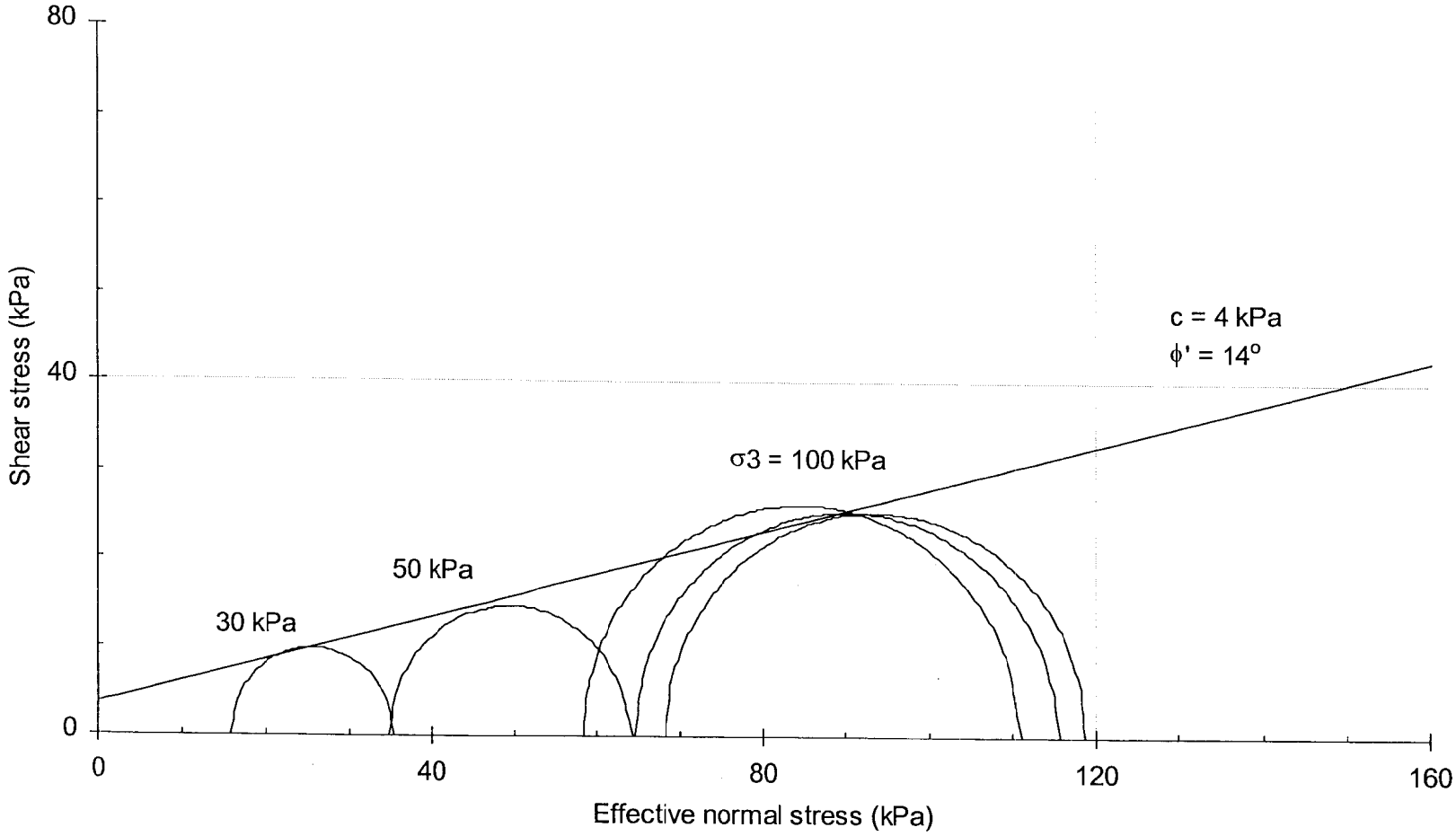

Figure B18 Manoa clay, CU strength tests: Effective stress failure envelope.

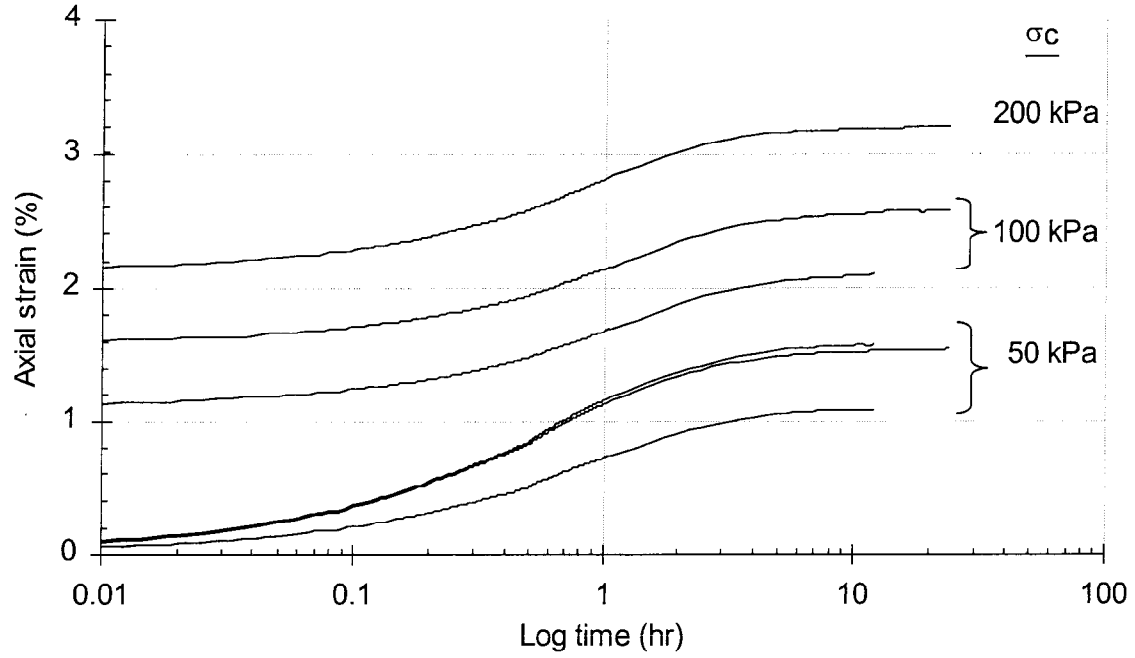

Figure B19 Kapolei Red silt, isotropic consolidation for CU strength tests: Axial strain vs. log time

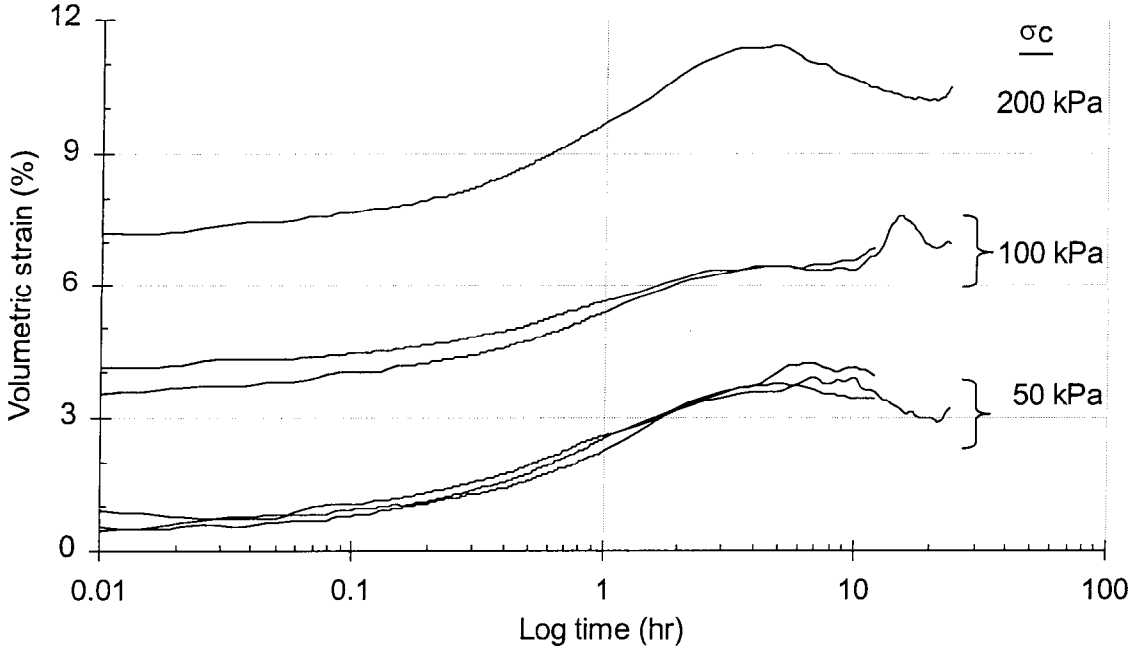

Figure B20 Kapolei Red silt, isotropic consolidation for CU strength tests: Volumetric strain vs. log time

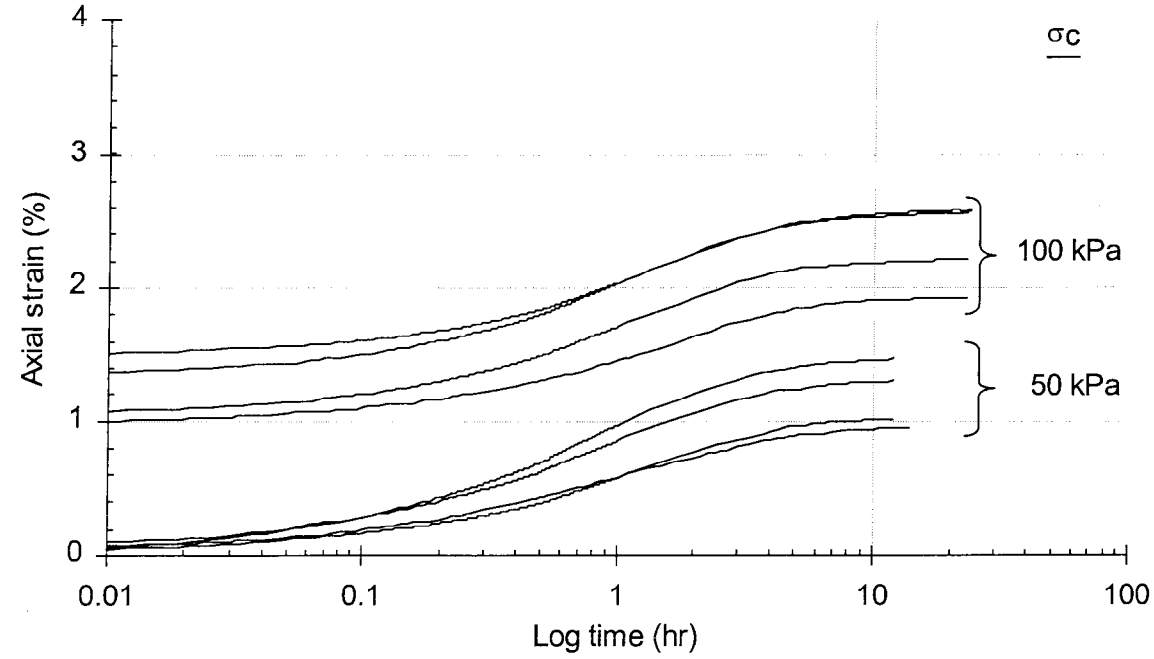

Figure B21 Kapolei Red silt, isotropic consolidation for CD strength tests: Axial strain vs. log time

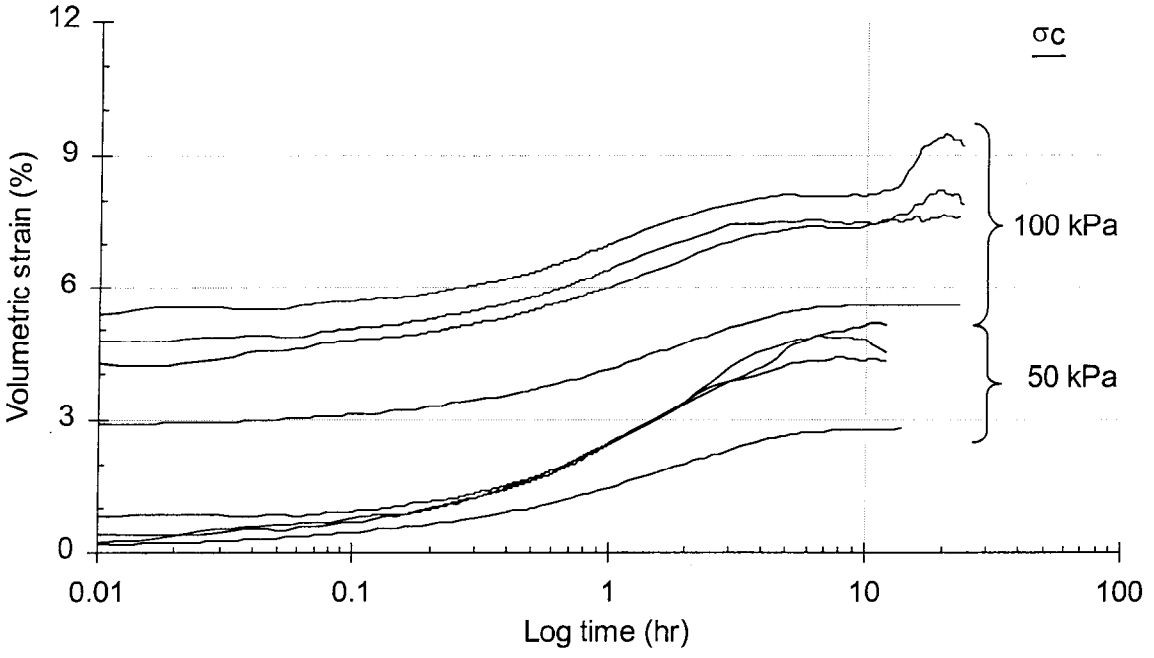

Figure B22 Kapolei Red silt, isotropic consolidation for CD strength tests: Volumetric strain vs. log time

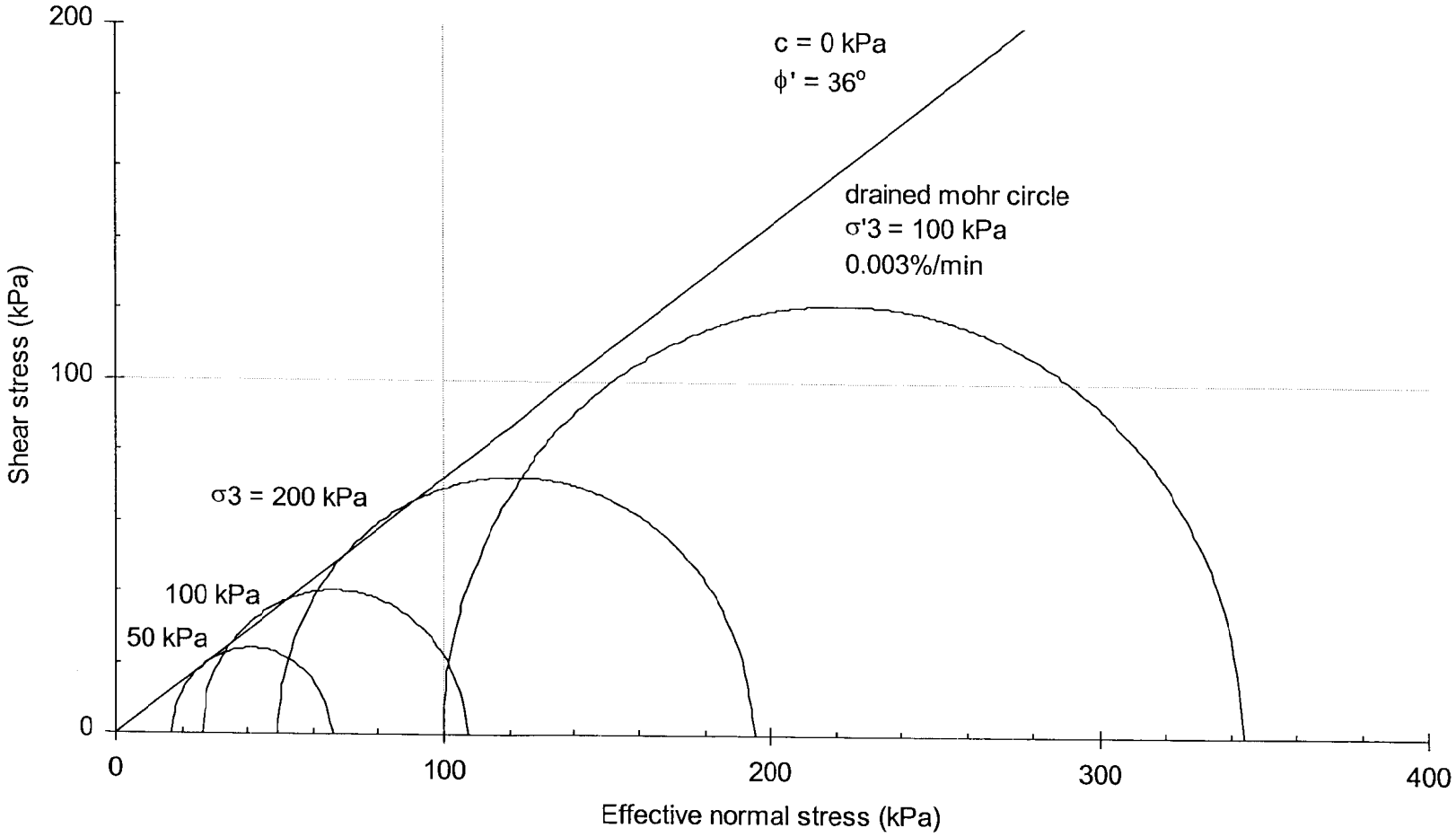

Figure B23 Kapolei Red silt, CU and CD strength tests: Effective stress failure envelope.

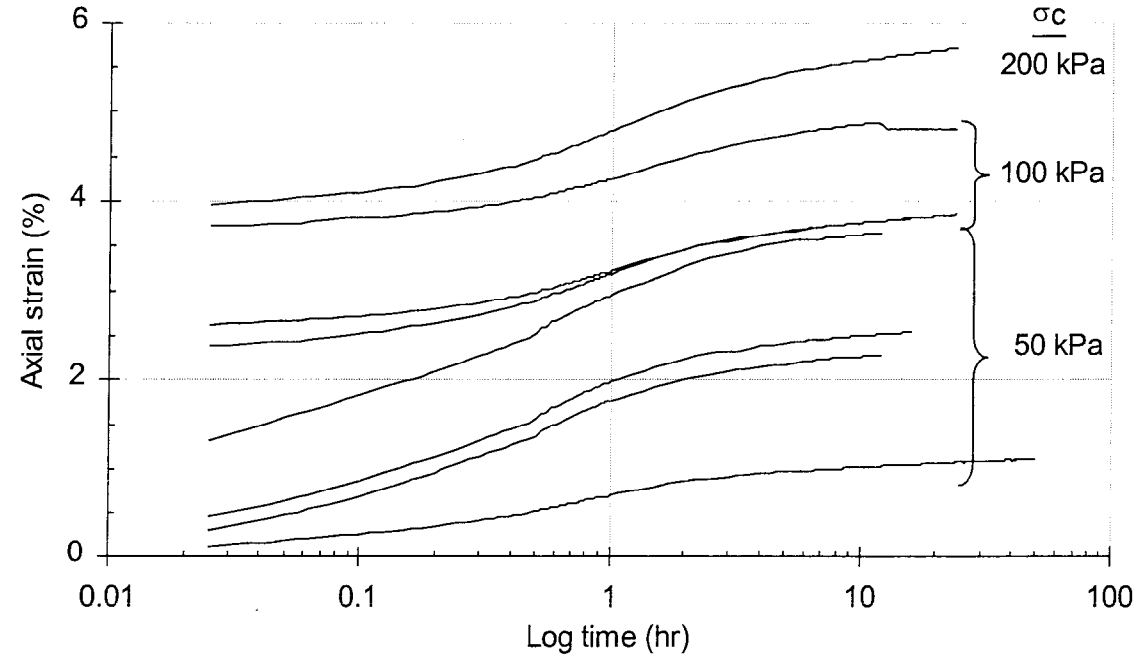

Figure B24 Hilo Ash soil, isotropic consolidation for CU and CD strength tests: Axial strain vs. log time

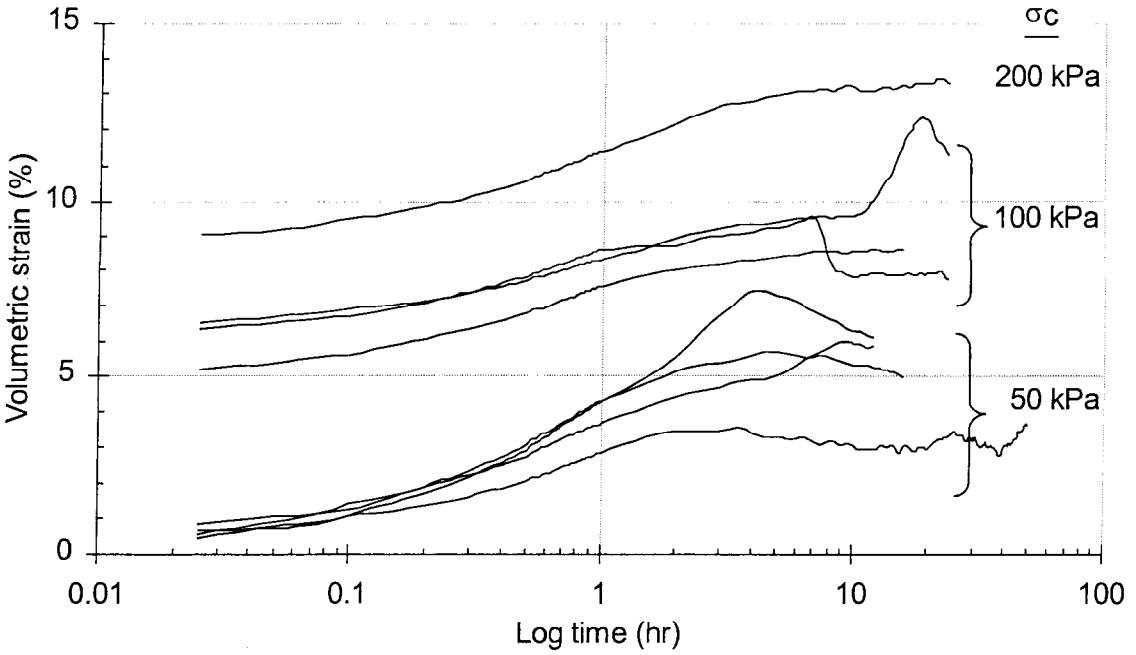

Figure B25 Hilo Ash soil, isotropic consolidation for CU and CD strength tests: Volumetric strain vs. log time

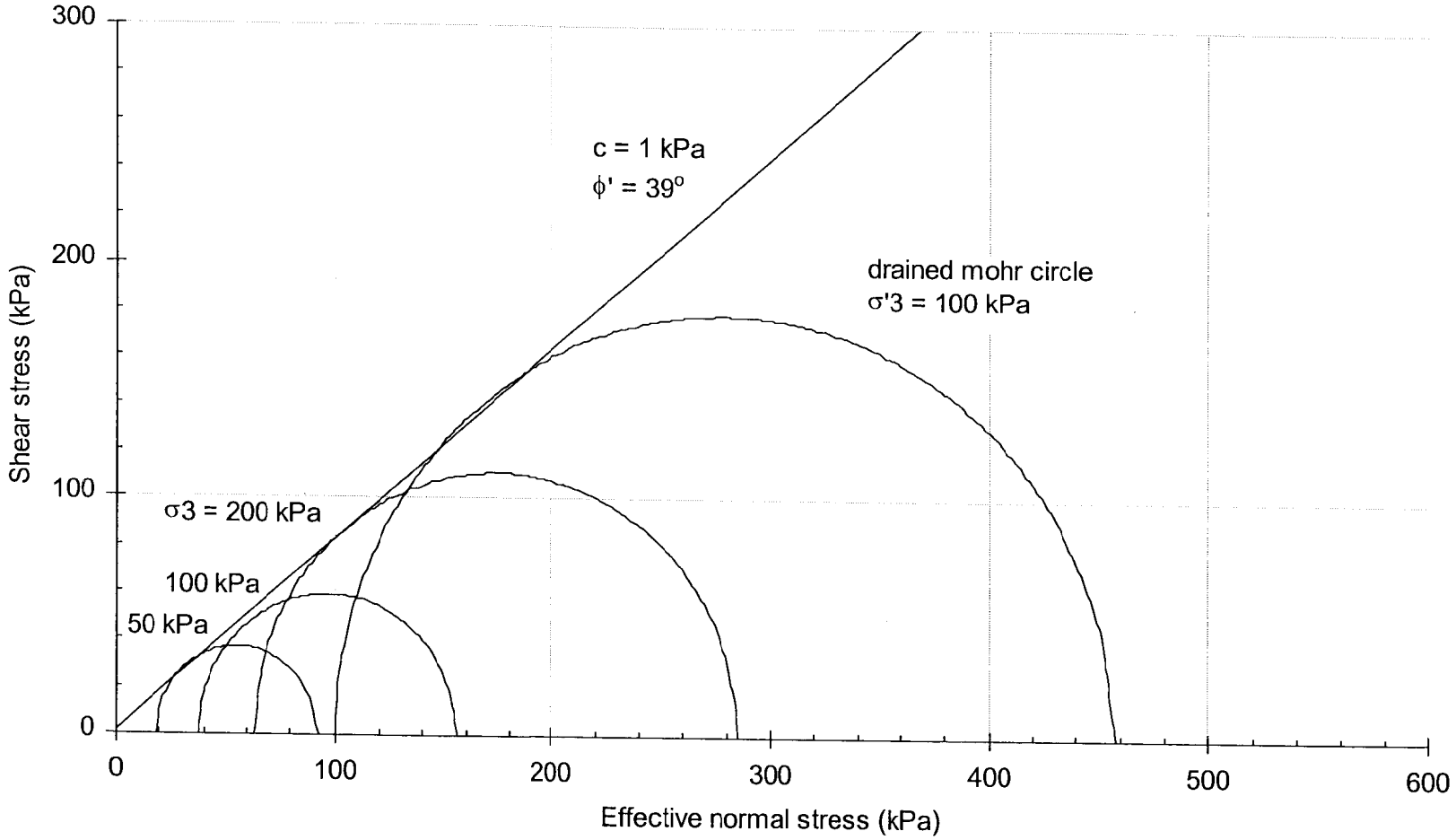

Figure B26 Hilo Ash soil, CU and CD strength tests: Effective stress failure envelope.

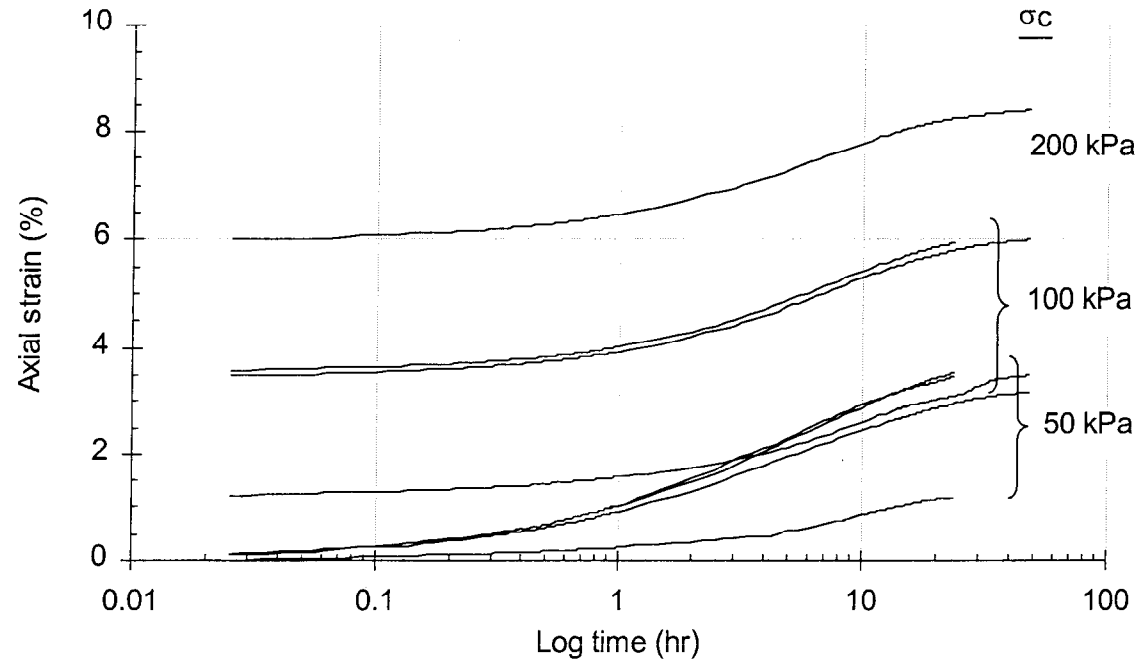

Figure B27 Kapolei Brown clay, isotropic consolidation for CU strength tests: Axial strain vs. log time

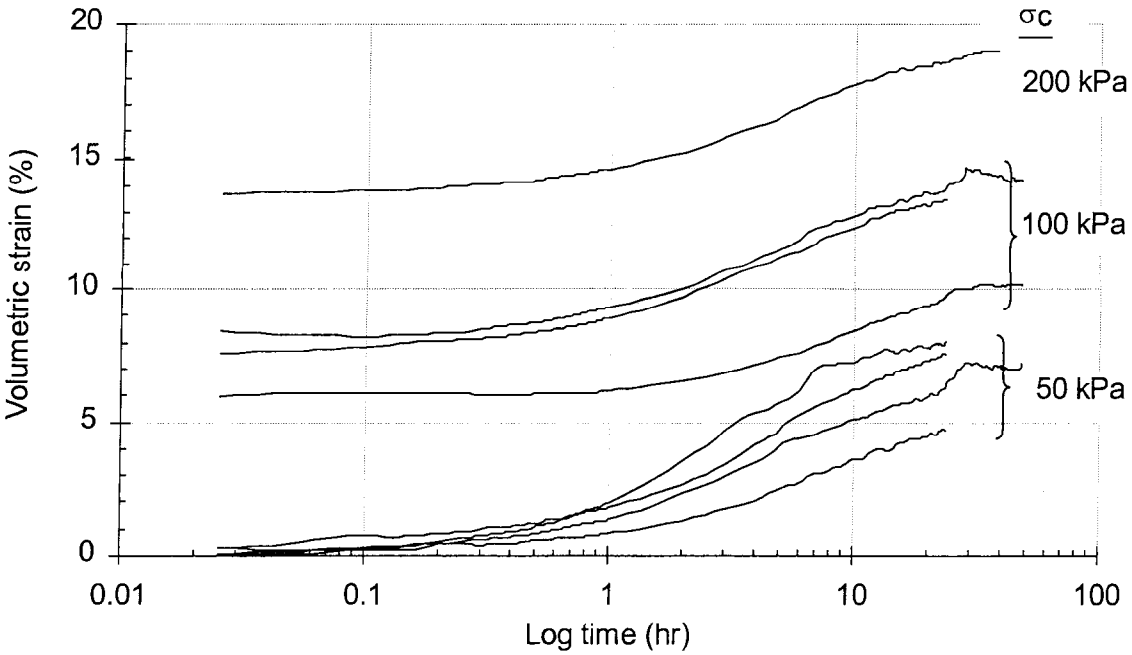

Figure B28 Kapolei Brown clay, isotropic consolidation for CU strength tests: Volumetric strain vs. log time

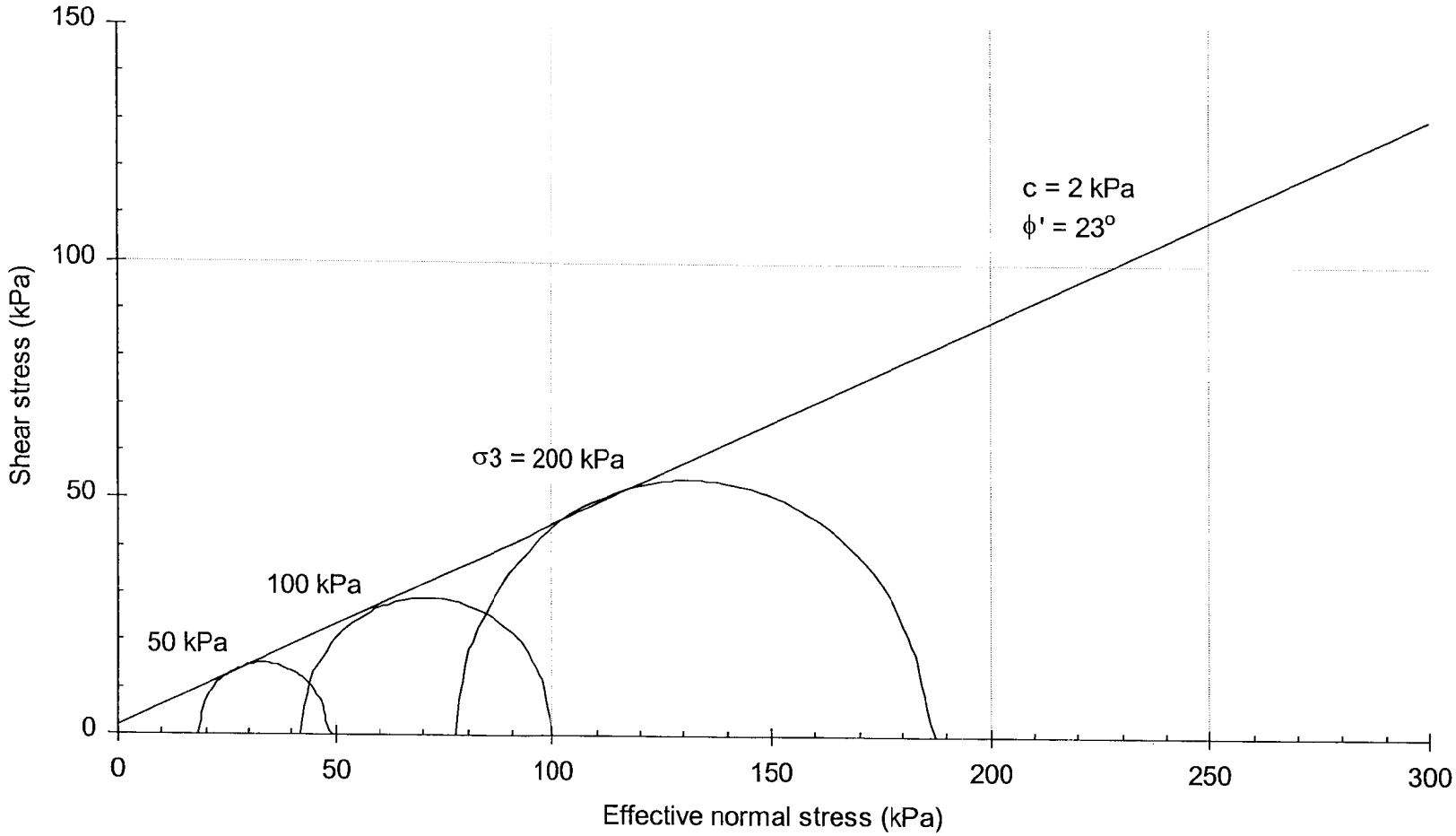

Figure B29 Kapolei Brown clay, CU strength tests: Effective stress failure envelope.

6. Appendix C – Creep Tests

Creep Tests

This appendix presents miscellaneous figures from the creep tests (Nakayama, 2000). Included are schematics of the testing equipment, consolidation data from the isotropic phases of all the creep tests, as well as stress-strain plots from the deviatoric loading phase of each test.

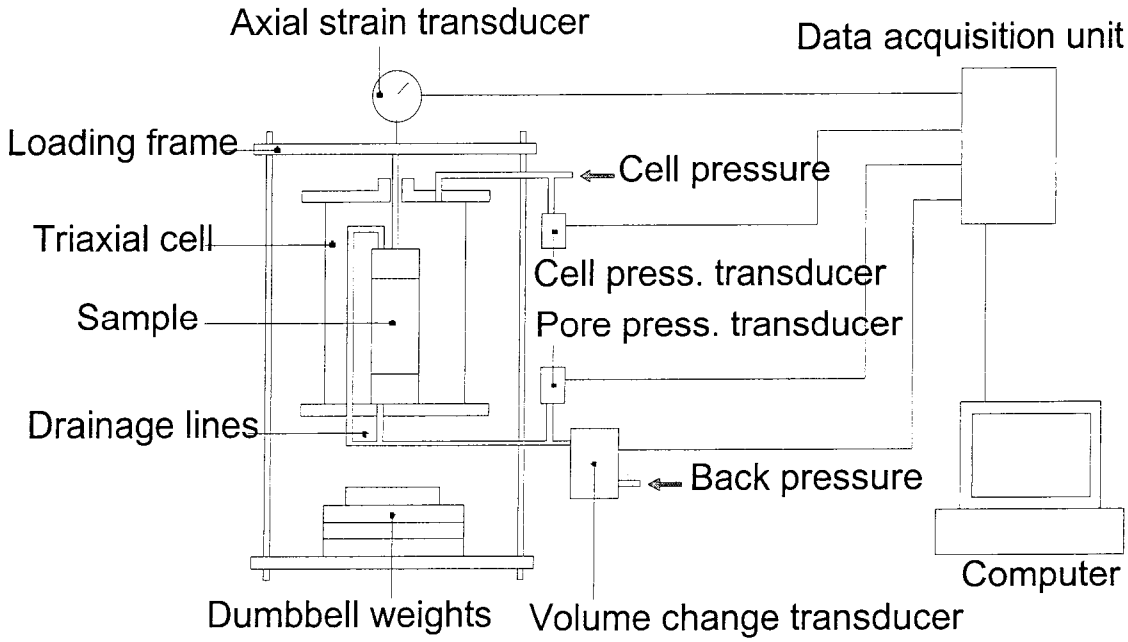

Figure C1. Creep test apparatus (not drawn to scale)

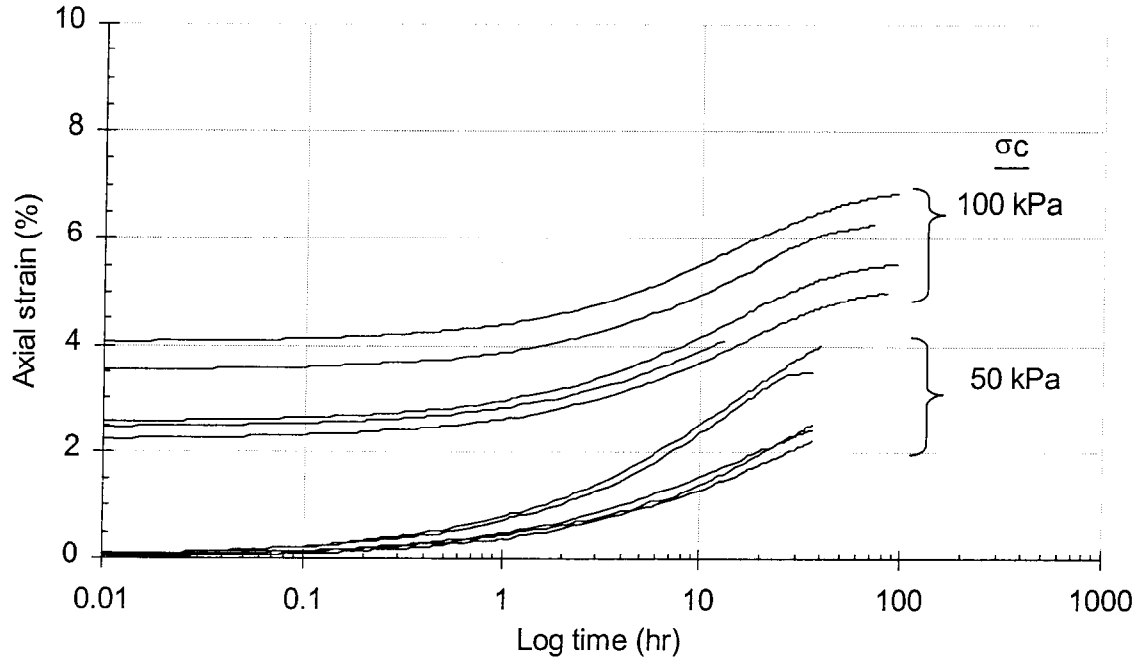

Figure C2. Manoa clay, isotropic consolidation for CD creep tests: Axial strain vs. log time

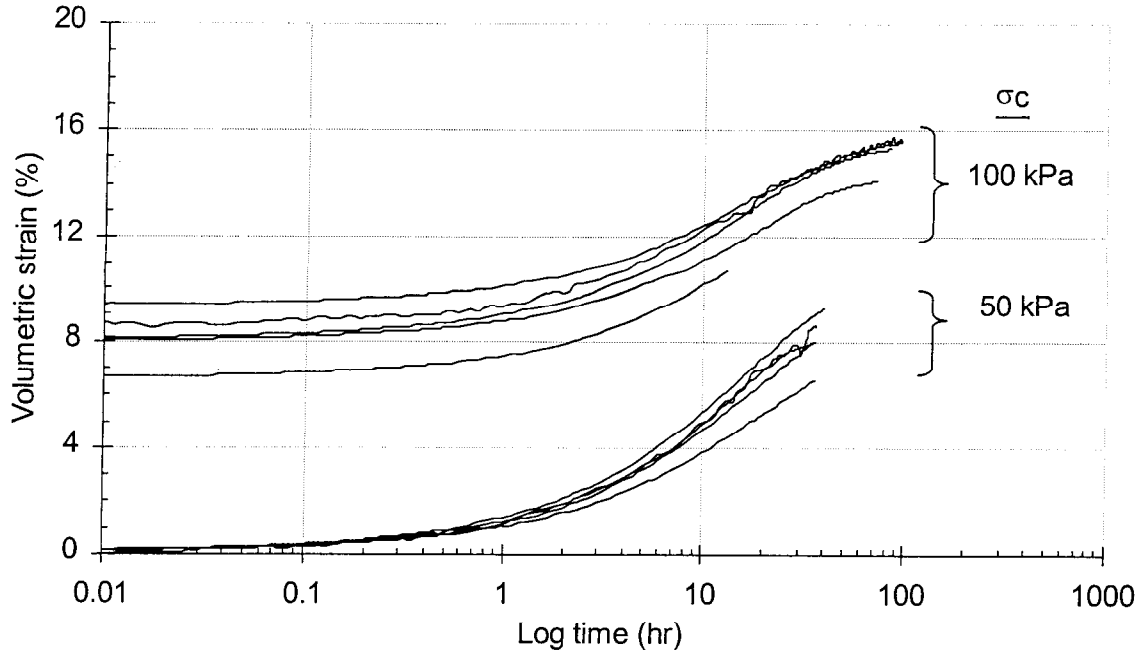

Figure C3. Manoa clay, isotropic consolidation for CD creep tests: Volumetric strain vs. log time

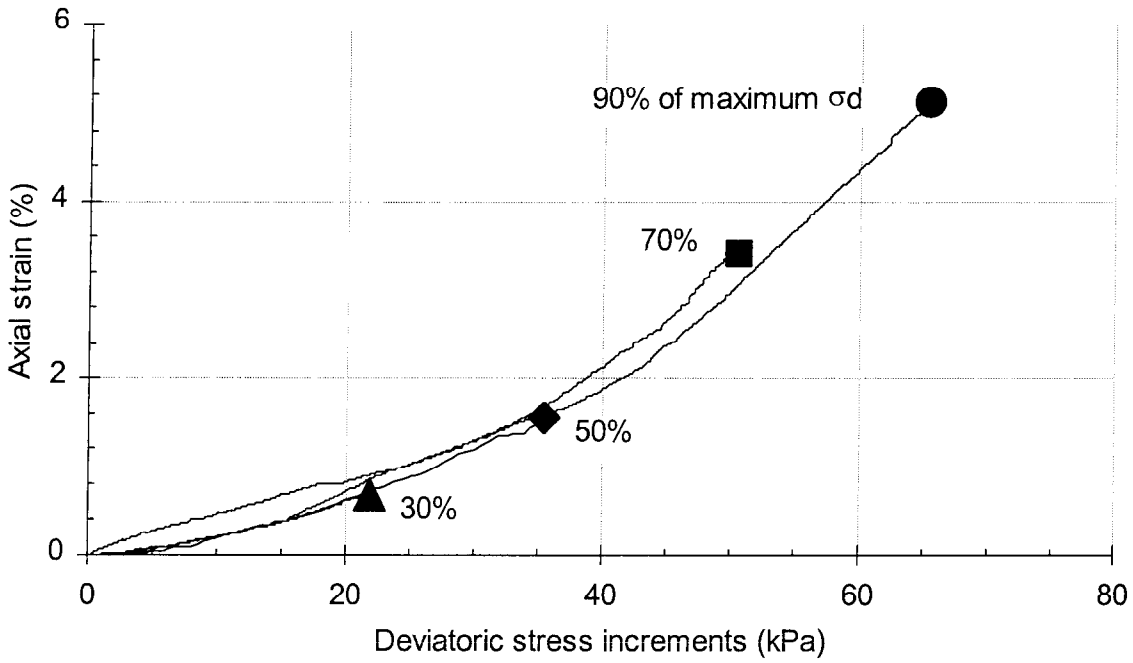

Figure C4. Manoa clay, loading increments for CD creep tests:
Axial strain vs. deviatoric stress increments

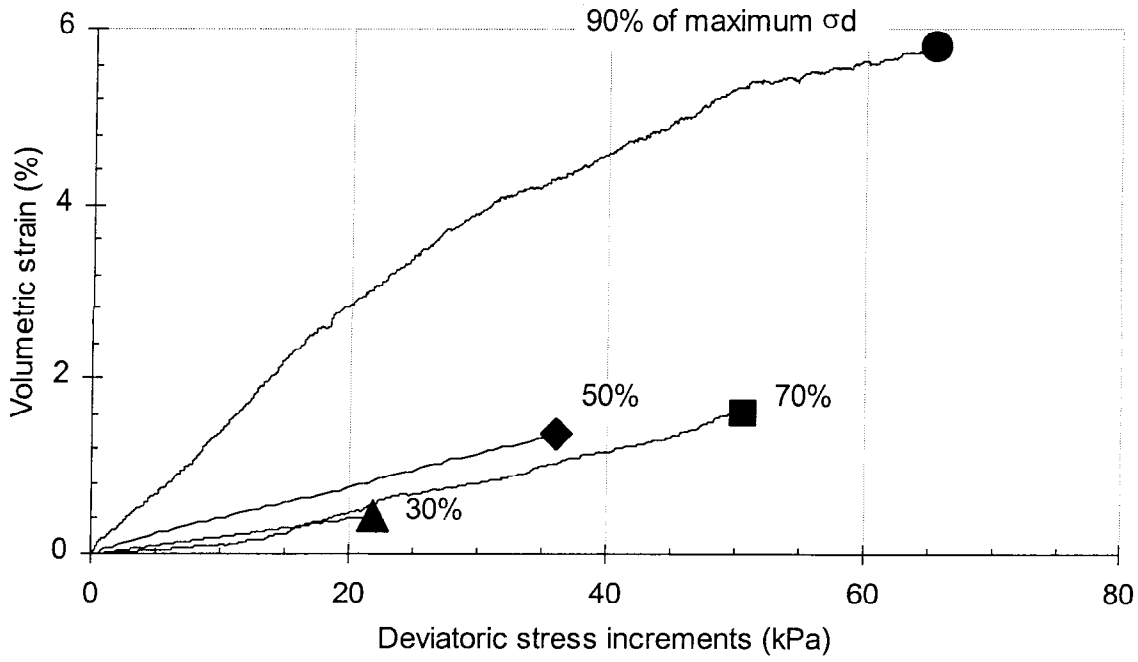

Figure C5. Manoa clay, loading increments for CD creep tests:
Volumetric strain vs. deviatoric stress increments

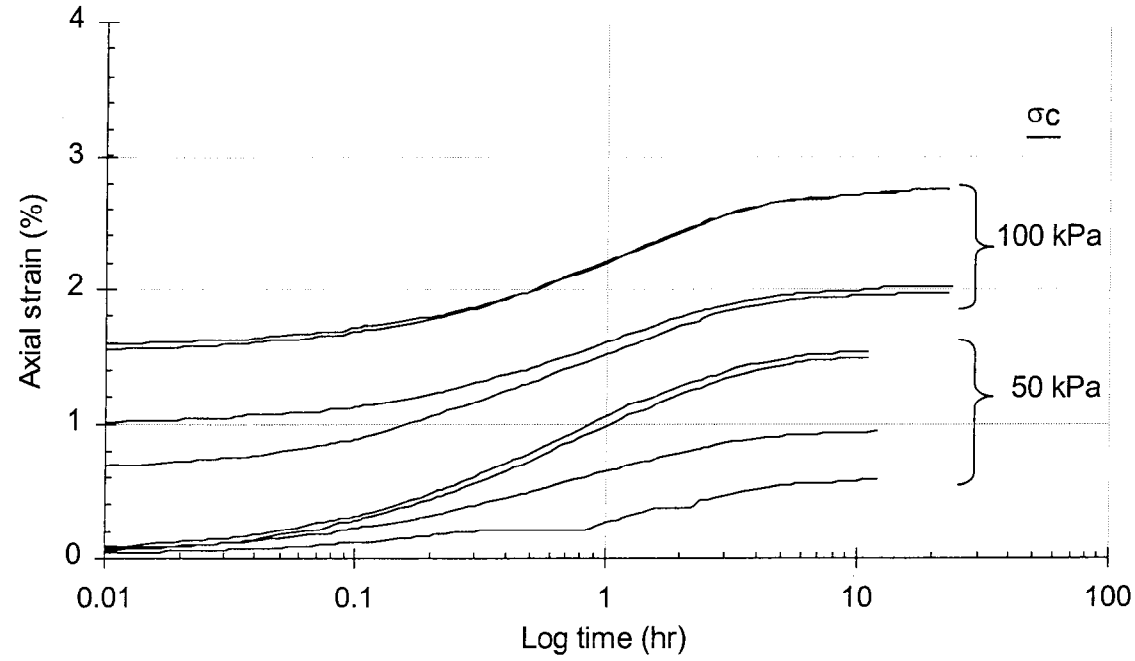

Figure C6. Kapolei Red silt, isotropic consolidation for CD creep tests: Axial strain vs. log time

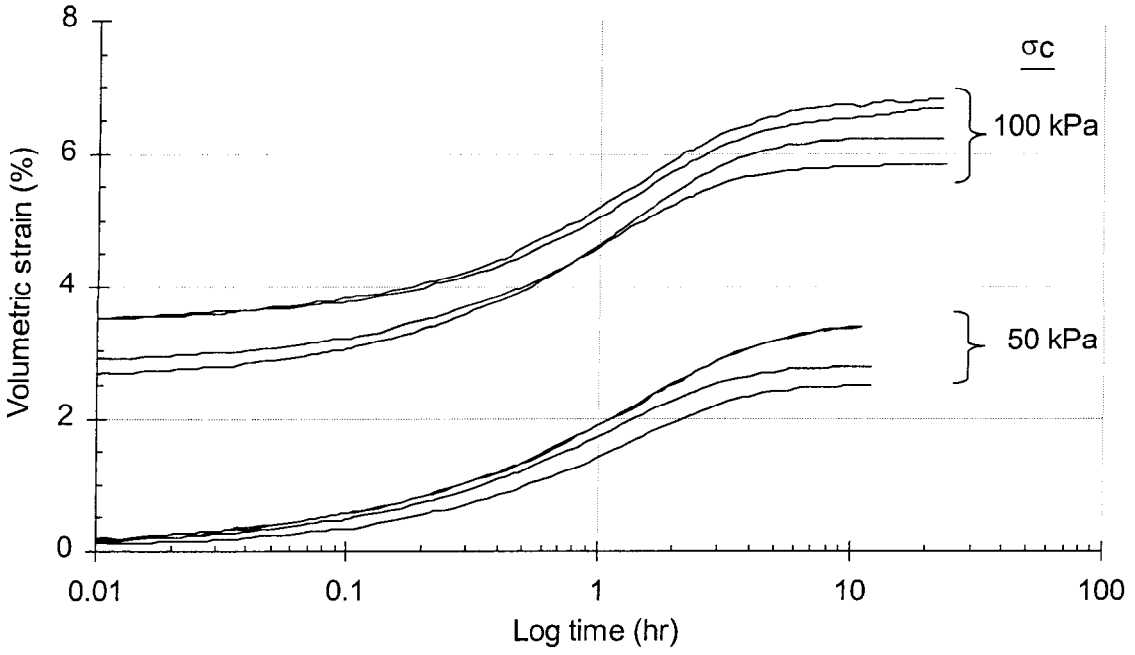

Figure C7. Kapolei Red silt, isotropic consolidation for CD creep tests: Volumetric strain vs. log time

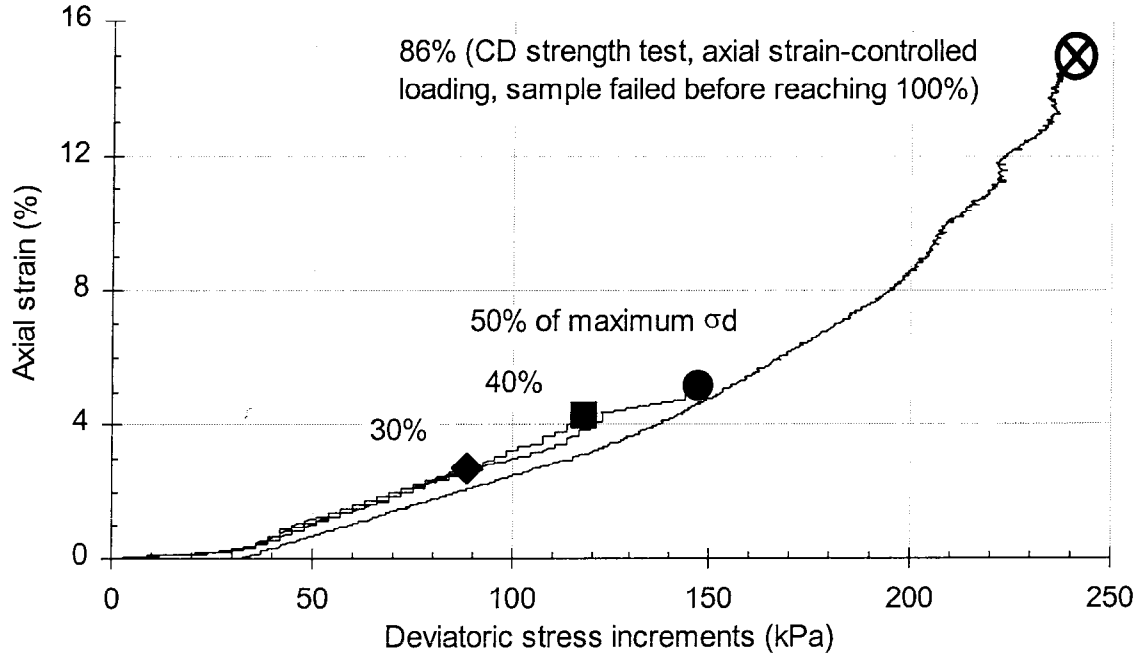

Figure C8. Kapolei Red silt, loading increments for CD creep tests: Axial strain vs. deviatoric stress increments

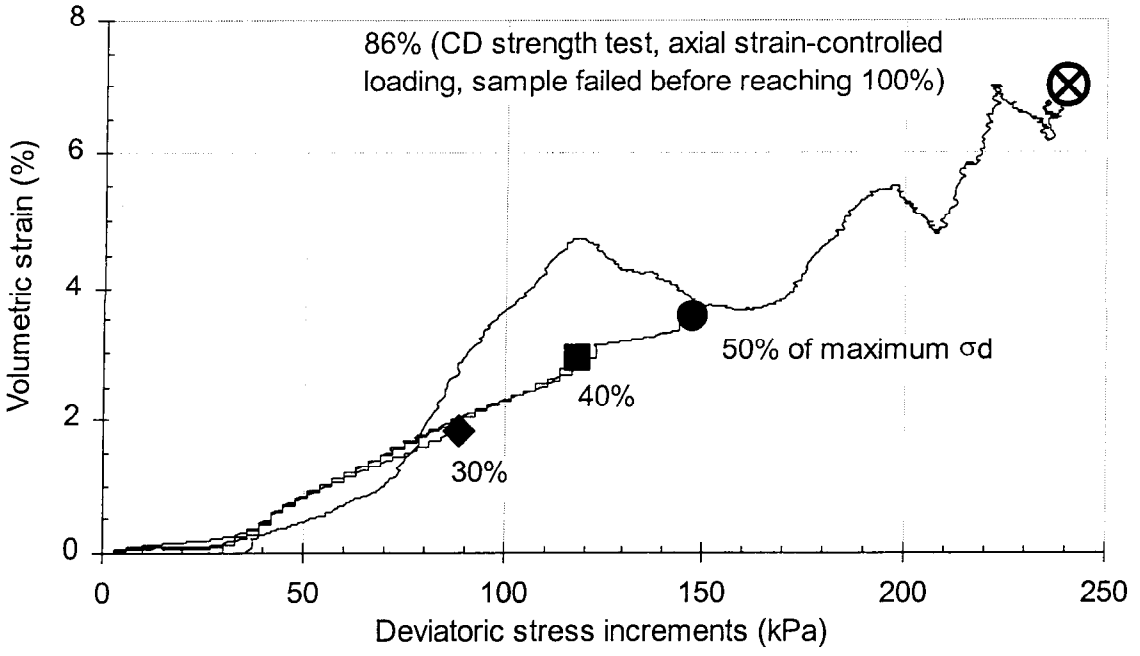

Figure C9. Kapolei Red silt, loading increments for CD creep tests: Volumetric strain vs. deviatoric stress increments

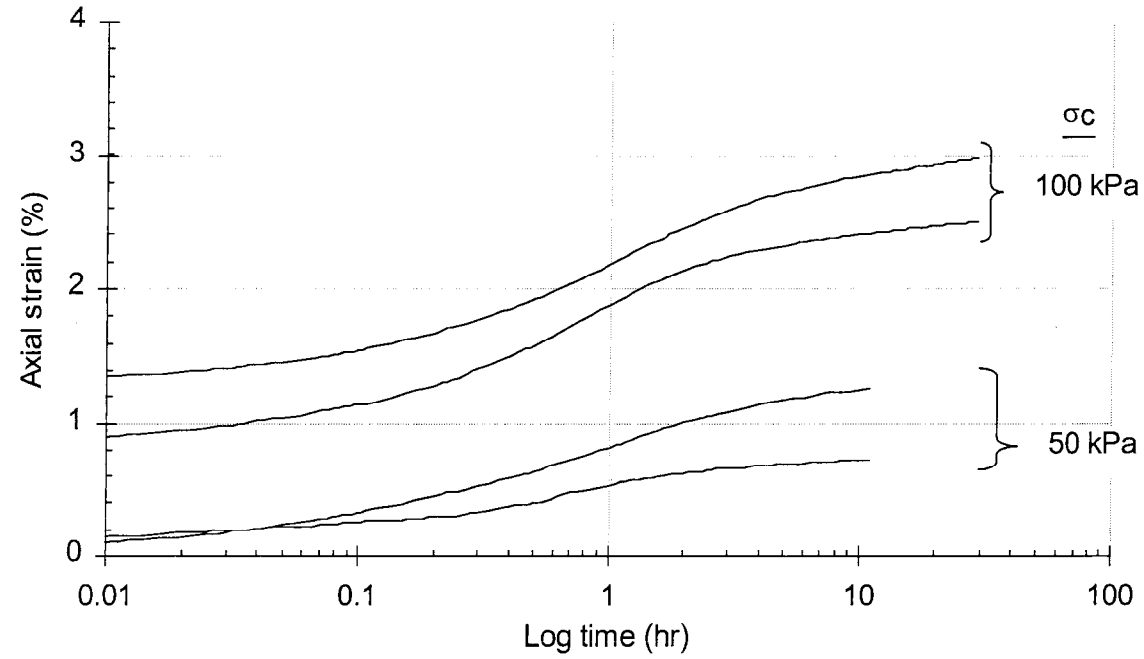

Figure C10. Hilo Ash soil, isotropic consolidation for CD creep tests: Axial strain vs. log time

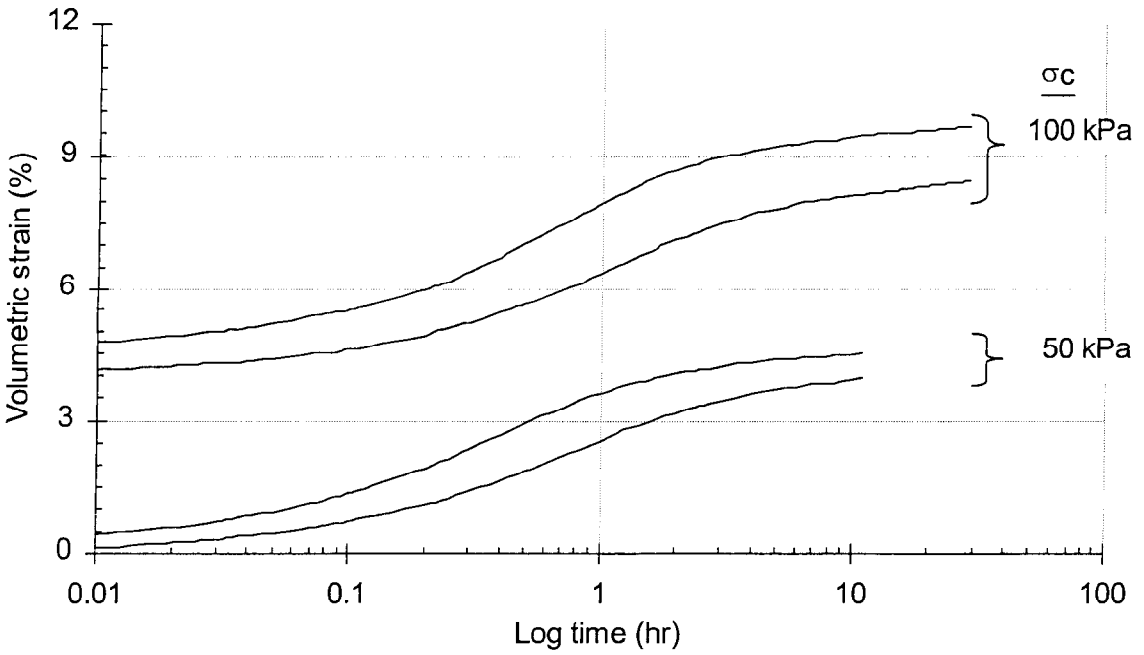

Figure C11. Hilo Ash soil, isotropic consolidation for CD creep tests: Volumetric strain vs. log time

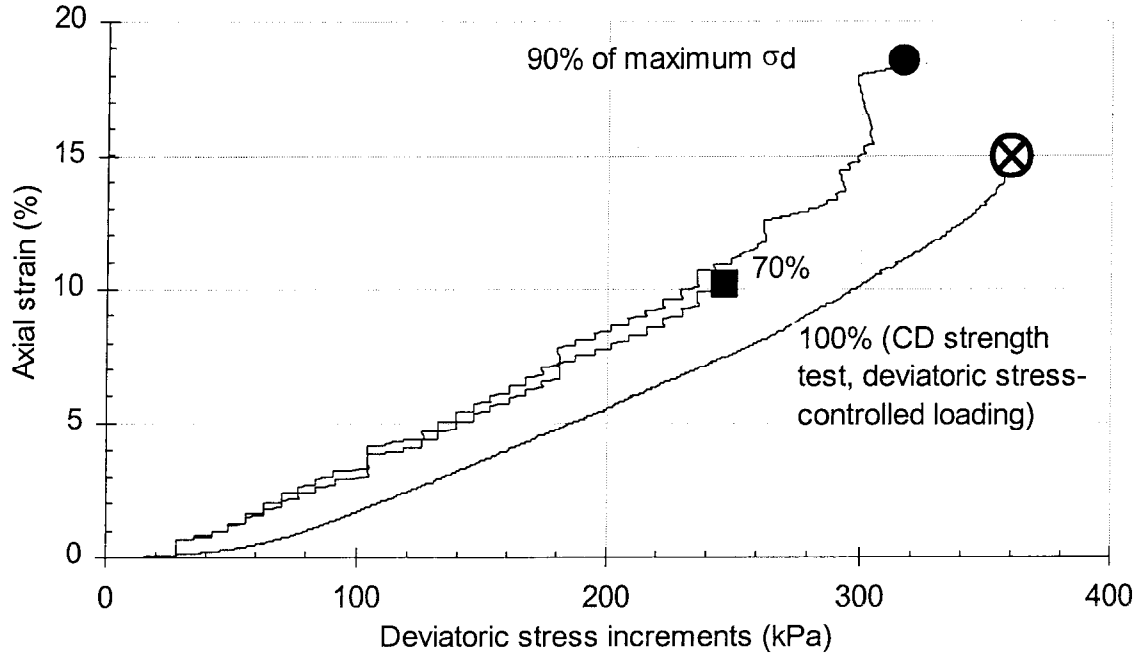

Figure C12. Hilo Ash soil, loading increments for CD creep tests: Axial strain vs. deviatoric stress increments

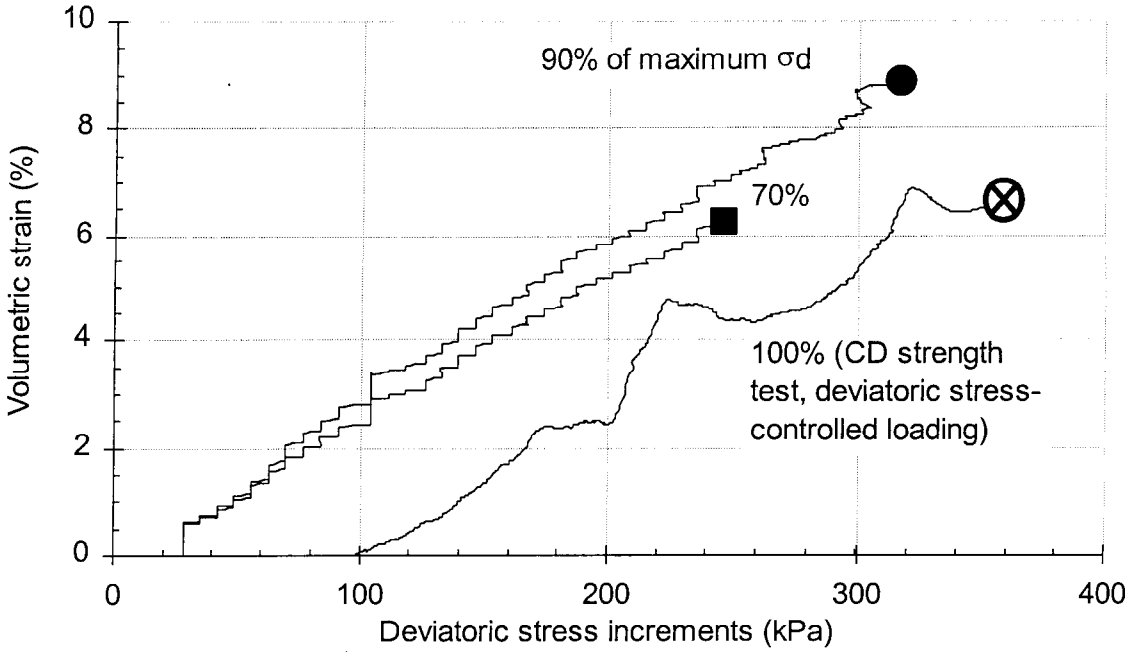

Figure C13. Hilo Ash soil, loading increments for CD creep tests: Volumetric strain vs. deviatoric stress increments

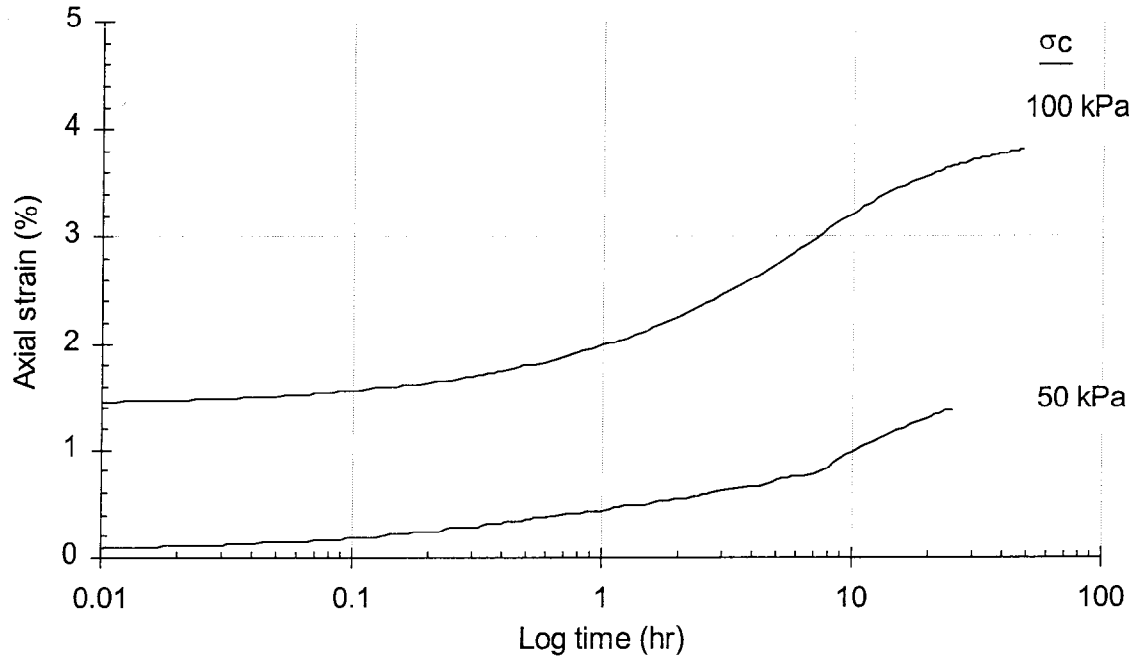

Figure C14. Kapolei Brown clay, isotropic consolidation for CD creep test: Axial strain vs. log time

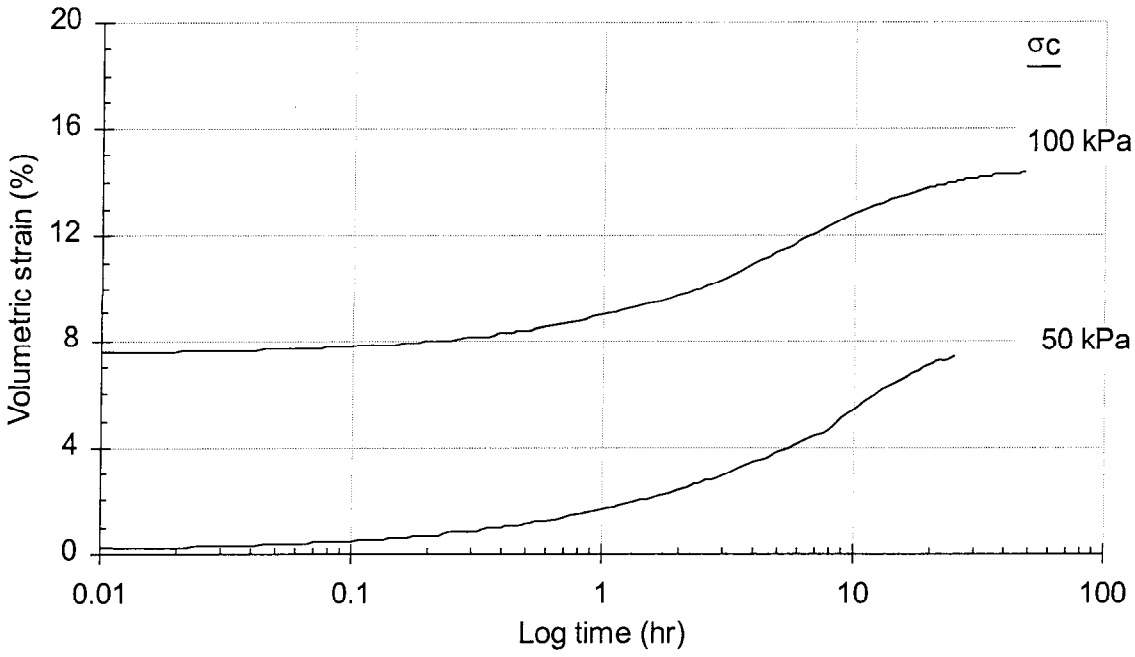

Figure C15. Kapolei Brown clay, isotropic consolidation for CD creep test: Volumetric strain vs. log time

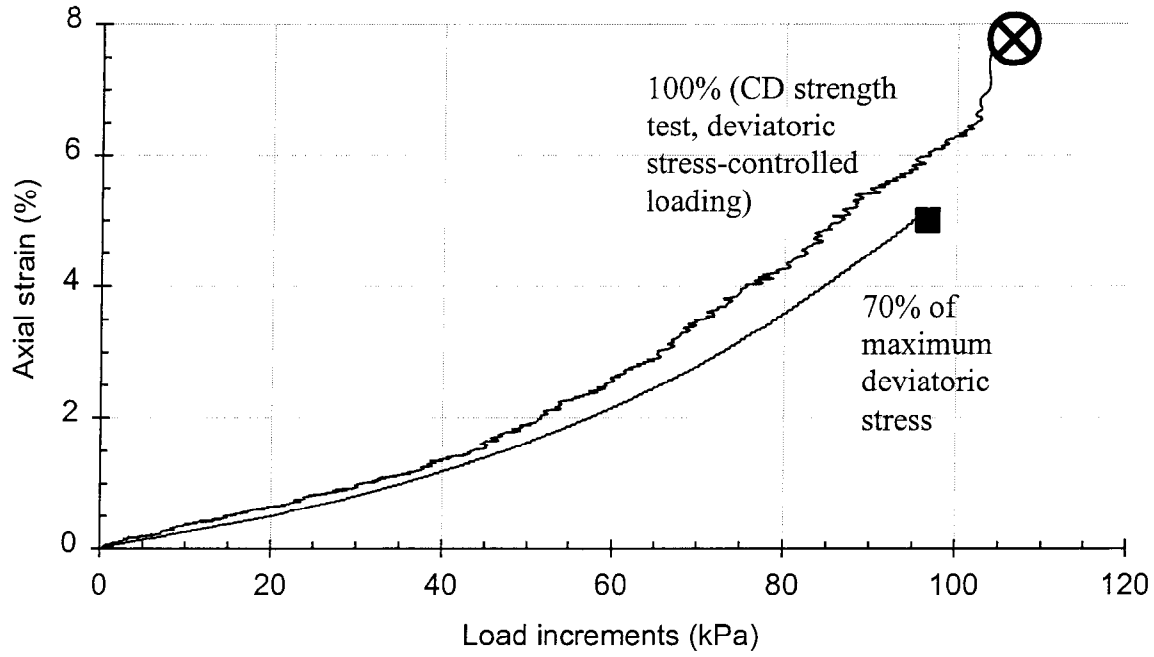

Figure C16. Kapolei Brown clay, loading increments for CD creep tests: Axial strain vs. deviatoric stress increments.

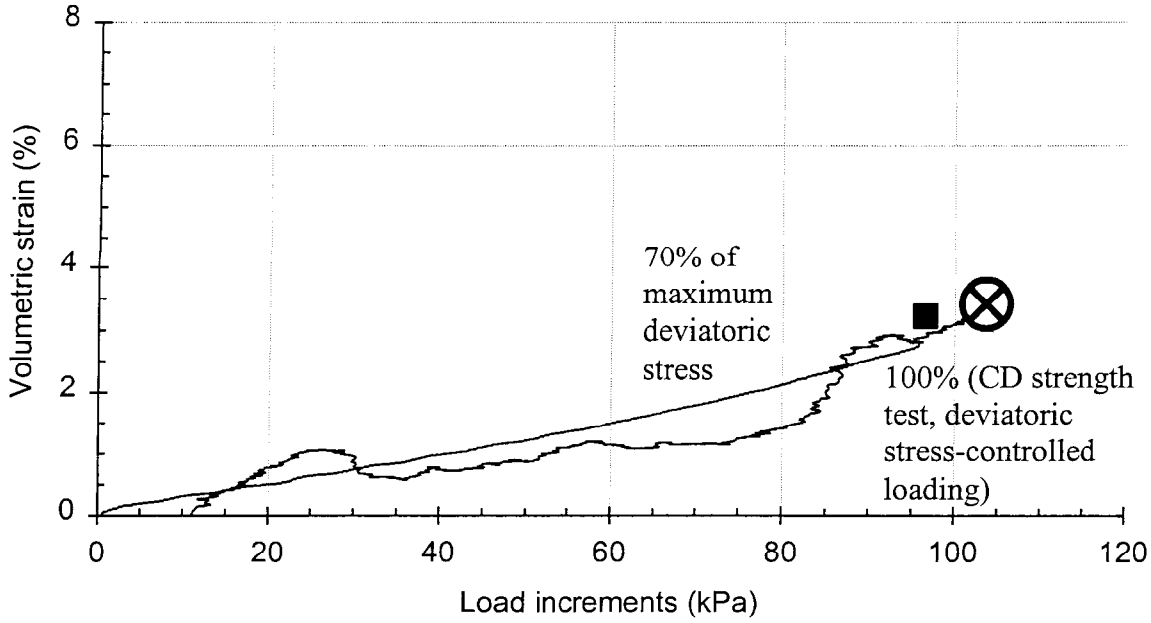

Figure C17. Kapolei Brown clay, loading increments for CD creep tests: Volumetric strain vs. deviatoric stress increments.

7. Appendix D – Post-Creep Strength Tests

Post-Creep Strength Tests

Four figures describing miscellaneous aspects of the post-creep strength tests are included in this appendix. They are discussed in some degree in Nakayama (2000).

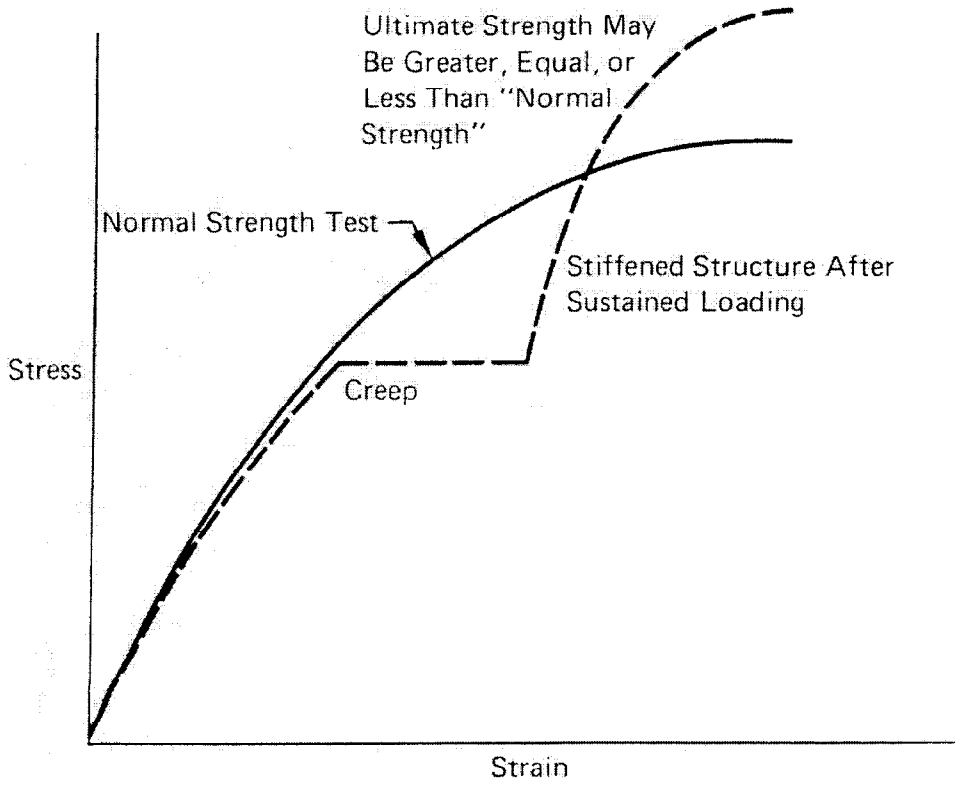

Figure D1. Effect of sustained loading on stress-strain and strength behavior (Mitchell, 1976)

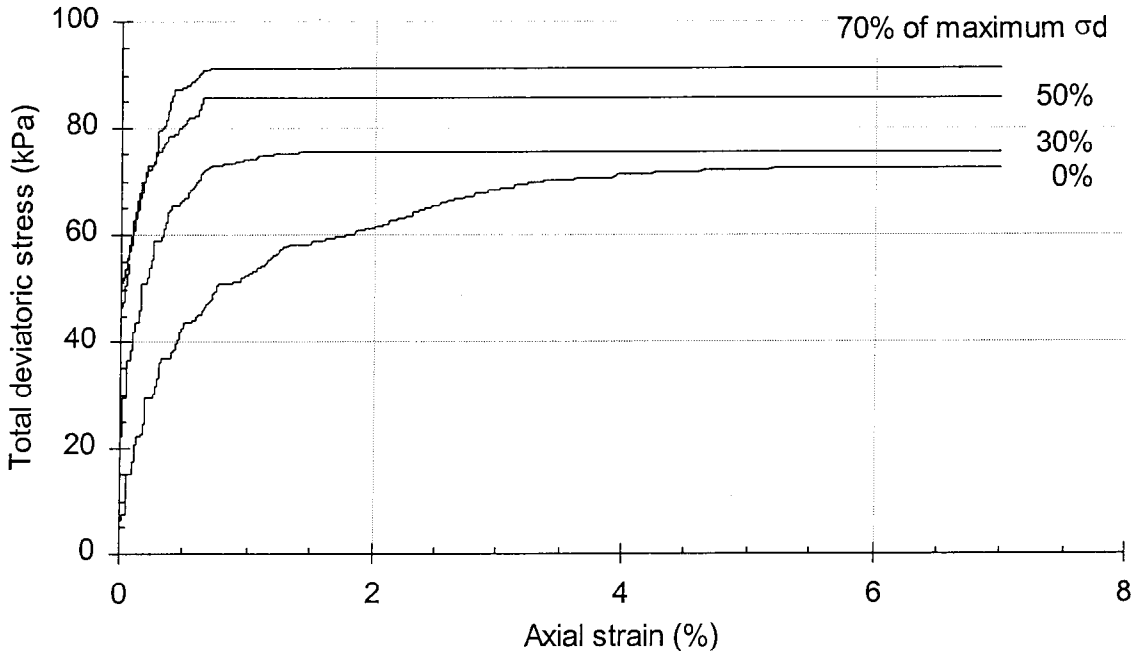

Figure D2. Manoa clay, post-creep undrained strength tests: total deviatoric stress vs. axial strain

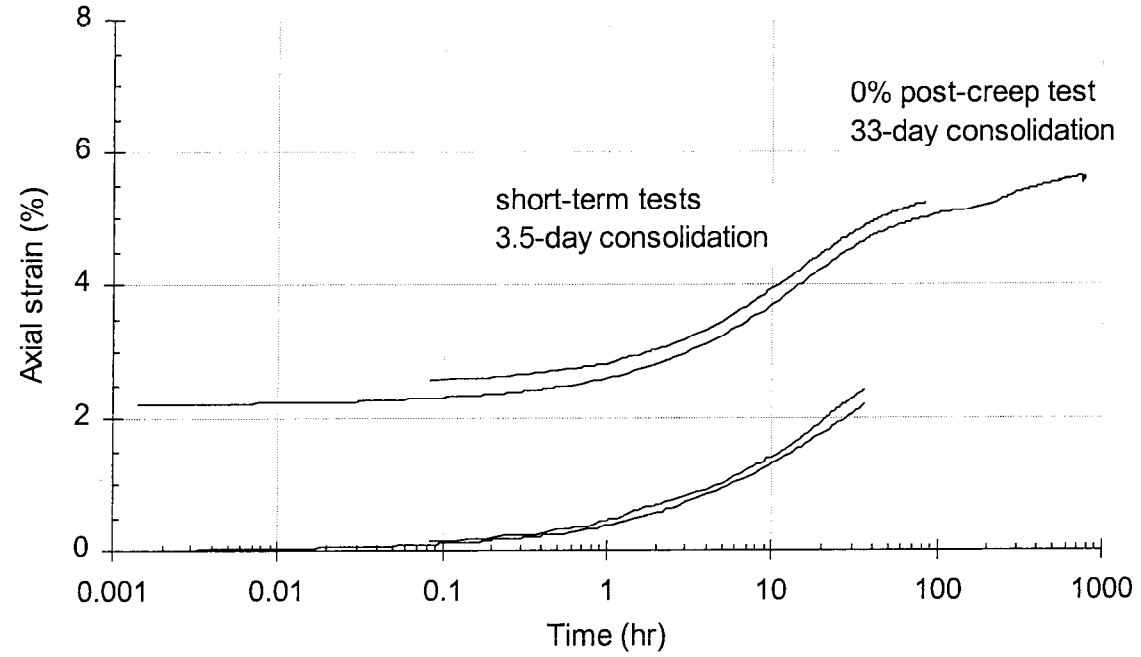

Figure D3. Manoa clay, triaxial consolidation for undrained strength tests: Axial strain vs. log time

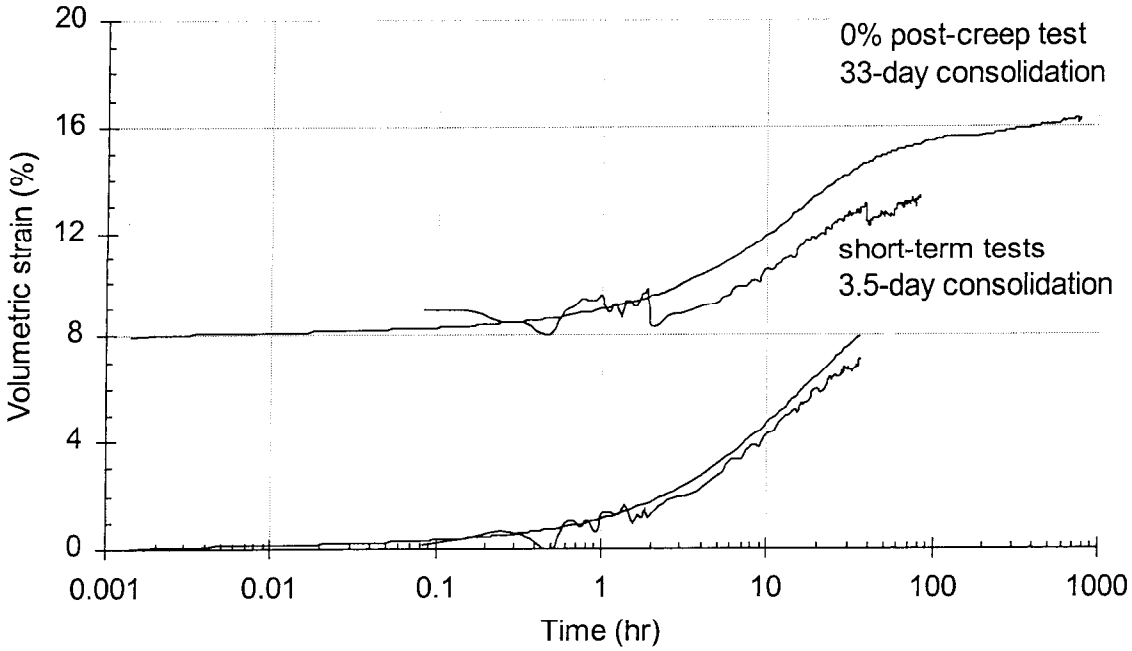

Figure D4. Manoa clay, triaxial consolidation for undrained strength tests: Volumetric strain vs. log time

8. Appendix E1 – Publication 1

Proceedings of the 10th International Conference on Computer Methods and Advances in Geomechanics, Vol. 1, pp. 1543-1547

Modeling the Effectiveness of Groundwater-Lowering Remediation Measures in the Alani-Paty Landslide Area, Oahu, Hawaii

H.G. Brandes
Associate Professor of Civil Engineering, Department of Civil Engineering, University of Hawaii, US

C.S.L. Tsui
Graduate Research Assistant, Department of Civil Engineering, University of Hawaii, US

ABSTRACT: In order to examine slope stability and creep problems in Manoa, one cross-section of the Alani-Paty landslide area was modeled using the computer software package SLOPE/W. The purpose of the study was to determine appropriate water elevations needed to insure adequate stability. The landslide area consists of fine-grained, very soft volcanic colluvium overlying basalt bedrock. The stability analysis suggests that local failures can continue to be expected in the upslope region. To avoid large-scale failure, the water table should be lowered to a depth at least 13 feet below to the ground surface in order to yield a factor of safety of one. This water elevation should be checked against piezometer readings to evaluate the effectiveness of the new drainage system.

1 INTRODUCTION

The Alani-Paty landslide in Manoa valley (Figure 1), on the island of Oahu, Hawaii, is typical of a series of slow-moving slides that occur on most flanks of the deep valleys that cut into the Koolau mountain range in East Honolulu. The volcanic colluvium that is found above the basalt bedrock is mostly fine-grained and very soft. In addition to continuous creep deformations, which are the focus of a companion paper (Tsui et al., 2001), these slopes are highly susceptible to reactivation in response to moderate and extreme rainfall events. Landsliding is a serious problem in these valleys since it typically occurs in high-density residential areas. Accumulated damages in Honolulu are estimated in the hundreds of millions of dollars.

Manoa valley has a relatively flat bottom and steep sides. Through intermittent debris flows and rock falls, weathered residuum, consisting of clasts and soil, has been transported downslope from the sides of Waahila Ridge to form an apron at the base of the ridge on which extensive failure and creep have taken place (Figure 2). This apron is concave upward, with a slope of 2°-6° near the valley floor and 10°-15° near the upslope edge. Average slope of the debris apron is 8°-12°. The affected deposits consist of crudely stratified clayey silt and silty clay containing boulder-, cobble-, and gravel-sized fragments of weathered basalt. The stratification of these deposits is complex and discontinuous, making it difficult to correlate layers even over short distances. The clasts of basalt constitute about 38% of the volume of the bulk soil, not sufficient to affect the stability or creep behavior of the area to a significant extent (Baum and Reid, 1992). The matrix containing the clasts consists of highly plastic silt and clay (Table 1). The head of the landslide has undergone at least 3 to 4 ft of displacement, with some offsets as large as 6 to 10 ft near Lanikaula street. Most of these displacements have occurred during or after intense rainfall events, although creep deformations continue to cause damage.

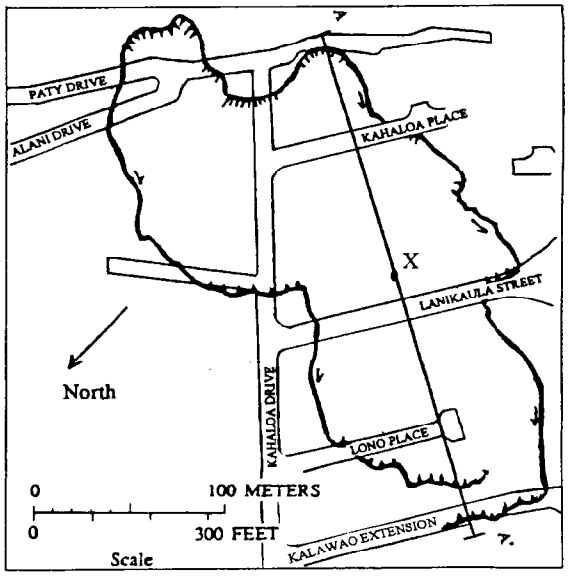

Figure 1. Approximate boundaries of the Alani-Paty landslide

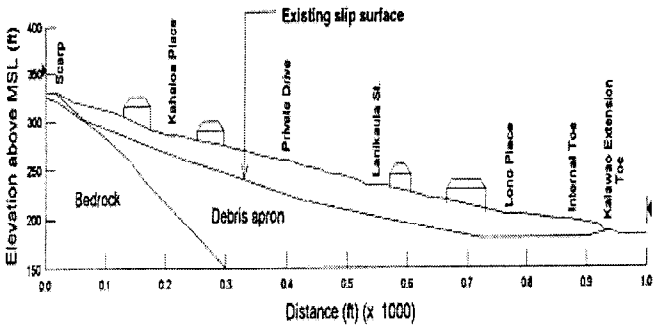

Figure 2. Cross section of landslide

2 REMEDIAL MEASURES

Extensive stabilization work in the area began in May 1993 (Polhemus, 1993). Following the advice of Peck and Wilson (1968) and others, remediation efforts have focused on controlling drainage to lower groundwater levels, grading, and installing tiebacks and various retaining structures. Drainage remedial measures included surface storm drains and repaving, horizontal and vertical subsurface drains, 80-ft deep groundwater pumps, and larger capacity water and wastewater pipes. In all, about 3,700 ft of new sewer lines were installed, along with 5,900 ft of new water lines and 2,600 ft of drains (Figure 3). In addition, an extensive tieback system was installed near the head of the landslide, consisting of side-by-side concrete blocks anchored to the bedrock by 100-ft long anchors (Civil Engineering Magazine, 1998). The purpose of this modeling study was to determine appropriate groundwater elevations that need to be maintained to insure adequate stability (Tsui, 1999).

Table 1. Index properties

Water content, w	47%
Liquid Limit, LL	87%
Plasticity Index, PI	54%
Average unit weight, γ_{sat}	138 pcf
Sand/Silt/Clay	7/27/66 %

3 SAFE GROUNDWATER TABLE

Computations were carried out using the software package SLOPE/W. This commercial code uses the limit equilibrium method to solve for the safety factor of any number of assumed failure surfaces. The complex soil profile was approximated by the residual strength parameters shown in Figures 4a and 4b. These values were determined from direct shear tests using remolded samples of the sand/silt/clay matrix (Baum et al., 1991). The low effective residual friction angles in Figure 4b have been confirmed by more recent triaxial tests conducted by these authors on remolded specimens. The stability analysis uses residual strength parameters since the soil in the landslide area has undergone substantial shearing. An average unit weight of 138 pcf was assumed for the entire area.

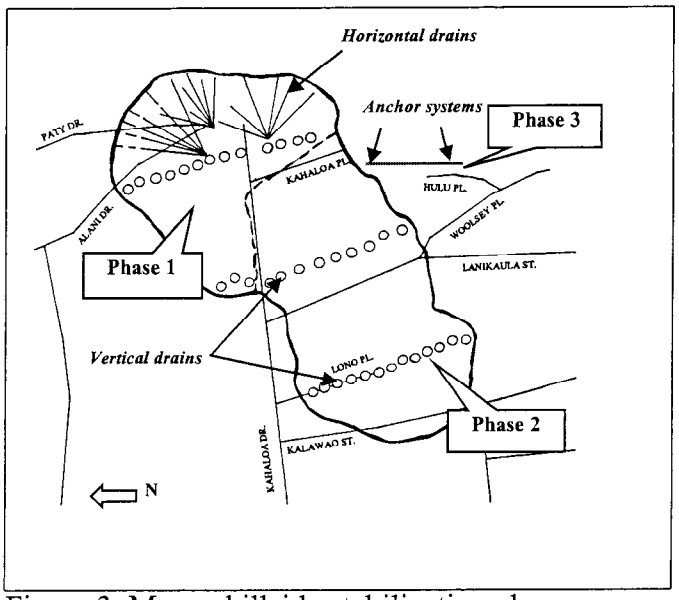

Figure 3. Manoa hillside stabilization phases

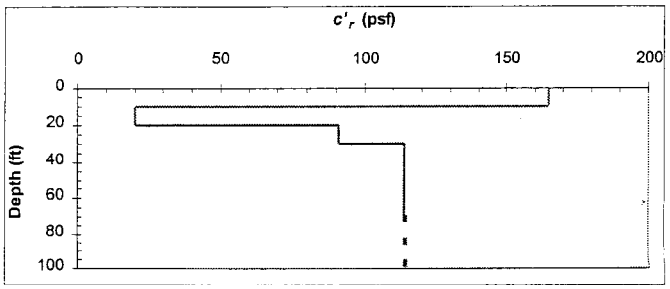

Figure 4a. Variation of residual effective cohesion with depth

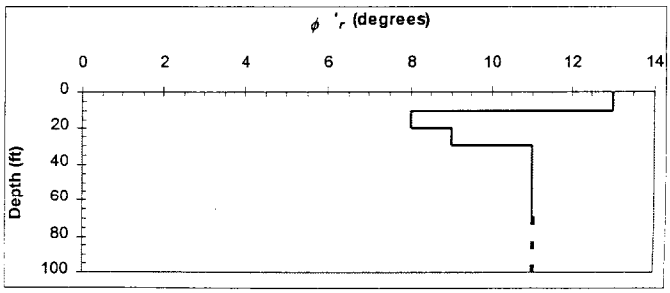

Figure 4b. Variation of residual effective frictional angle with depth

The predominant failure surface in the landslide (Figure 2) has been inferred indirectly, in part from hydraulic conductivity measurements and recorded water elevations. Piezometer data indicates that the

freshwater groundwater table is located some 150 ft below the basal slip surface. Nonetheless, piezometer readings also indicate the presence of a prevalent perched water table above the major slip surface. Slug tests reported by Baum et al. (1991) and Baum and Reid (1992) suggest a hydraulic conductivity profile as shown in Figure 5. The location of the predominant failure surface is associated with the interval of low permeability between 20 and 30 ft. Most of the piezometers shallower than 29 ft or deeper than 60 ft responded to rainfall, whereas those between 30 and 60 ft were dry or gave steady readings during the monitoring period.

Hundreds of failure surfaces were investigated. These included numerous circular sections of varying radius, size and location, as well as fully specified surfaces roughly parallel to the presumed major failure surface (Figure 2). In each case, the factor of safety was calculated using the rigorous Morgenstern-Price method, which satisfies both force and moment equilibrium. A constant interslice function equal to 1 was assumed.

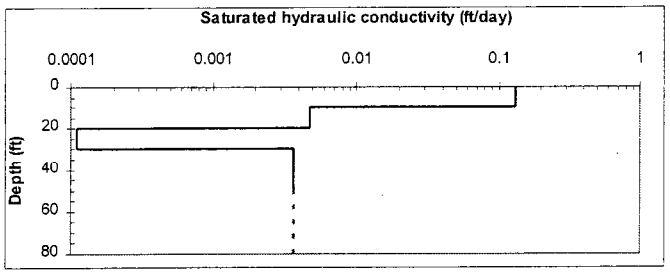

Figure 5. Variation of hydraulic conductivity with depth

Circular slip surfaces near the head of the slide gave minimum safety factors slightly less than one, even with a groundwater table 20 ft below the ground surface (Figure 6). The upslope area is less stable because it has a steeper geometry. However, the fact that the soil in this area is sandier and presumably somewhat stronger than elsewhere may result in true safety factors that are slightly higher. Nonteheless, observations indicate significantly more damage to structures in the upslope area, particularly near Alani Drive and Paty Drive, than anywhere else. The head of the landslide was found to be moving downslope during a number of rainy periods when the United States Geological Survey was monitoring the slope, but the main body of the landslide only moved during two of those rainy periods. A complicating factor, not considered in this study, is that pressure head changes in the upslope region are more rainfall-dependent than in the downslope region.

Twenty fully specified failure surfaces along transect AA' in Figure 1 were analyzed to determine the effect of regional groundwater level on stability throughout the landslide area (Table 2, Figure 7). Slip surface number 12, located 5 ft above the major failure surface and parallel to it, yielded the critical groundwater elevation Figure 8 indicates that a groundwater table of at least 13 ft below the ground surface is required in order to have a safety factor larger than one, and hence avoid large-scale failure. In fact, to allow for uncertainties, the warning elevation should probably be closer to 20 ft below ground. Water levels in the piezometers need to be checked against this value to gauge overall stability, particularly during rain events. If these depths are not maintained, the overall drainage system needs to be reevaluated.

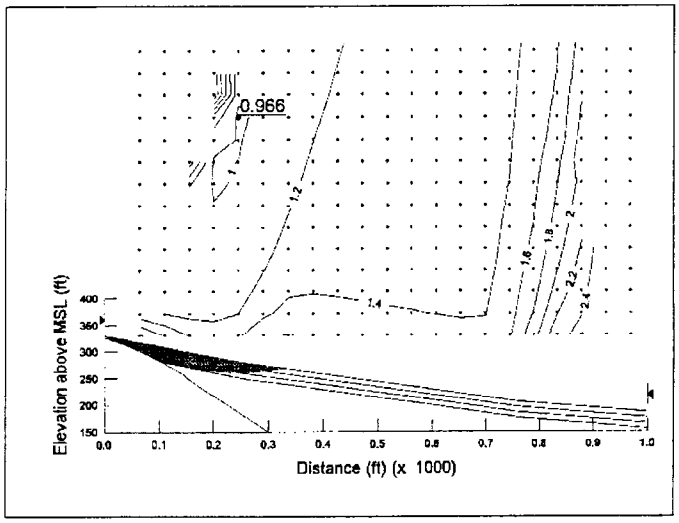

Figure 6. Critical slip surface and contours of safety factors (Water table 20 ft below ground surface)

Table 2. Identification numbers and descriptions for fully specified slip surfaces

Set 1 - Parallel to existing slip surfaces		
	1	Existing slip surface
	2	5 ft above the existing slip surface
	3	10 ft above the existing slip surface
	4	15 ft above the existing slip surface
	5	5 ft below the existing slip surface
Set 2 - Parallel to ground surface		
	6	5 ft below ground surface (about 900 ft long)
	7	10 ft below ground surface (about 900 long)
	8	15 ft below ground surface (about 900 ft long)
	9	20 ft below ground surface (about 900 ft long)
	10	25 ft below ground surface (about 900 ft long)
Set 3 - Parallel to existing slip surface and of limited length		
	11	Existing slip surface (first 750 ft portion)
	12	5 ft above the existing slip surface (first 750 ft portion)
	13	10 ft above the existing slip surface (first 750 ft portion)
	14	15 ft above the existing slip surface (first 750 ft portion)
	15	5 ft below the existing slip surface (first 750 ft portion)
Set 4 - Parallel to ground surface and of limited length		
	16	5 ft below ground surface (about 750 ft long)
	17	10 ft below ground surface (about 750 long)
	18	15 ft below ground surface (about 750 ft long)
	19	20 ft below ground surface (about 750 ft long)
	20	25 ft below ground surface (about 750 ft long)

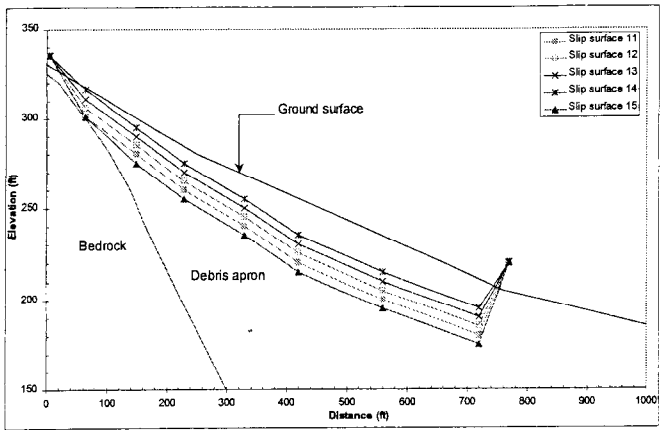

Figure 7. Locations of fully specified slip surfaces

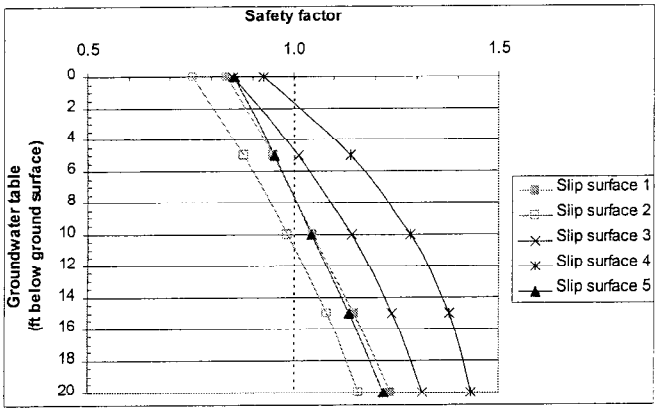

Figure 8. Safety factors for different groundwater conditions

4 ADDITIONAL CONSIDERATIONS

The safety factors determined from this study are conservative in a number of ways. First of all, the new anchor system was not considered in the analysis. The anchor system in the upslope region serves to tie the weak soil to the stronger bedrock underneath, thus improving the safety of the slope. Because presumably only the soil close to the pre-existing slip surface has undergone failure, only this region currently has soil with shear strength parameters reduced to residual values. The soil above and below this region could still be characterized by strength parameters that are closer to peak values. Since residual strength was used for the whole slope, the results for slip surfaces above or below the existing surface are conservative. Furthermore, the residual strength parameters used are based on laboratory tests on remolded samples, which probably underestimate the true residual values. Also, capillary tension above the piezometric line was ignored. Since all the soil below the perched water table was assumed to be submerged, the pressure heads in some regions inside the slope were overestimated, resulting in underestimated safety factors. Finally, no vertical downward movement of water was considered.

Because of all these factors, the field safety factors could actually be higher than those determined from this study. Despite these uncertainties, this study does include realistic cross sections, and to a certain soil properties, and provides meaningful preliminary estimates.

5 BACK-ANALSYSIS

Back-analysis can be used to estimate the peak soil strength parameters at the time of original failure by assuming that such failure occurred when the safety factor reached one. One of the benefits of this type of analysis is that the strength parameters that are obtained represent in situ values, averaged over the length of the failure surface, and take into account fissures, pre-existing shear planes and other imperfections that are difficult to simulate in the laboratory. However, the slope geometry and groundwater conditions need to be known at the time of failure. The assumed geometry used for the analysis is as shown in Figure 9.

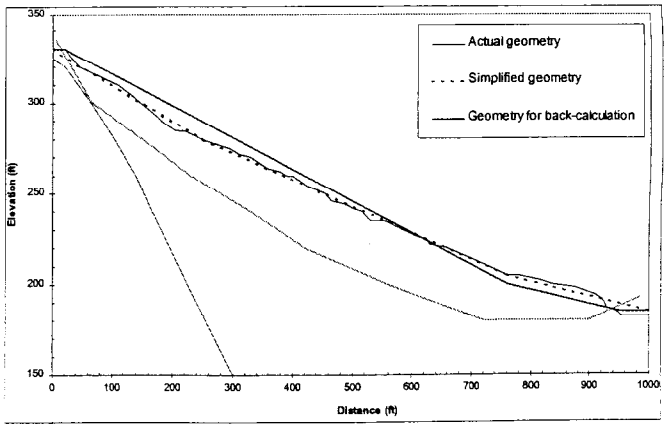

Figure 9. Slope geometry along section AA' used for back-analysis

The results of the back-analysis are summarized in Figure 10, where the strength parameters have been normalized by the baseline values indicated on that figure. Shown in Figure 10 are combinations of ϕ'/ϕ'_r and c/c_r that result in a factor of safety of one for various groundwater locations at the time of

failure. Above each straight line the factor of safety is larger than one and below it is less than one. For example, if we assume that the cohesion has not changed due to failure, and we further assume an original groundwater level located at the ground surface (perhaps due to a long rainstorm event), than the peak friction angle would be about 40% higher than the residual value of 10.2^0.

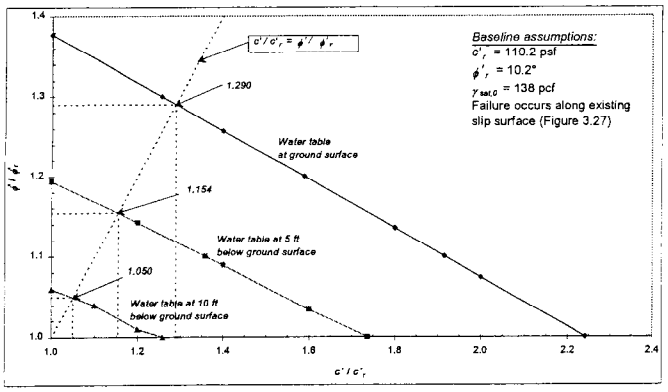

Figure 10. Combinations of c'/c'_r and ϕ'/ϕ'_r for FS = 1 from back-analysis

6 CONCLUSIONS

Morgenstern-Price's slope stability analysis indicates that local circular failures are likely to occur in areas of the upslope region that have not been stabilized, even with the water table as low as 20 ft below the ground surface. These types of failures have indeed been observed in the field, particularly in response to intense rainfall events. Any future large-scale failure will probably develop close to the existing predominant slip surface. To avoid this type of instability, water levels should be kept at least 13 ft below the ground surface, and preferably deeper than that.

7 ACKNOWLEDGEMENTS

This study was supported in part by a grant from the Hawaii Department of Transportation and the Federal Highway Administration. Their support is gratefully acknowledged.

8 REFERENCES

Baum, R.L., M.E. Reid, C.A. Wilburn & J.D. Torikai 1991. Summary of Geotechnical and Hydrologic Data Collected from May 1, 1990 through April 30, 1991, for the Alani-Paty Landslide, Manoa Valley, Honolulu, Hawaii. *U.S. Geologic Survey Open-File Report 91-598*: 102.

Baum, R.L. & M.E. Reid 1992. Geology, Hydrology and Mechanics of the Alani-Paty Landslides, Manoa Valley, Oahu, Hawaii. *U.S. Geological Survey Open-File Report 92-501*: 87.

Civil Engineering, 1998. Soil Anchors, Drains Halt Hawaiian Landslide. *Civil Engineering Magazine*, September 1989: 13-14.

Peck, R.B. & S.D. Wilson 1968. Report on The Hind Iuka Landslide and Similar Movements, *Honolulu, Hawaii*: 21.

Polhemus, D. 1993. "Halting the Manoa slip-slide". *The Honolulu Advertiser*, March 7, A: 18.

Tsui, C.S.L., H.G. Brandes & D.D. Nakayama 2001. Creep Behavior and Modeling of the Slow-Moving Alani-Paty Landslide, Oahu, Hawaii. *Proceedings of the 10th International Conference on Computer Methods and Advances in Geomechanics*, Tucson, AZ.

Tsui, C.S.L. 1999. Modeling the Slope Stability and Creep Behavior of the Alani-Paty Landslide Area, Manoa Valley, Honolulu, Hawaii. *MS Thesis, University of Hawaii*: 159p.

9. Appendix E2 – Publication 2

Proceedings of the 10th International Conference on Computer Methods and Advances in Geomechanics, Vol. 1, pp. 1629-1633

Creep Behavior and Modeling of the Slow-Moving Alani-Paty Landslide, Oahu, Hawaii

C.S.L Tsui
Graduate Research Assistant, Department of Civil Engineering, University of Hawaii, US

H.G. Brandes
Associate Professor, Department of Civil Engineering, University of Hawaii, US

D.D. Nakayama
Graduate Research Assistant, Department of Civil Engineering, University of Hawaii, US

ABSTRACT: The Alani-Paty landslide area is underlain by soft, high plasticity soils that are susceptible to time-dependant deformation. In order to estimate creep displacements in the field, one cross-section of the landslide area was modeled using the Soft-Soil creep model in the PLAXIS software code. A combination of field measurements over a limited period of time, along with finite element modeling, have allowed for preliminary predictions of future creep displacements.

1 INRODUCTION

The Alani-Paty landslide in Manoa valley, on the island of Oahu, Hawaii, is typical of a series of slow-moving slides that occur on most flanks of the deep valleys that cut into the Koolau mountain range in East Honolulu. The volcanic colluvium that is found above the basalt bedrock is mostly fine-grained and very soft. Laboratory creep tests show that this type of soil is highly susceptible to time-dependent deformations (Nakayama, 2000), which is also evident in the field by slow but continuous surface deformations that have required millions of dollars in stabilization measures.

This article discusses creep modeling efforts for a representative cross section of the Alani-Paty area, aimed at estimating past and future deformations. A companion paper that focuses on overall stability expands on the geologic setting and geotechnical characteristics of the soils in the landslide area, as well as on recent remediation measures (Brandes and Tsui, 2001). Creep computations were carried out with the commercial code PLAXIS using the SSC (Soft-Soil Creep) model.

2 PROBLEM GEOMETRY AND MODELING APPROACH

Modeling of creep deformations focused on representative cross section AA' in Figure 1. Section AA' can be broadly characterized by inclinations of 5H:1V in the upslope region near the head, 6.8H:1V in the midslope region, and 12H:1V in the downslope region near the toe. In order to simplify the analysis, a single inclination of 6.8H:1V (8.4^0) was used throughout. Initially, a 50-ft long and 5-ft deep section was selected (Figure 2), although the effect of choosing different dimensions is considered as well. The left and right boundaries of the slope section are fixed horizontally, but are free to move vertically. The bottom of the section, on the other hand, is fixed. This means that the height of the slope, *H*, represents the maximum depth to which creep occurs. Remedial measures installed in the area are not considered in this study. Also, the groundwater table is assumed to be at the slope surface to simulate the worst case scenario. The finite element mesh consists of triangular elements with three integration points as shown in Figure 2. Plain strain and drained conditions throughout are assumed.

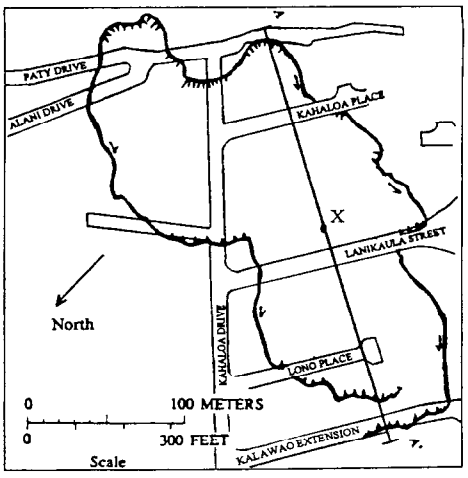

Figure 1. Approximate boundaries of the Alani-Paty landslide

The initial stress due to soil weight is applied to the soil to begin the analysis. An initial time equal to 1 day is input to correspond to the initial stress state. The resulting deformation due to this *gravity turn-on* is reset to zero prior to the second phase,

which is the creep phase. During the creep portion of the analysis the soil is allowed to relax and deform with no changes in external loads.

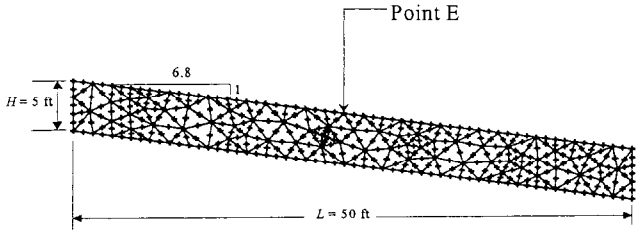

Figure 2. Problem geometry

3 CONSTITUTIVE MODEL AND MATERIAL PARAMETERS

Values of unit weight, cohesion and friction angle are taken from published United States Geological Survey reports (Baum and Reid, 1992). An average saturated unit weight of 138 pcf, an average residual cohesion of 110.2 psf, and an average residual friction angle of 10.2^0 are adopted (Table 1).

Table 1. Index properties

Quantity	Description	Value	Remarks
γ_{sat}	Saturated unit weight	138 lbf/ft^3	
k	Hydraulic conductivity	0.037 ft/d	Same in all direction
c	Cohesion	110.2 psf	$= c'_{residual}$
ϕ	Friction angle	10.2^o	$= \phi'_{residual}$
ψ	Dilatancy angle	0	
λ^*	Modified compression index	0.0703	
κ^*	Modified swelling index	0.0105	= 15% of λ^*
μ^*	Modified creep index	0.0035	= 5% of λ^*

The SSC constitutive model in PLAXIS allows for the elasto-plastic, time-dependent analysis of near-normally consolidated fine-grained soils. The basic volumetric creep equation is given as follows:

$$\dot{\varepsilon}_v^{\,t} = \frac{\mu^*}{t}\left(\frac{p^{eq}}{p_p^{\,eq}}\right)^{\frac{\lambda^*-\kappa^*}{\mu^*}} \qquad (1)$$

where:

λ^*= modified compression index (ε_v vs. e)

κ^*= modified swelling index (ε_v vs. e)

μ^*= modified creep index ($\varepsilon_v^{\,t}$ vs. t')

p^{eq} = final equivalent pressure applied

$p_p^{\,eq}$ = final equivalent isotropic pre-consolidation pressure after creep

$p_{p,0}^{\,eq}$ = initial equivalent isotropic pre-consolidation pressure before loading

t = total time for consolidation and creep

t' = effective creep time

ε_v = total volumetric strain

$\varepsilon_v^{\,t}$= volumetric creep strain

Deviatoric creep strains are computed from Equation (1) with the use of the associated flow rule and by assuming p^{eq} as the plastic potential function. Additional details about this model can be found elsewhere (Tsui, 1999; PLAXIS, 1998). Specific parameters selected for the analysis were based on laboratory 1-D consolidation and triaxial. They are listed in Table 1.

4 DISCUSSION OF COMPUTER PREDICTIONS

Figure 3 shows the deformed mesh after 10,000 days. Given that section AA' is approximately 1000 ft long and that the depth of creep is unlikely to reach anything near this length, the geometry of the problem is close to that of a semi-infinite slope. In fact, the deformation pattern in Figure 3 bears this out. After 10,000 days, the mesh reflects shearing caused by the downslope component of gravity and reduction in height due to volumetric compression. The central portion of the slope undergoes nearly uniform changes in stress and displacement, without undue influence from either the left or the right boundaries. Slope lengths of 75 ft and 100 ft were tried as well, but displacements and stresses in the central region, near point E, did not vary much.

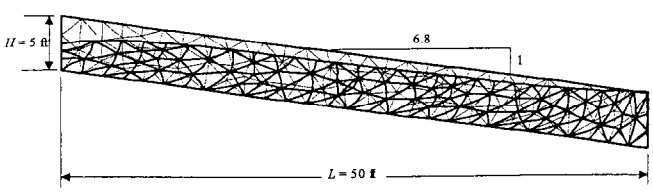

Figure 3. Deformed mesh after t = 10,000 days; displacements are magnified by a factor of 5

However, the same can not be said about the effect of slope height, H. A thicker creep zone

results in larger surface creep displacements. A number of analyses were conducted using different values of H to evaluate its effect on resulting creep deformations. Because a change in H also affected selection of a representative length, a new appropriate length was calculated for each H so that relative displacements and stresses between points near the center of the slope remained about the same. The variation of surface downslope displacement U_d at point E for slope sections with thicknesses of 2.5 ft, 7.5 ft, 10 ft, 12.5 ft, 15 ft and 17.5 ft are shown in Figure 4. The downslope deformation U_d at point E can be normalized as shown in Figure 5.

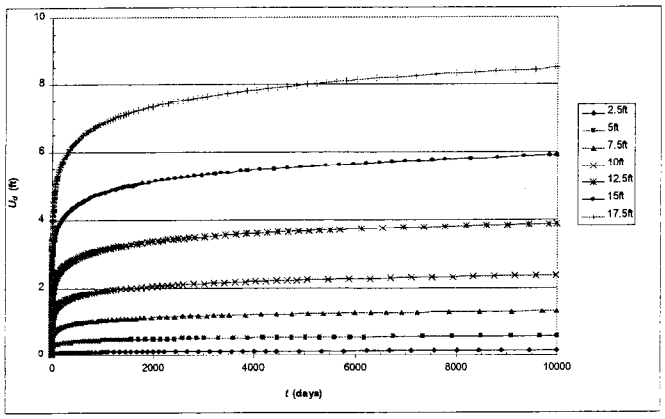

Figure 4. Downslope displacement at point E for different creep depths

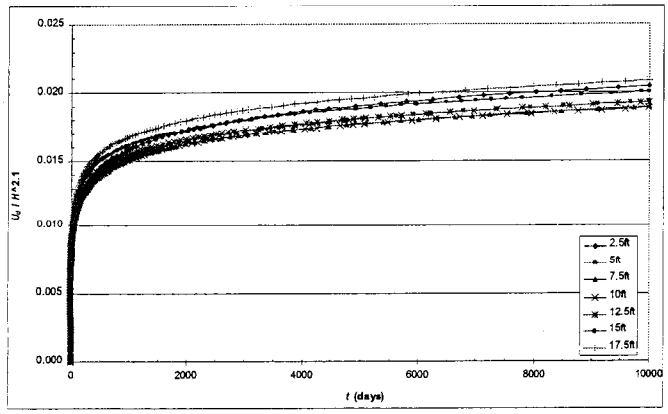

Figure 5. Normalized downslope displacement at point E

Downslope velocity may be a more useful quantity then displacement for estimating past and future deformations due to creep. Normalized velocity as a function of time (Figure 6) can conveniently be expressed by a single relationship:

$$t\, v_d / H^{2.1} = 0.002 \qquad (2)$$

where:

t = time under sustained loading (in days)
v_d = surface downslope velocity (in ft/day)
H = thickness of slope subjected to creep movement (in ft)

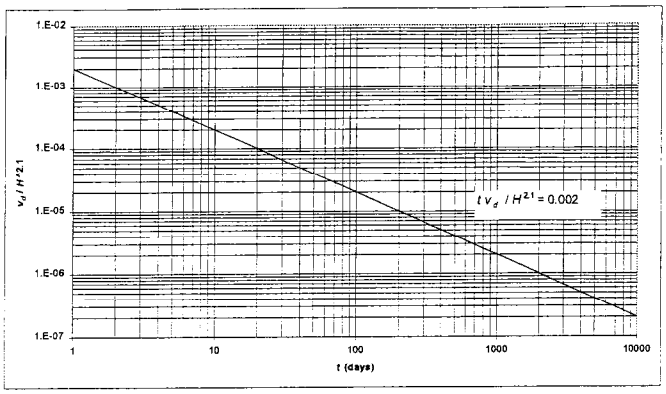

Figure 6. Relationship between surface downslope velocity at point E and effective creep time

Equation (2), in combination with inclinometer measurements, can be used to estimate downslope deformations. However, the start of creep, i.e. $t = 0$, is hard to determine for field slopes. In fact, it is unlikely that such a time even exists for natural slopes that have developed over hundreds or thousands of years. In case of constructed slopes, such an initial time may be more obvious (Brandes et al., 1994). Because the Alani-Paty slope has existed for thousands of years, a small value of t would not be realistic and may lead to overestimating creep deformations. A large value for t is therefore suggested for predictions of future creep movements.

Since the thickness of the Alani-Paty landslide above the inferred failure surface is about 25 ft, a height of 25 ft is a reasonable first choice for the depth to which creep occurs. As an example, downslope velocity v_d can be estimated for two times since the initiation of creep as follows:

Case 1: t = 1,000 days
$v_d = 0.002 \times H^{2.1} / t$
$v_d = 0.002 \times 25^{2.1} / 1000$
v_d = 0.0017 ft/day = 0.63 ft/year = 7.6 in/year

Case 2: t = 100 years
$v_d = 0.002 \times 25^{2.1} / (100 \times 365)$
$v_d = 4.73 \times 10^{-5}$ ft/day
v_d = 0.017 ft/year = 0.2 in/year

The USGS collected inclinometer measurements during a 20-month period from October 1989 through March of 1991 (Baum and Reid, 1992). During this time, the downslope deformation near the head of the slope attributed to creep was estimated to be about 0.05 ft (Baum et al., 1991). The average creep rate was therefore about 0.0025 ft/month, or 8.33×10^{-5} ft/day. It is interesting to

note that by using this value for v_d, along with a height of 25 ft, Equation (2) would give a time from creep initiation of about 57 years. This value of t obviously does not correlate with the actual age of the Alani-Paty slope area. Creep must have been occurring for much longer than that. However, this initial time can be used to make rough predictions on how creep velocity may decrease with time. For example, ten years after the USGS monitoring period one may estimate a velocity of about 0.0022 ft/month. These values need to be correlated with additional field measurements.

Because the results of the above analysis are dependent on the selected soil parameters, a sensitivity study was conducted to evaluate the effects of these parameters on creep predictions. A 10-ft thick and 300-ft long section was selected for this analysis. The results are summarized in Table 2, which indicates what happens if each parameter in turn is increased by 10%. It is apparent that the results are most sensitive to parameters c, ϕ, and μ^*. As with any sensitivity analysis involving soil parameters, the results need to be viewed with caution since it is unreasonable to expect that any of these parameters vary independently of the others.

Table 2. Summary of sensitivity analysis

Parameter in question	Change in parameter	Change in U_d
γ_{sat}	+10%	+4%
k	+10%	0%
c	+10%	-14%
ϕ	+10%	+12%
λ^*	+10%	+1%
κ^*	+10%	0%
μ^*	+10%	+9%

The stability analysis in the companion paper (Brandes and Tsui, 2001) indicated that a groundwater table of at least 15 ft or so below the ground surface is required in order for the slope to be safe. Therefore, creep predictions were carried out using a groundwater table located at an equivalent depth. Because of numerical difficulties encountered when the slope was thicker than about 20 ft, computations were carried out instead on a 10 ft-thick slope with a groundwater elevation at the surface and also at 6 ft below the surface. This depth of 6 ft represents 60% of the slope height, which corresponds to a groundwater depth of 15 ft in the 25-ft slope section used for the stability analysis. The downslope displacement and velocity at point E are shown for both water elevations in Figures 7a and 7b. A 60% drop in the groundwater table results in about a 36% decrease in v_d, independent of the value of H. It is therefore apparent that a lower groundwater table will not only increase slope stability, but it will also reduce creep deformations.

5 CONCLUSIONS

Downslope creep velocity was found to decrease with time according to Equation (2). However, the time for creep initiation is hard to determine for slopes such as the Alani-Paty one which have existed for thousands of years. However, when combined with field measurements, creep modeling can provide estimates of surface displacements as was demonstrated by a specific example. The effect of lowering the groundwater is, as expected, to decrease the amount of creep.

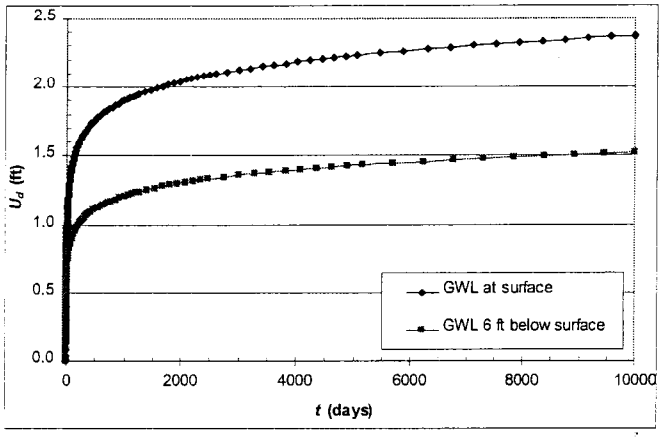

Figure 7a. Effect of groundwater table on surface downslope displacement at point E (H = 10 ft, L = 300 ft, t = 10,000 days)

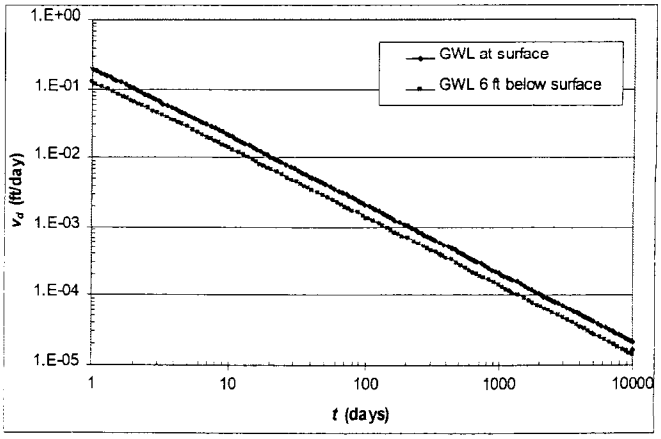

Figure 7b. Effect of groundwater table on surface downslope velocity at point E (H = 10 ft, L = 300 ft, t = 10,000 days)

6 ACKNOWLEDGEMENTS

This study was supported in part by a grant from the Hawaii Department of Transportation and the Federal Highway Administration. Their support is gratefully acknowledged.

7 REFERENCES

Baum, R.L., M.E. Reid, C.A. Wilburn & J.D. Torikai 1991. Summary of Geotechnical and Hydrologic Data Collected from May 1, 1990 through April 30, 1991, for the Alani-Paty Landslide, Manoa Valley, Honolulu, Hawaii. *U.S. Geologic Survey Open-File Report 91-598*: 102.

Baum, R.L. & M.E. Reid 1992. Geology, Hydrology and Mechanics of the Alani-Paty Landslides, Manoa Valley, Oahu, Hawaii. *U.S. Geological Survey Open-File Report 92-501*: 87.

Brandes, H.G. & C.S.L. Tsui 2001. Modeling the Effectiveness of Groundwater-Lowering Remediation Measures in the Alani-Paty Landslide Area, Oahu, Hawaii. *Proceedings of the 10th International Conference on Computer Methods and Advances in Geomechanics*, Tucsion, AZ.

Brandes, H.G., A.J. Silva, M.H. Sadd & G.E. Veyera 1994. Stress-Strain-Time Modeling of Submarine Slopes. *Proceedings of the 8th International Conference on Computer Methods and Advances in Geomechanics*, Morgantown, WV, 3:2435-2445.

PLAXIS, 1998. *PLAXIS Version 7 Users Manual.* R.B.J. Brinkgreve and P.A. Vermeer Eds., Netherlands.

Nakayama, D.D. 2000. Creep Characterization of Tropical Soils. *MS Thesis, University of Hawaii*: 195p.

Tsui, C.S.L. 1999. Modeling the Slope Stability and Creep Behavior of the Alani-Paty Landslide Area, Manoa Valley, Honolulu, Hawaii. *MS Thesis, University of Hawaii*: 159p.